AD NUMBER

AD809319

NEW LIMITATION CHANGE

TO

Approved for public release, distribution unlimited

FROM

Distribution authorized to U.S. Gov't. agencies and their contractors; Critical Technology; FEB 1967. Other requests shall be referred to Air Force Aero Propulsion Lab., ADSC, Wright-Patterson AFB, OH 45433.

AUTHORITY

AFAPL ltr, 12 Apr 1972

AFAPL-TR-66-143

EVALUATION OF POLE FACE LOSSES FOR THE 467 KVA EXPERIMENTAL GENERATOR

J. L. McCabria
C. C. Kouba
Westinghouse Electrical Corporation

TECHNICAL REPORT AFAPL-TR-66-143

February, 1967

Air Force Aero Propulsion Laboratory
Research and Technology Division
Air Force Systems Command
Wright-Patterson Air Force Base, Ohio

NOTICES

When Government drawings, specifications, or other data are used for any purpose other than in connection with a definitely related Government Procurement operation, the United States Government thereby incurs no responsibility nor any obligation whatsoever; and the fact that the Government may have formulated, furnished, or in any way supplied the said drawings, specifications, or other data, is not to be regarded by implication or otherwise as in any manner licensing the holder or any other person or corporation, or conveying any rights or permission to manufacture, use, or sell any patented invention that may in any way be related thereto.

Copies of this report should not be returned to the Research and Technology Division unless return is required by security considerations, contractual obligations, or notice on a specific document.

EVALUATION OF POLE FACE LOSSES FOR THE 467 KVA EXPERIMENTAL GENERATOR

J. L. McCabria
C. C. Kouba

FOREWORD

The work discussed in this report was performed by the Westinghouse Electric Corporation, Aerospace Electrical Division, Lima, Ohio under United States Air Force Contract AF33(615)2326 from January 1965 to July 1966. This contract was administrated by the Air Force Aero Propulsion Laboratory, Research and Technology Division, Air Force System Command, Wright-Patterson Air Force Base, Ohio with Mr. C. H. Armbruster acting as Project Engineer.

This work represents a continuation of work performed on Contracts AF33(657)10922 and AF33(615)1551 from January 1964 to January 1965.

This report is assigned supplementary report number WAED 66.55E by Westinghouse

This report was submitted by the authors for review in December, 1966.

Publication of this report does not constitute Air Force approval of the report's findings or conclusions. It is published only for the exchange and stimulation of ideas.

Glenn M. Kevern
Chief, Energy Conversion Branch
Aerospace Power Division

ABSTRACT

The pole face losses associated with the alternating flux density that is produced by the slot and teeth in the armature for the 467 kva experimental generator were experimentally evaluated by using an eddy-current dynamometer. The design factors which influence pole face losses in the generator were duplicated in the test fixture as close as possible. Centrifugal stress in the rotor limited the tooth ripple frequency to one-half the tooth ripple frequency of the generator and it was necessary to extrapolate the data from 24,000 cps to 48,000 cps to determine the pole face losses at these conditions. No attempt was made to control the temperature of the pole faces. Therefore, the test results had to be corrected for a change of resistivity since the pole faces will operate at a much higher temperature in the generator.

A complete analysis of the pole face loss problem based upon theoretical considerations is presented in the report. The problem of dealing quantitatively with the magnetic flux density distribution at the surface of the poles is treated analytically. Harmonic frequencies and the losses due to each harmonic frequency were considered. The effect of grooves in the pole faces were also considered in the theoretical analysis. The theoretical equations show that the eddy-current losses are a function of permeability of the pole face material. In the actual problem this quantity is a variable and a method for determining the applicable value of this variable is presented.

The general conclusions derived from this work are: (1) materials which offer the best combination of d-c magnetic and strength properties for a high speed, high temperature, solid rotor have inferior properties from the standpoint of pole face losses and (2) a 16-fold decrease of eddy-current losses can be obtained by using a laminated material for the pole tips which has been chosen for its high a-c magnetic permeability when compared with the losses associated with material that has been selected for its creep strength or other criteria except its a-c magnetic permeability.

TABLE OF CONTENTS

LIST OF ILLUSTRATIONS

LIST OF ILLUSTRATIONS - Continued

LIST OF ILLUSTRATIONS - Concluded

LIST OF SYMBOLS WHICH ARE NOT DEFINED WITHING THE BODY OF THE REPORT

Vector Quantities

B	Magnetic flux density, gauss
D	Electric flux density
E	Electric field strength
H	Magnetic field strength, oersteds
J	Current density, abampere/cm^2

LIST OF SYMBOLS WHICH ARE NOT DEFINED
WITHIN THE BODY OF THE REPORT - Continued

Vector Quantities (Continued)

i,j,k	Unit vectors in a rectangular coordinate system

Scalar Quantities

A,B,C,D,E	Arbitrary Constants
$A_{-1},B_{-1},C_{-1},D_{-1},E_{-1}$	Arbitrary Constants
a_1,a_2,a_3	Separation Constants
B_x,B_y,B_z	Rectangular components of Magnetic flux density, gauss
f	Tooth ripple frequency, cycles/second
i	$\sqrt{-1}$
J_x,J_y,J_z	Rectangular components of current density, abampere/cm^2
k,n	Arbitrary integers
m	Order of harmonic associated with flux distribution
P	Eddy-current loss, ergs/sec/cm^2
t	Time seconds
U_m	$= \left[\left(0.25 + \frac{f^2\mu^2\lambda^4}{\rho'^2 m^2}\right)^{1/2} + 0.5\right]^{1/2}$, dimensionless
V_m	$\left[\left(0.25 + \frac{f^2\mu^2\lambda^4}{\rho'^2 m^2}\right)^{1/2} - 0.5\right]^{1/2}$, dimensionless

Scalar Quantities

x,y,z	Rectangular coordinates, cm

LIST OF SYMBOLS WHICH ARE NOT DEFINED WITHIN THE BODY OF THE REPORT - Continued

Greek Symbols

β	$\tan^{-1} \frac{2f\mu_\lambda{}^2}{\rho' m}$
ϵ	Dielectric constant
Θ	$\frac{2\pi}{\lambda} (f\lambda t + x - V_m y)$
λ	Slot pitch, cm
μ	Permeability
ρ	Resistivity, ohm-cm
ρ'	Resistivity, abohm-cm
ϕ	Flux, maxwells

LIST OF REFFRENCES

1. Aston, K., and Rao, M.V.K.:"Pole Face Losses due to Open Slots," Journal I.E.E., 1941, Vol. 88.

2. Barello, G.: "Eddy-Currents Produced in the Solid Pole Pieces of Alternators by the Stray Rotating Fields of the Armature Reaction," Revue Generale de l'Electricite Vol. 64, No. 11, November 1955.

3. Kouba, C. and Muir, J.: "Spur Pole Face Loss Evaluation," Report No. WAED 64.57E, Aerospace Electrical Division, Westinghouse Electric Corporation, Lima, Ohio, October, 1964.

4. Gibbs, W. J.: "Tooth Ripple Losses in Unwound Pole Shoes" Institution of Electrical Engineers Journal (London) Vol. 94, 1947.

5. Bozorth, R.M.: "Ferromagnetism" by D. Van Nostrand Co., Inc., 120 Alexander St., Princeton, New Jersey, reprinted Nov. 1964.

SECTION I

INTRODUCTION

Accurate evaluation of the power losses in the rotor pole faces is required to determine the thermal state of a rotor. The mechanical integrity of the rotating mass depends upon these losses since the allowable stresses depends upon the thermal state of the rotor. Losses which produce heat energy in the pole faces are caused by two sources of flux oscillations. The first is due to the fact that as the pole face passes under a slotted armature all points on the pole face experience a varying flux density. At one instant a point on the pole face is under a tooth where the radial component of the flux density is a maximum and at the next instant it is under a slot where the radial component of the flux density is a minumum. The varying flux density in the radial direction within the poles is associated with a varying flux in the tangential direction since all flux lines must form a closed loop. The varying flux density produces an emf which gives rise to eddy-currents that produce losses in the pole. The varying flux also produces minor hysteresis loops which cause additional losses. The losses produced by the slots and teeth in the armature are generally called "tooth ripple losses". These losses exist whenever the machine is magnetized.

A second source of losses in the poles is produced by the varying flux that is generated by harmonic mmf's associated with the armature windings. These losses exist only when current is flowing in the windings.

Many investigators have published equations for evaluating the power losses due to eddy-currents and, for the most part, they have been collated in a paper by Aston and Rao (reference 1). Equations for the evaluation of the losses associated with the varying flux produced by the armature windings are presented in Reference 2. Most investigators have used semi-empirical or purely empirical means based upon the results of several experiments to establish their formulas. Other investigators have based their equations upon theoretical considerations by admission of certain approximations. In general, the theoretical treatments assume that only eddy-current loss has importance and is always predominant over hysteretic loss. Admission of approximations are necessary to deal with the permeability of the material, which is a variable quantity and is always treated as a constant. Admission of certain approximations are also necessary to obtain numerical results for the distribution of flux density on the surface of the pole faces.

The value of the parameters which influence pole face losses for the 467 kva experimental generator is far above the range previously investigated. Hence, empirical equations which contain numerical constants that are based upon experimental results from average designs are apt to give erroneous results for the novel 467 kva generator. Hence, equations which are based upon theoretical considerations are preferred, since this method can be employed for a wider range of values of the variables. One of the important variables which has a significant influence upon eddy-current losses is the resistivity of material in the poles. The pole faces in the experimental generator will operate at approximately 1000°F and the material in the poles will have a higher resistivity than the average design. Therefore, experimental results obtained with average designs can not be used to predict the eddy-current losses in a high temperature generator unless the formulas correctly describe the influence of resistivity. The experimental generator tooth ripple frequency will be 48,000 cps, which is approximately eight times greater than the frequency previously investigated. Thus, formulas based upon experimental results from low frequency tests must correctly describe the influence of frequency before they can be used to predict the losses for the experimental generator.

Several of the available equations were used to evaluate the tooth ripple losses for the generator and the results were presented in Reference 3. A wide disagreement was found to exist.

In general, pole face losses are of minor importance in slow-speed machines and an order of magnitude difference between the calculated and actual values may be of little significance with regard to machine performance. For the high speed experimental generator, where the rotor material is being used near its maximum stress and temperature capabilities, an error of less than 50 percent could result in a complete failure of the machine. For this reason and since the accuracy of available equations is questionable, it was deemed necessary to perform experiments to determine the tooth ripple losses with material and design factors as close as possible to those contemplated for the generator. The design of a pole face loss test fixture was initiated in 1963. The fixture was built and tests were accomplished during 1964 and reported in Reference 3. In general, the results from these tests were inconclusive with regard to pole face losses. The test fixture and instrumentation was modified to reduce the experimental error and the program was continued. In addition, a complete theoretical analysis of the problem was performed. The results from this analysis and the experimental effort are presented in in this report.

SECTION II

TEST FIXTURE

The distinguishing features of the test fixture employed for this investigation are illustrated by Figure 1. In effect, the fixture was an eddy-current dynamometer or a magnetic brake in which a toothed rotor was rotated between two poles of an electromagnet. Torque reaction on the trunnion mounted stator was measured on a scale to obtain the electrical and windage losses in the machinery. The air gap was controlled by adjusting the radial position of the poles.

The tooth pitch and slot configuration in the rotor duplicated the tooth pitch and slot configuration of the armature for the 467 kva experimental generator shown in Figure 2. Centrifugal stress limited the speed of the 120-tooth rotor to 12,000 rpm. Thus, the maximum tooth ripple frequency that could be attained was 24,000 cps or one-half the tooth ripple frequency of the generator.

The pole specimens used in the fixture are shown in Figures 3a and 3b. The specimens were made of H-11 steel and were heat treated to hardness specified for the full scale rotor. The grooves in the pole faces duplicated the grooves used in the rotor pole faces except for width; they were approximately 0.010 inches wide at the surface of the pole or approximately 0.005 inches wider than desired.

It would have been highly desirable to construct a test fixture in which no losses except the tooth ripple losses could have existed. In general, this is not capable of being realized. Designers of a pole face loss test fixture must cope with the problem of separating the pole face losses from the other losses in the machine. Ingenious methods are always required. The losses in the test fixture shown in Figure 1 which caused a torque reaction on the scale were: (1) the loss associated with the aerodynamic drag on the stator, (2) rotor iron losses, (3) magnetic circuit pulsation loss, and (4) pole face losses. The reaction in the bearings which support the high speed rotor and the aerodynamic reaction on the rotor were not imposed upon the trunnion mounted stator. The initial tests performed in 1964 (reference 3) showed that the aerodynamic reaction on the stator was approximately ten times greater than the reaction due to electrical losses in the machine at operating conditions pertinent to the generator.

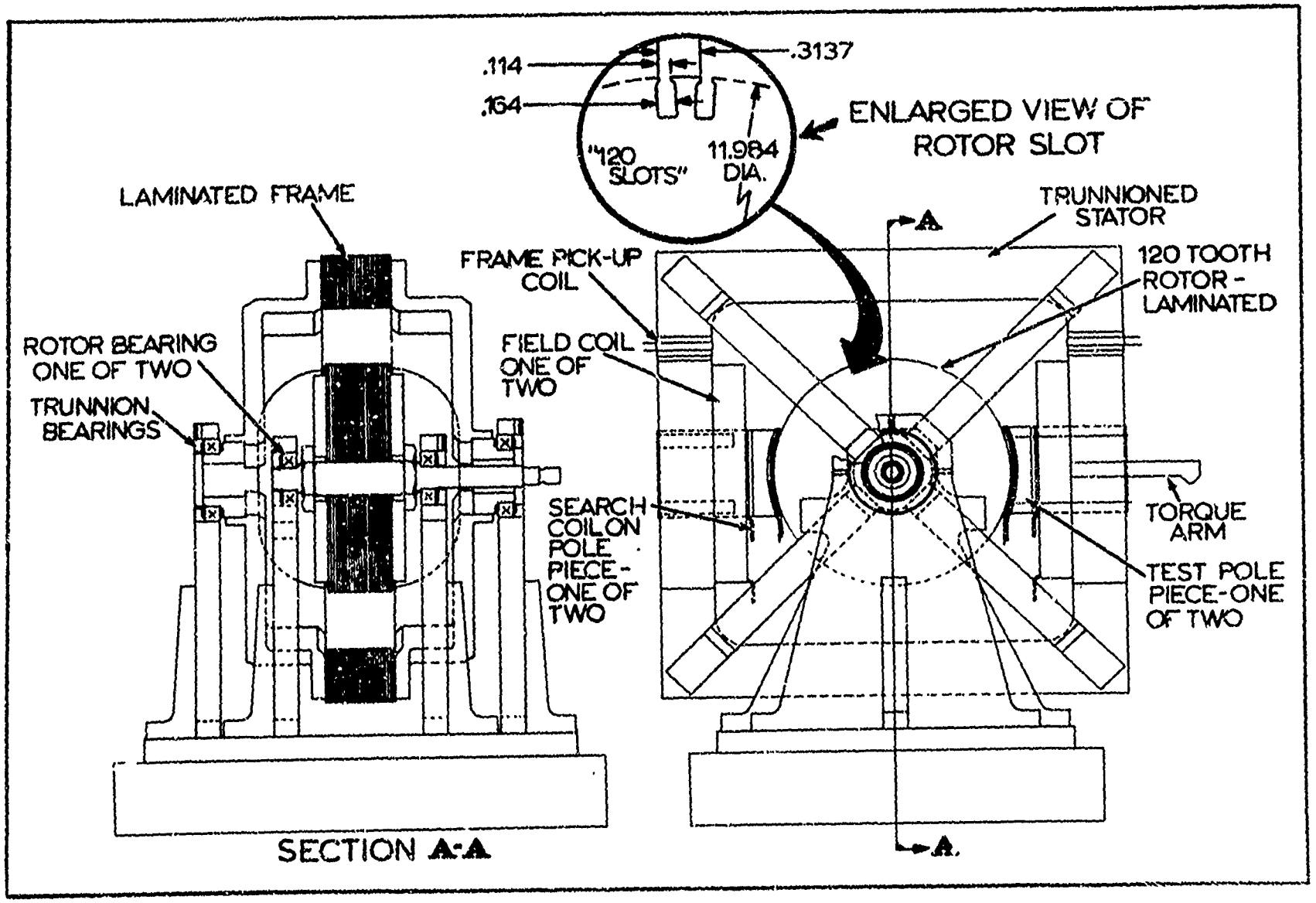

Figure 1. Pole Face Loss Test Fixture

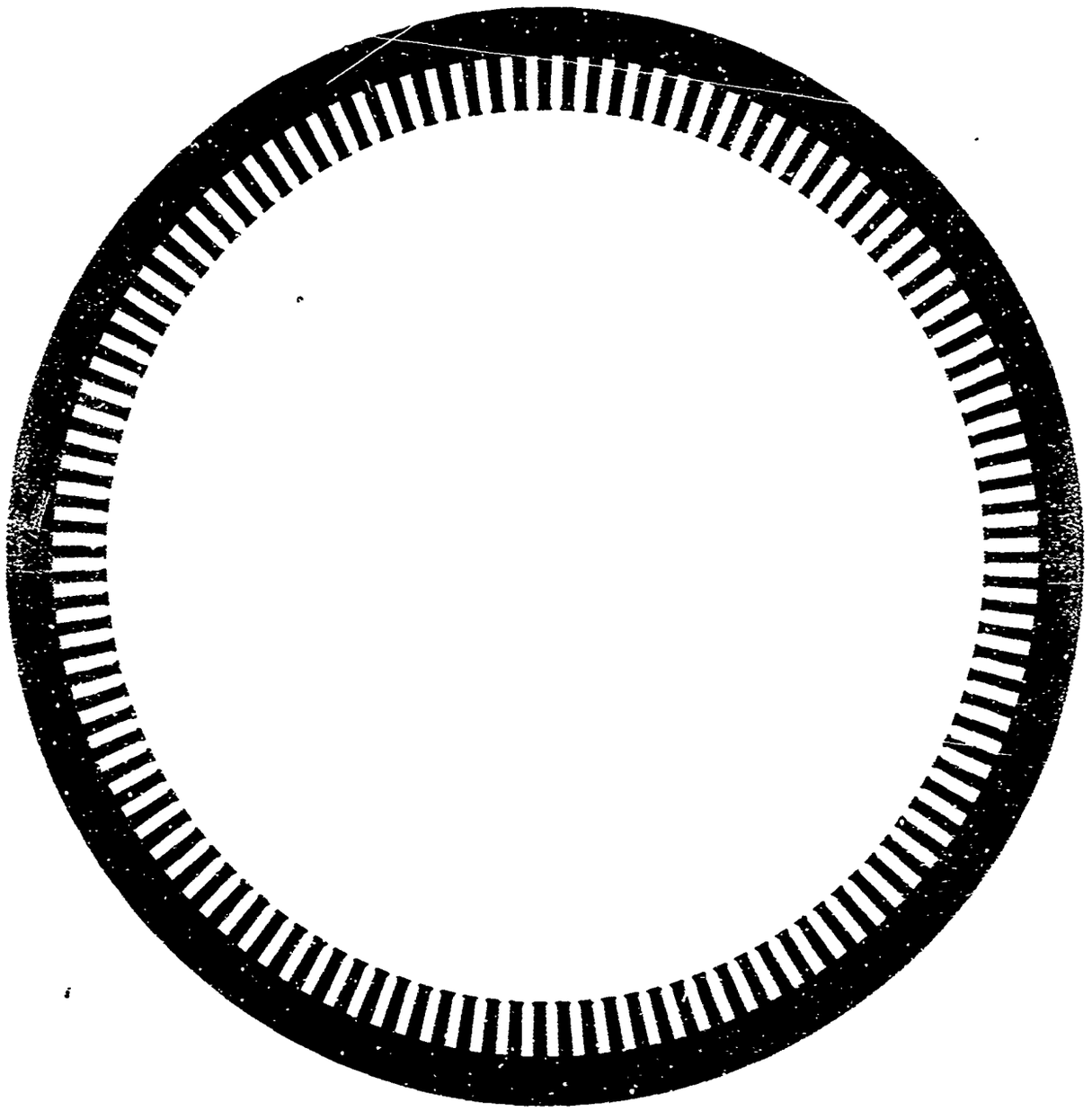

Figure 2. Slot Configuration in Experimental Generator

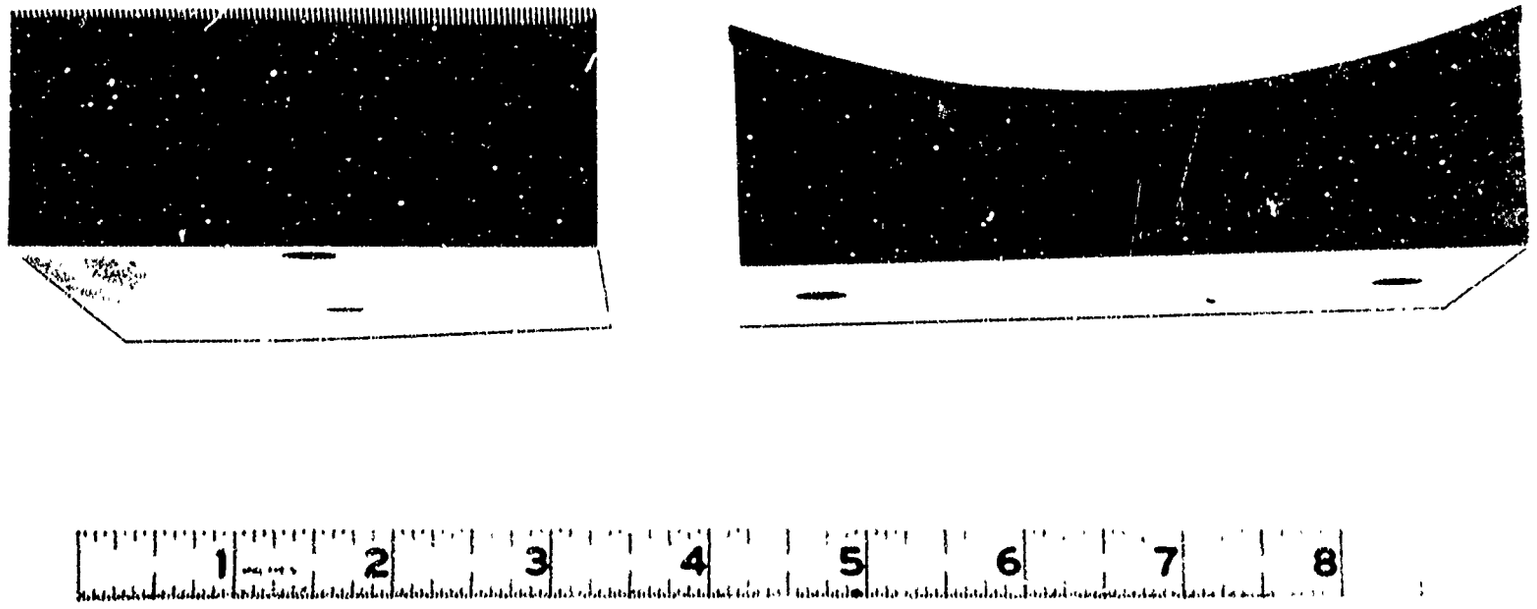

Figure 3a. Side View of Poles

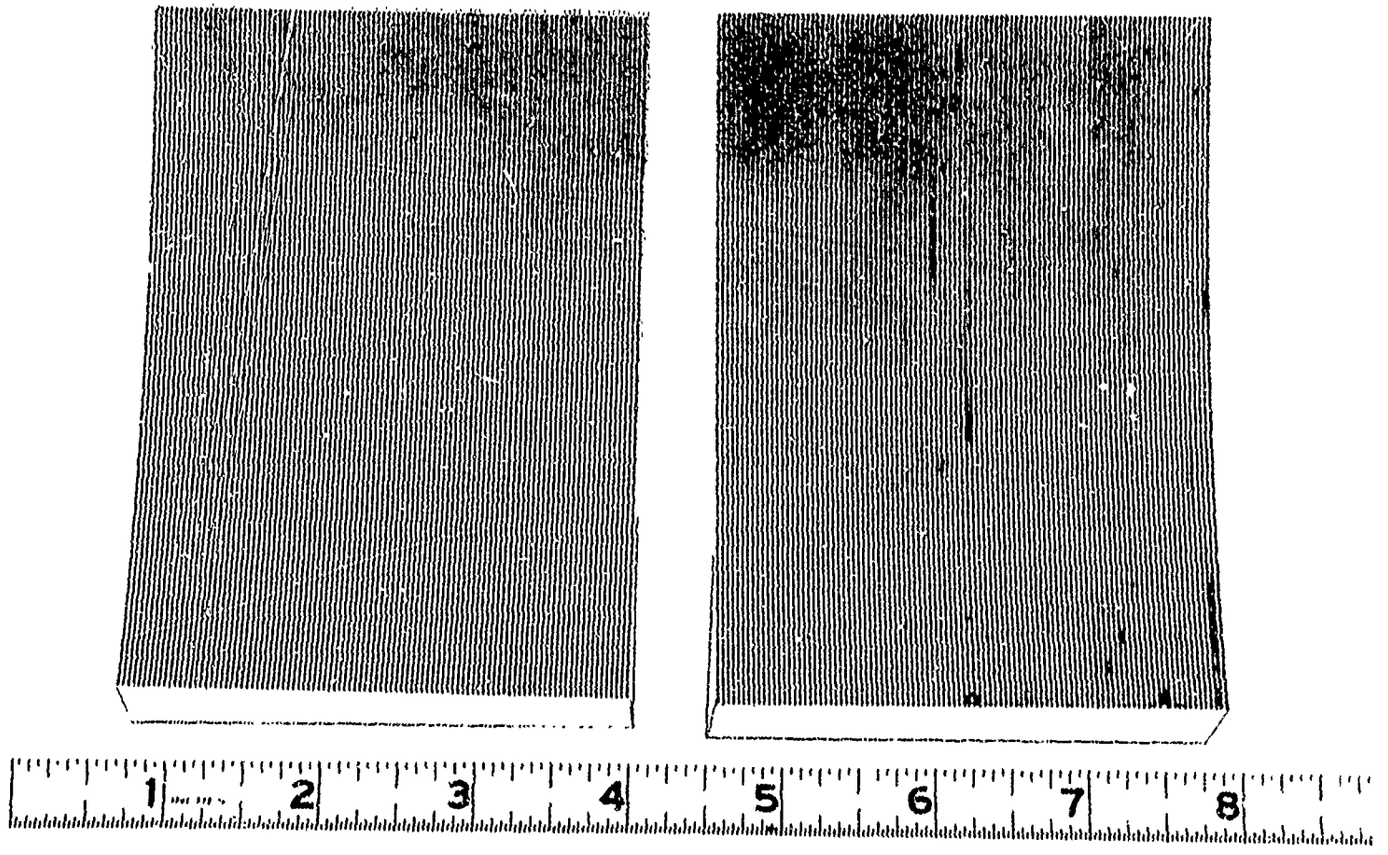

Figure 3b. Poles for Pole Face Loss Test Fixture

Stationary shrouds were installed on the windward side of the poles to decrease the aerodynamic reaction on the stator after the initial tests were performed. With this modification the windage reaction was decreased to approximately two times the reaction due to electrical losses at conditions relevant to the actual generator. The windage reaction was measured by noting the scale reading with the fixture demagnetized for each test speed and air gap. This value was then subtracted from the readings taken with the fixture magnetized. The net reaction represented the electrical losses in the magnetic circuit. Magnetic circuit pulsation losses could not be separated from the other losses. Pulsation losses are caused by a variation of air gap reluctance and are theoretically present when the pole arc covers a non-integral number of slot pitches and is most severe when the fractional part of the number is one-half for an integral slot winding. Since the test fixture had an armature with an integral slot winding feature or sixty slot pitches per pole pitch, the number of slot pitches per pole arc was made an integral number, or fifteen in order to reduce the pulsation losses.

To verify that the test fixture design was such that pulsation losses were negligible, a forty turn coil was wound on the stator frame so that any flux pulsation in the magnetic circuit could be measured. This was accomplished by connecting a calibrated oscilloscope to the coil and measuring the induced voltages and frequency. Figure 4 shows the induced coil voltage as taken from polaroid pictures; curves are presented for several air gaps.

The maximum magnitude of the flux pulsation for the smallest air gap was approximately 2 lines per square inch and it is reasonable to conclude that the loss produced by this magnitude of pulsation was very minute.

The electrical losses in the fixture were separated into rotor iron loss and pole face loss by determining the rotor iron loss for a given rotor speed and frame flux at large air gaps. Since pole face loss is a function of air gap, this loss decreased when the air gap increased.

Since rotor iron loss is independent of air gap, it was obtained by plotting the measured electrical losses for constant values of flux and speed as a function of air gap and extrapolating the curves to infinite air gap where pole face losses are zero. The rotor iron loss was then subtracted from the total electrical loss to obtain the pole face loss for a given frame flux, air gap, and rotor speed.

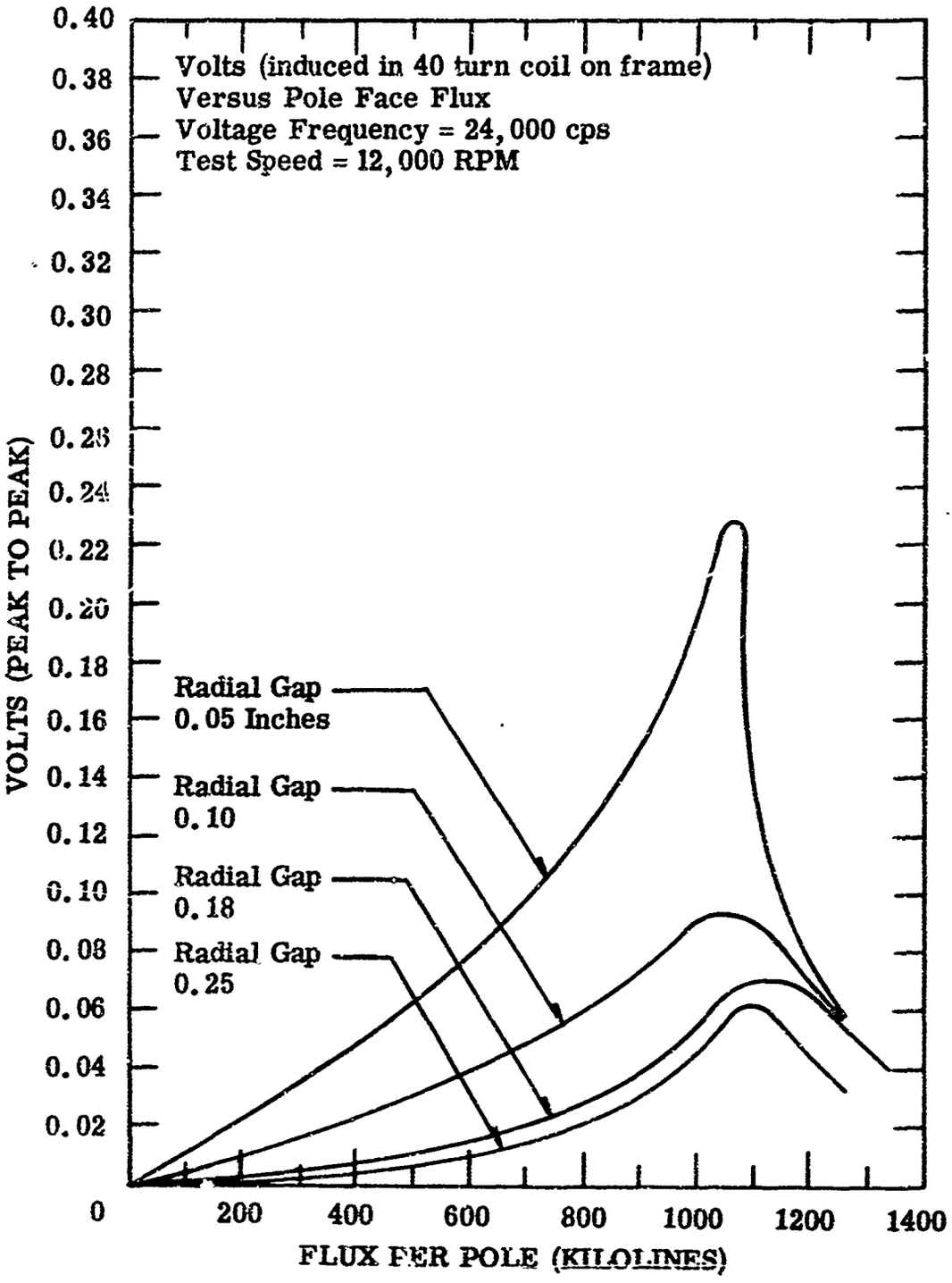

Figure 4. Frame Tooth Pulsation Voltage

SECTION III

TEST RESULTS

The initial test runs had indicated that a considerable amount of flux was fringing around the pole face flux coils and that the total flux through the rotor was higher than that indicated by the pole face coil readings. To verify this, another set of coils were wound on the stator frame so that all of the flux entering the rotor could be measured. Figure 5 shows a plot of measured flux as a function of the field coil excitation current for both the pole face and frame flux coils for the case of a radial gap of 0.092 inches. These curves verify the conclusion that the total rotor flux is significantly higher than the flux in the stator pole faces.

Curves of rotor flux and pole face flux plotted as a function of field coil current for the four test air gap are shown in Figures 6 and 7 respectively. These curves are independent of rotor speed.

One of the initial test runs included an air gap of 0.054 inch but it was later found when plotting the data that an insufficient number of data points were taken for rotor flux values between 0 and 1000 kilolines (only two points were included). Because of the steep slope of the air gap line for this small gap length, smaller increments of field current should have been used to obtain more points. For this reason, test data for the 0.054 inch air gap was omitted from the analysis.

Figures 8, 9, and 10 show plots of measured test fixture electrical loss (i.e., total measured loss minus windage loss) plotted as a function of field coil current for the rotor speeds of 4,000 rpm, 8,000 rpm, and 12,000 rpm respectively. The high speed limit for the test fixture is 12,000 rpm.

From the curves of rotor flux versus field current and electrical loss versus field current for the various test air gaps, plots of electrical loss as a function of air gap length for constant values of rotor flux were obtained. These curves are shown in Figures 11, 12, and 13 for rotor speeds of 4,000 rpm, 8,000 rpm, and 12,000 rpm respectively. The rise in electrical loss with smaller air gaps due to increased pole face loss, is very evident. The right hand side of the curves, where the rate of change of loss with air gap is practically zero, represents the rotor tooth and core loss. The difference

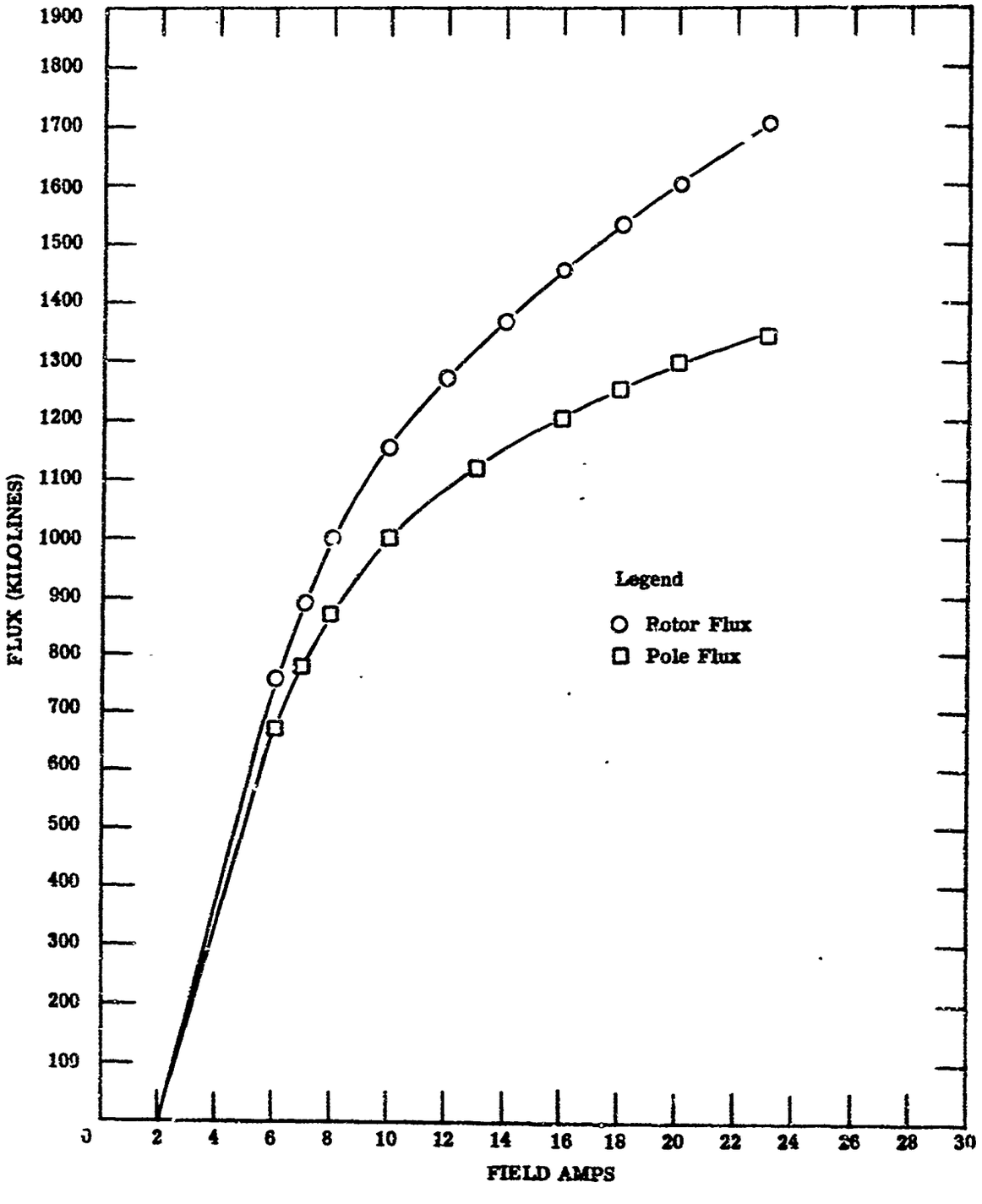

Figure 5. Rotor and Pole Face Flux Versus Field Current for 0.092 Inch Radial Gap

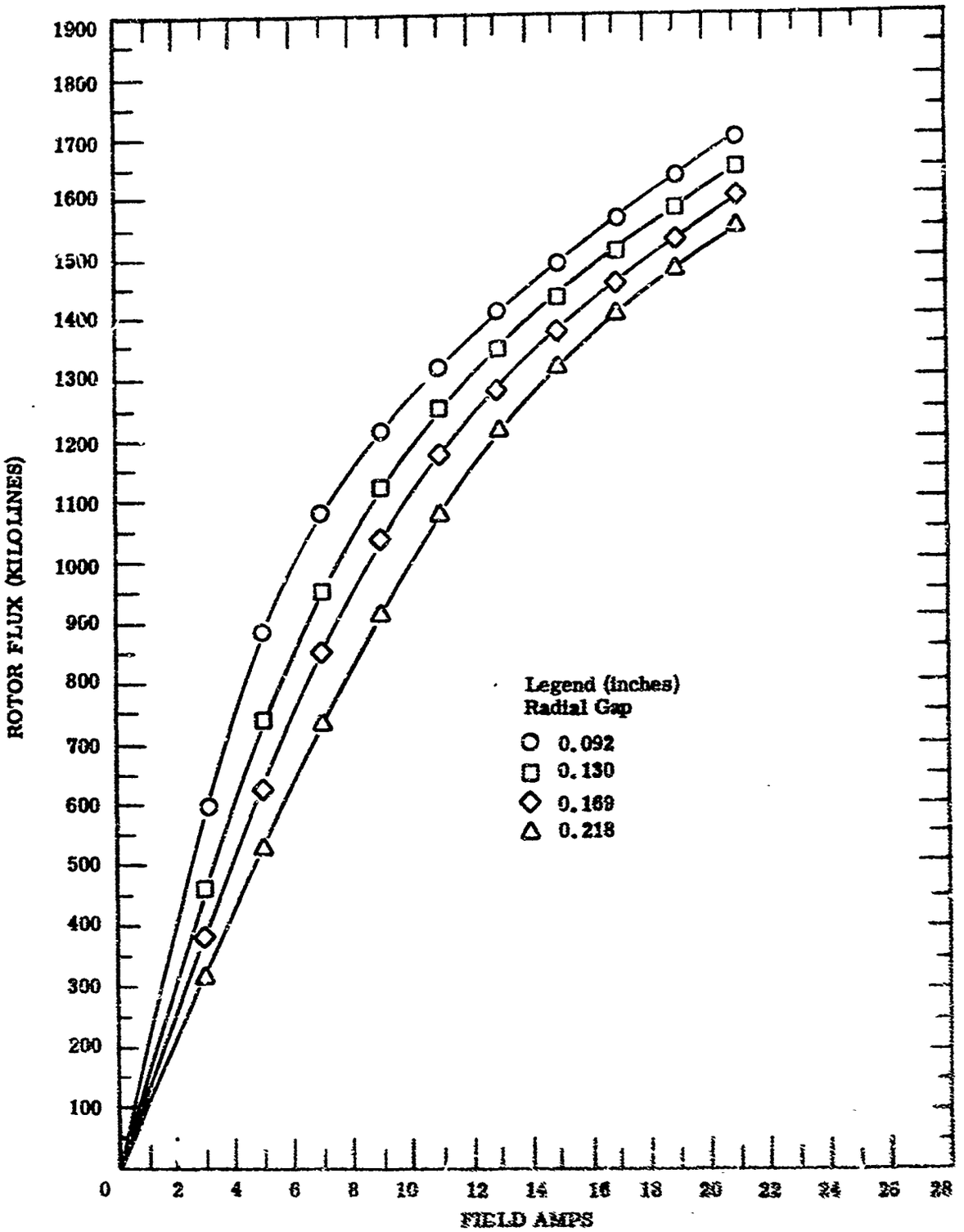

Figure 6. Rotor Flux Versus Field Current

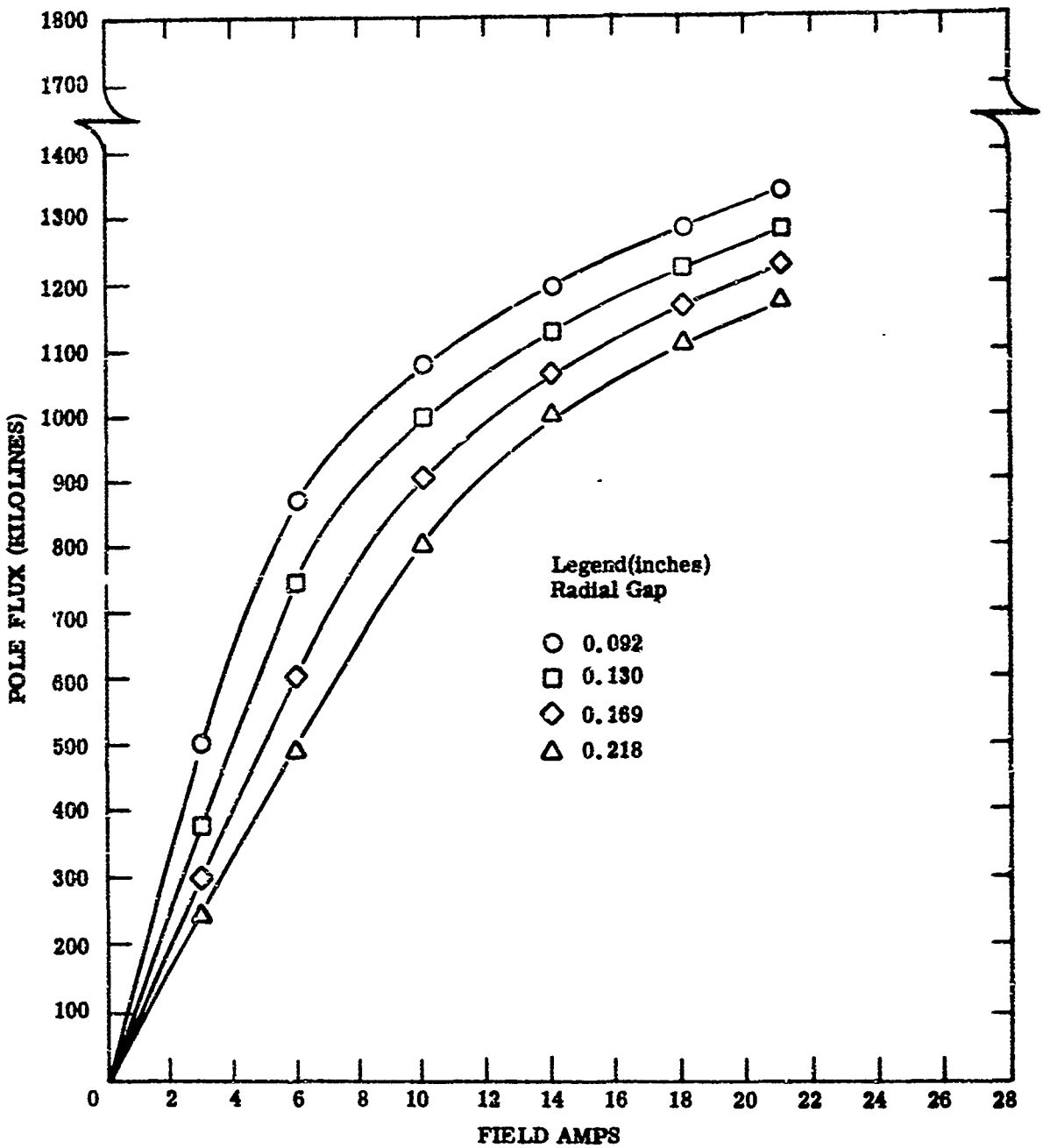

Figure 7. Pole Face Flux Versus Field Current

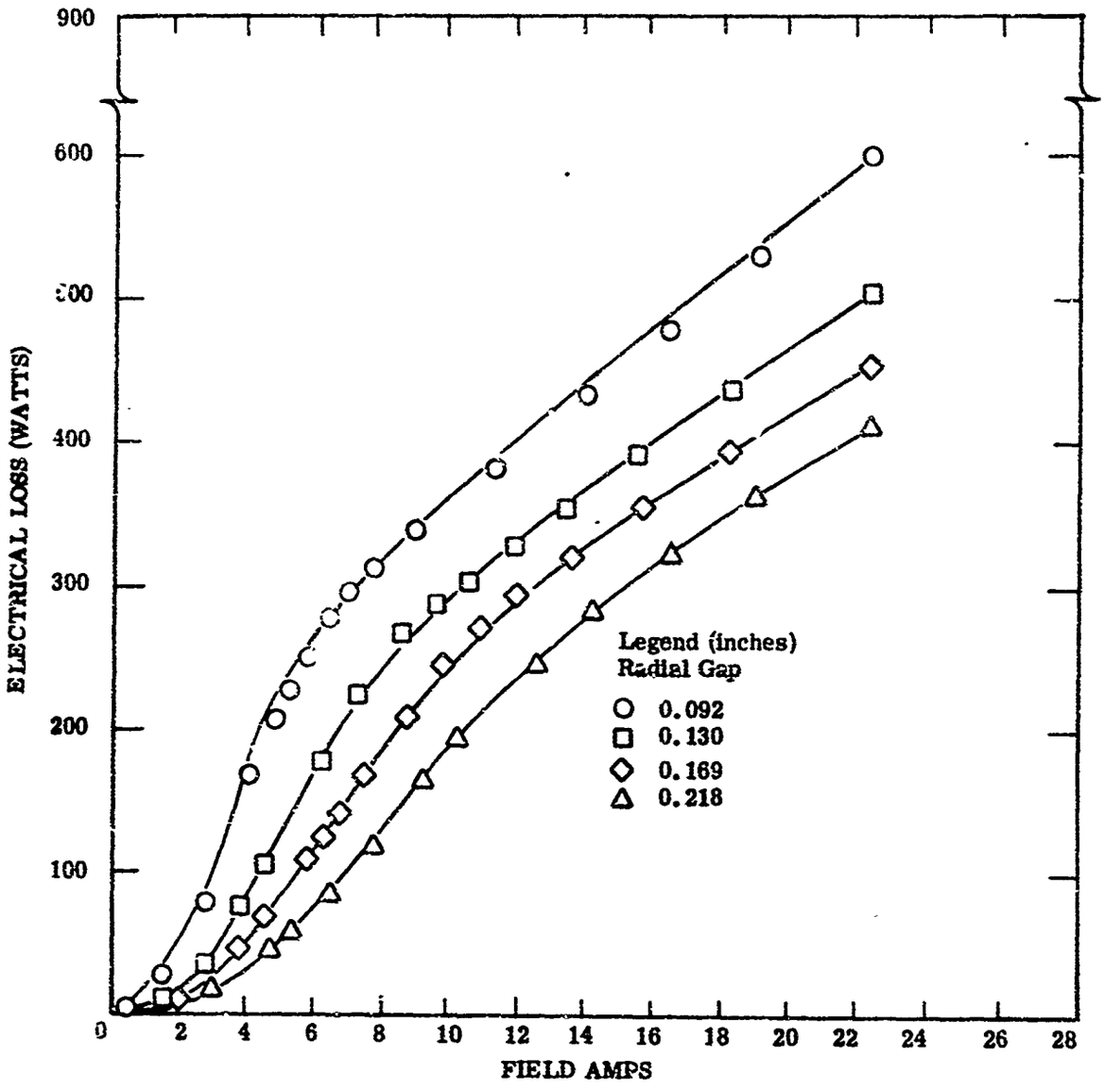

Figure 8. Electrical Losses Versus Field Current at 4,000 rpm

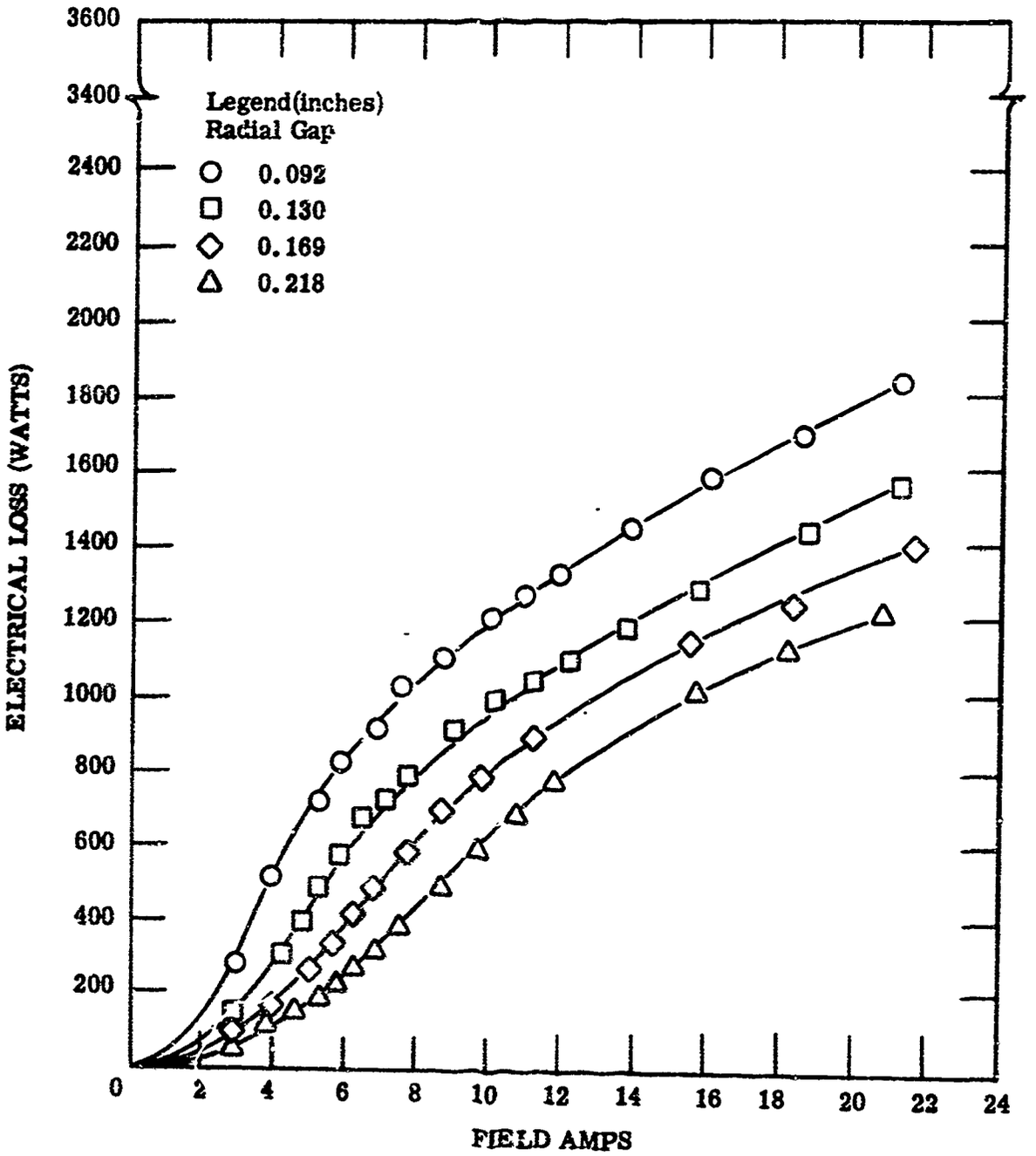

Figure 9. Electrical Losses Versus Field Current at 8,000 rpm

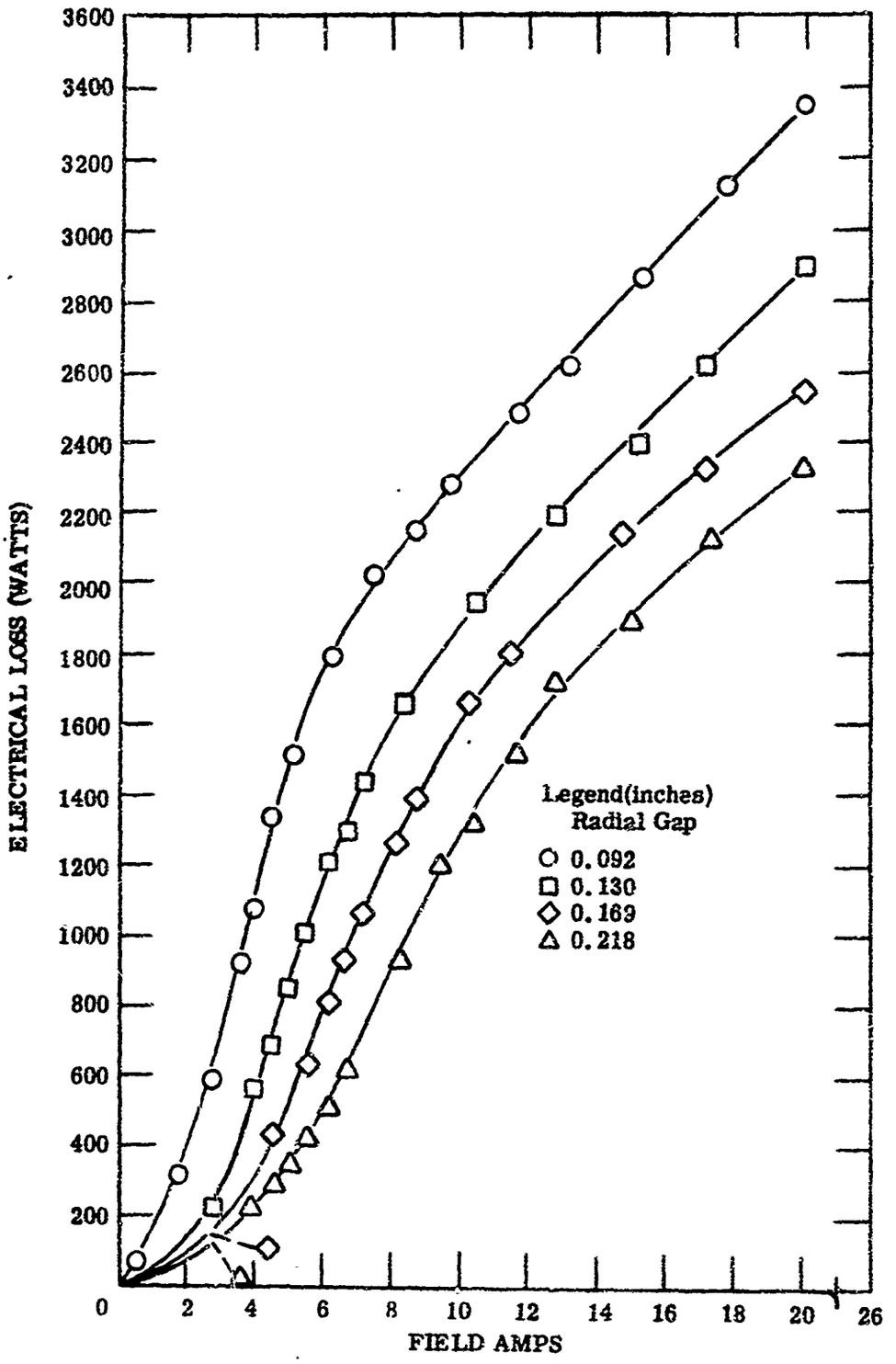

Figure 10. Electrical Losses Versus Field Current at 12,000 rpm

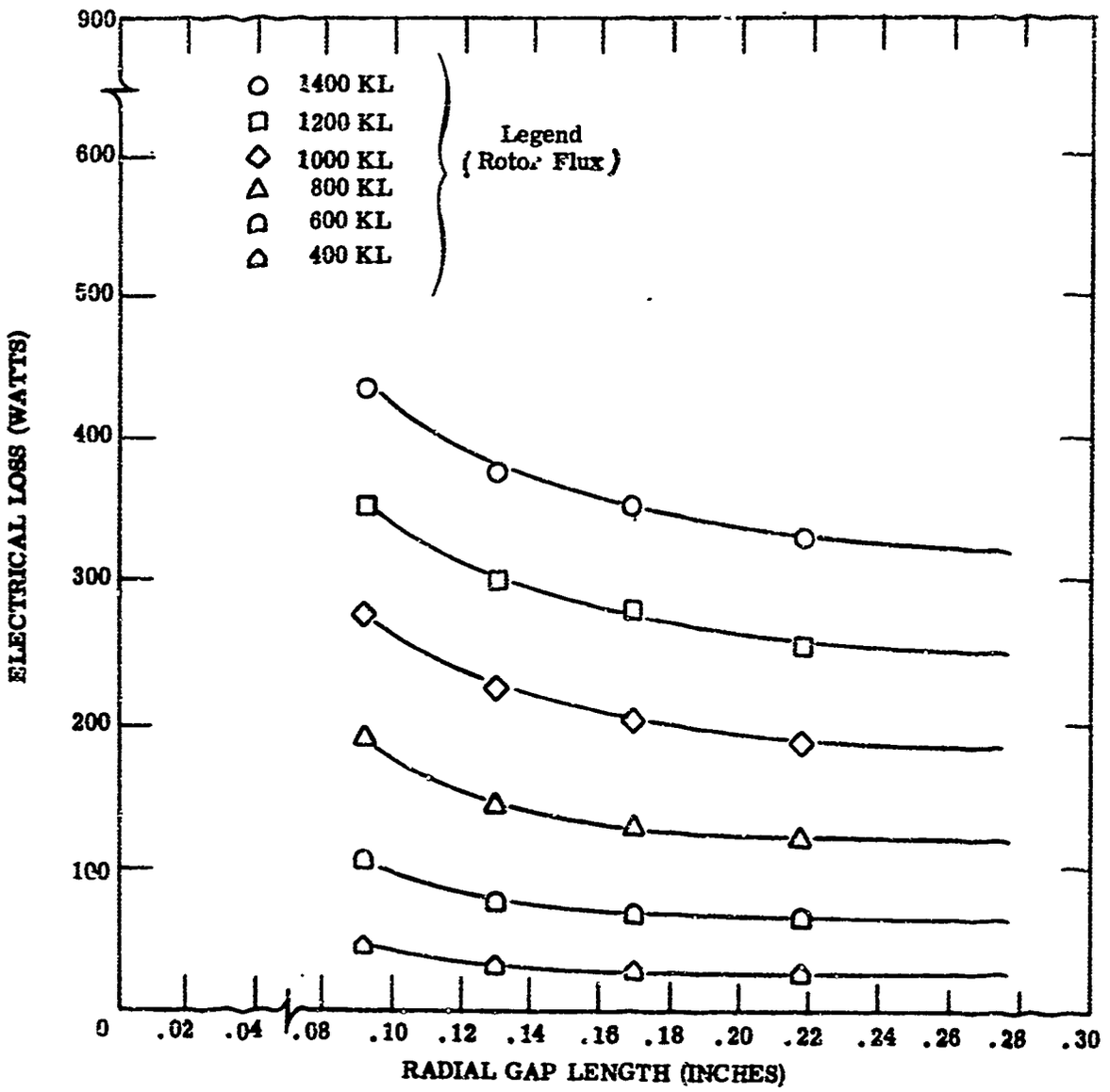

Figure 11. Electrical Losses Versus Radial Gap at 4,000 rpm

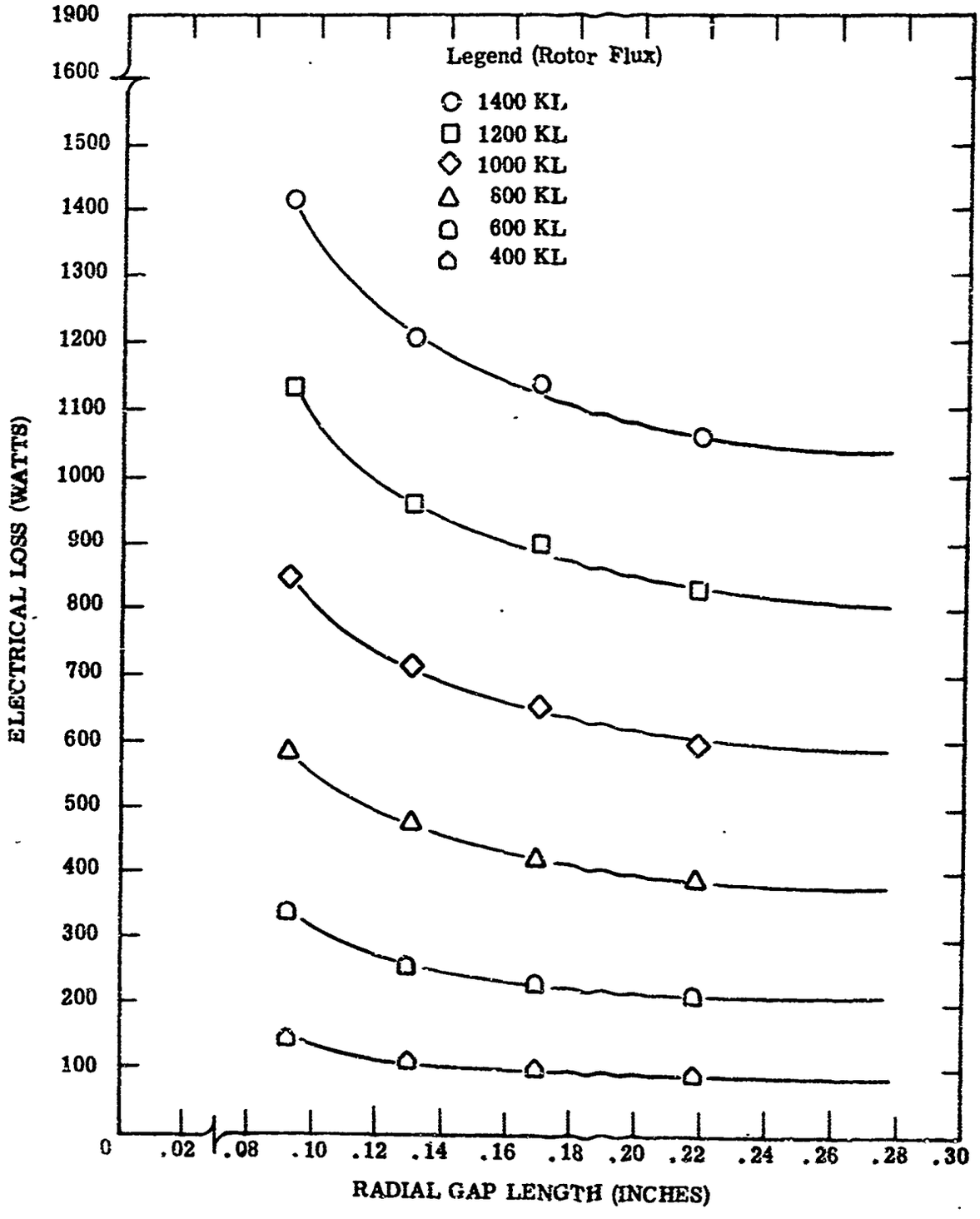

Figure 12. Electrical Losses Versus Radial Gap at 8,000 rpm

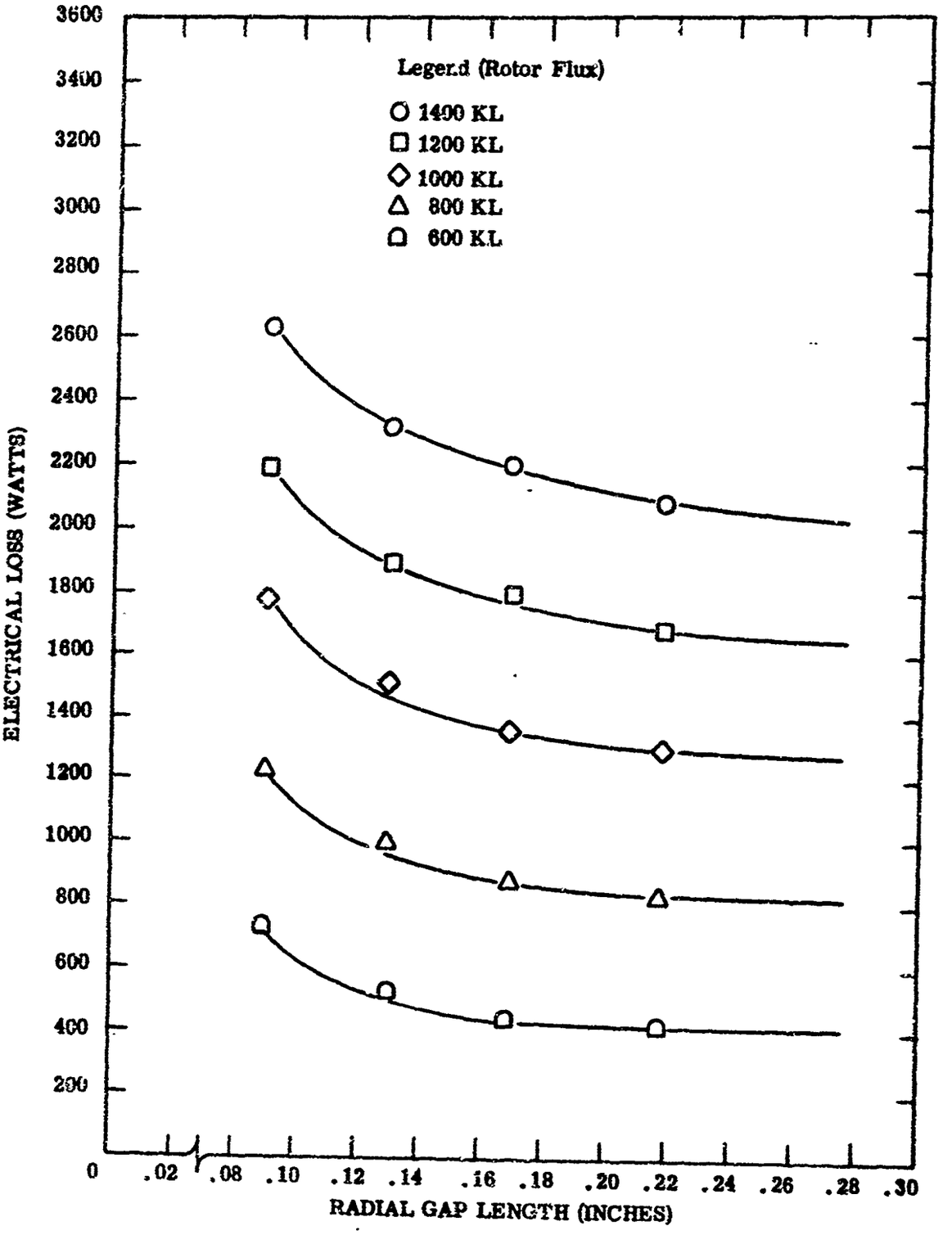

Figure 13. Electrical Losses Versus Radial Gap at 12,000 rpm

between the loss values given by the curves at a particular air gap and the rotor tooth and core loss represents the fixture pole face loss. Pole face loss is a function of flux in the pole faces and not the total flux in rotor. The flux in the pole faces for a given value of rotor flux was determined from the curves of Figures 6 and 7. Pole face loss, expressed in units of watts per square inch, and plotted as a function of pole face flux density and tooth frequency, are shown in Figures 14, 15, and 16. The units of flux density, and tooth frequency were used since these units are more descriptive of the factors involved in the creation of pole face loss. A tooth frequency of 24,000 cps corresponds, in this case, to a rotor speed of 12,000 rpm.

Effects of tooth saturation are clearly evident on the test curves as shown by the decreasing slope of the loss curve for pole face flux densities above approximately 60 kilolines per square inch. Saturation of the teeth decreases the amplitude of the flux ripple in the pole surface thereby reducing losses.

The radial gap length for the experimental generator is 0.100 inch. Since test data was not obtained for this exact gap length, the loss corresponding to a 0.100 inch air gap was obtained by plotting the test loss values versus the air gap lengths tested as shown in Figure 17. Figure 18 shows a plot of pole face loss as a function of tooth frequency. Loss values derived from the test data are shown by the circled points. The tooth frequency for the experimental generator is 48,000 cps. It was therefore necessary to extrapolate these data points to 48,000 cps as indicated in Figure 18. The accuracy of the extrapolated loss is sensitive to errors in the data points that were obtained from the experimental values. Since the torque on the trunnion mounted stator due to pole face loss was small in comparison with the combined torque, the accuracy of torque measurement had a predominant influence upon accuracy of the experimental data. Measurement error associated with the torque on the stator was approximately $\pm$ one percent. For a pole face flux of 56.5 kilolines per square inch the windage loss torque was less than or equal to 200 percent of the electrical loss. Thus the maximum error associated with the electrical loss which was obtained by substracting the windage loss was

$$\text{error} = (1+0.01)\ (1+W/E) - (1-0.01)W/E - 1 = 0.02W/E+0.01$$

where W = windage loss, E = electrical loss. For W/E = 2.0 the error becomes $\pm$ five percent. The error associated with the pole face loss, which was obtained by subtracting the electrical loss for a large air gap, becomes

$$\text{error} = (1+0.05)E/P - (1-0.05)E/P - 1 \approx 0.1E/P + 0.05$$

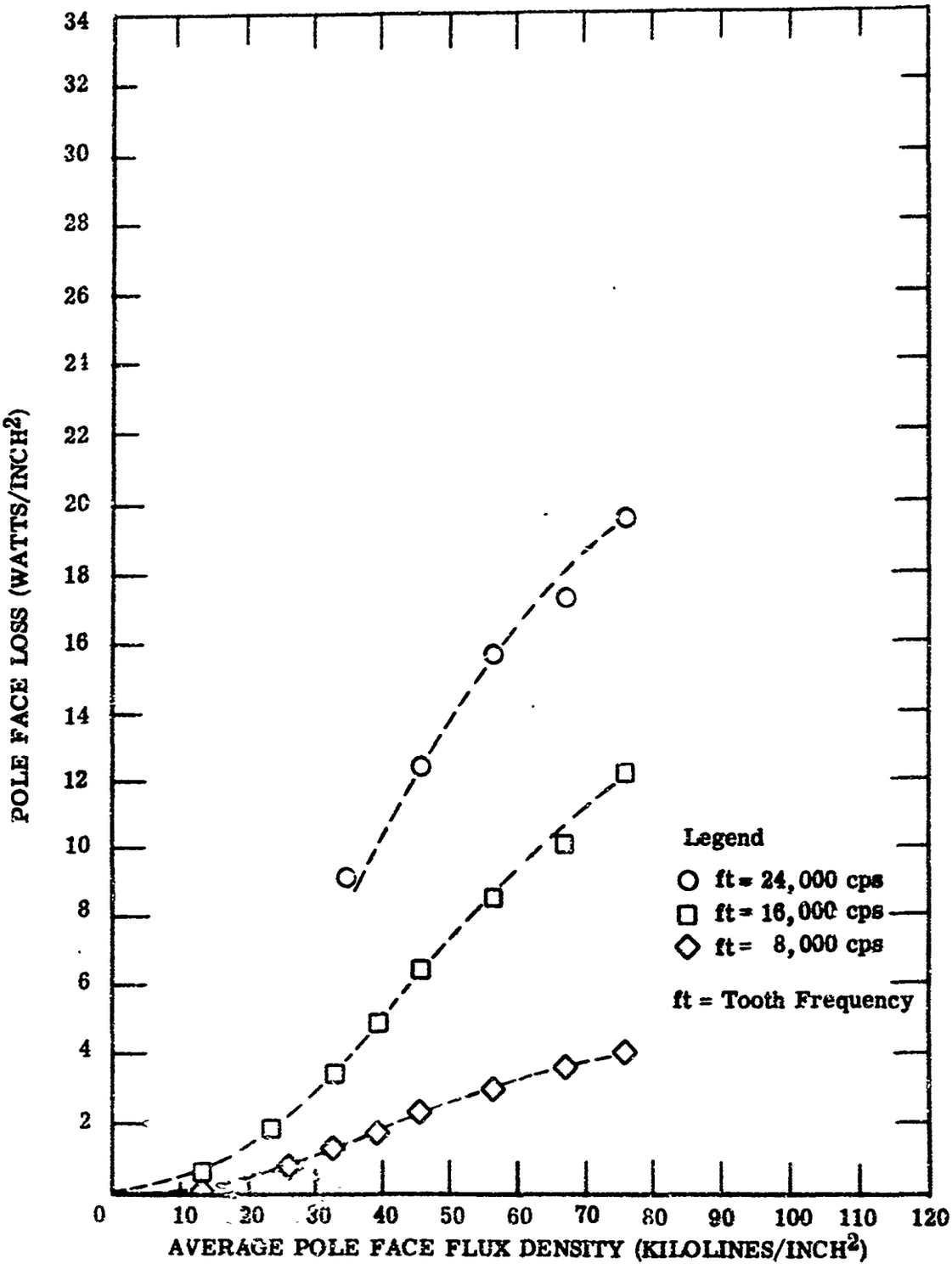

Figure 14. Pole Face Loss Versus Average Pole Flux Density for 0.092 Inch Radial Gap

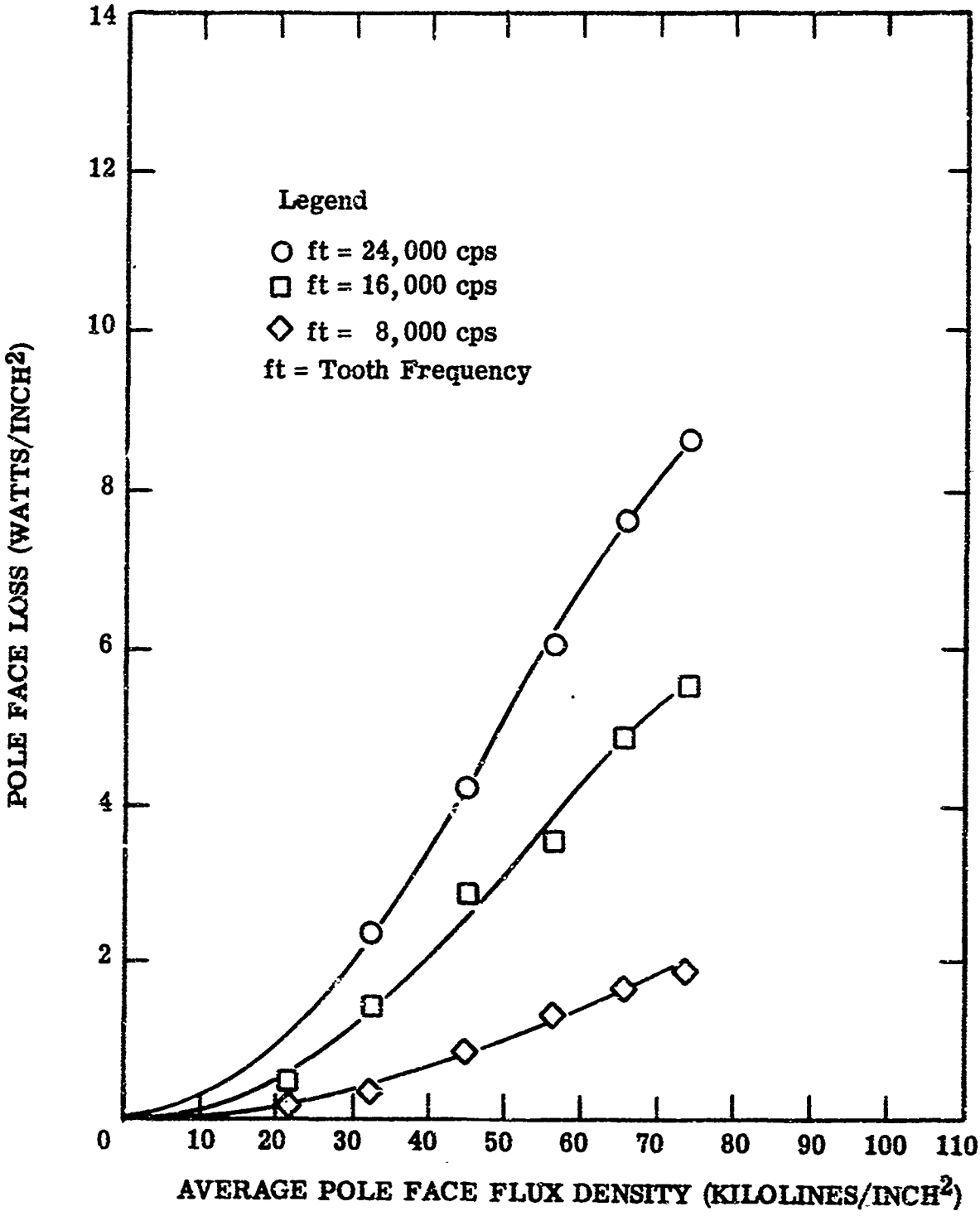

Figure 15. Pole Face Loss Versus Average Pole Flux Density for 0.130 Inch Radial Gap

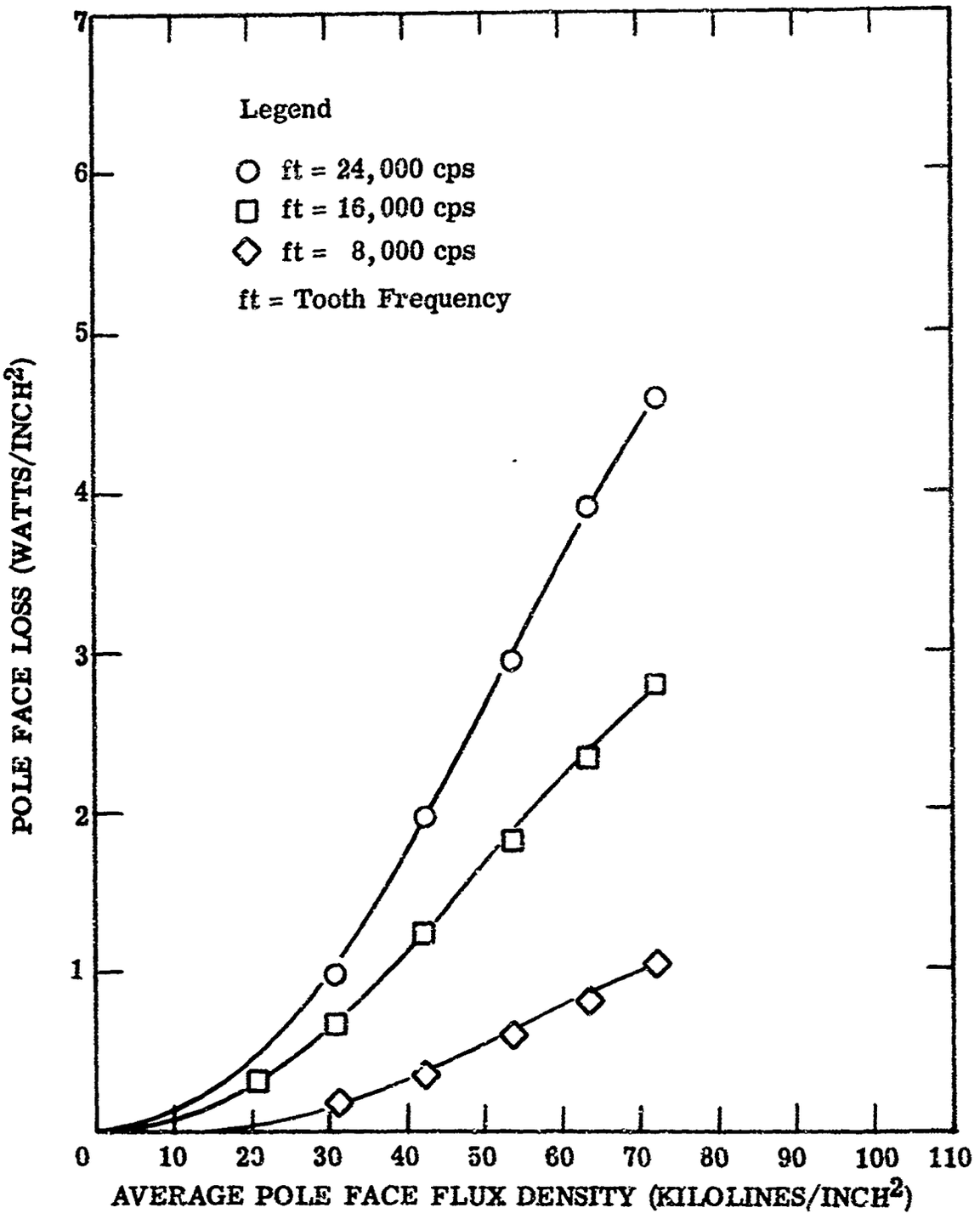

Figure 16. Pole Face Loss Versus Average Pole Flux Density for 0.169 Inch Radial Gap

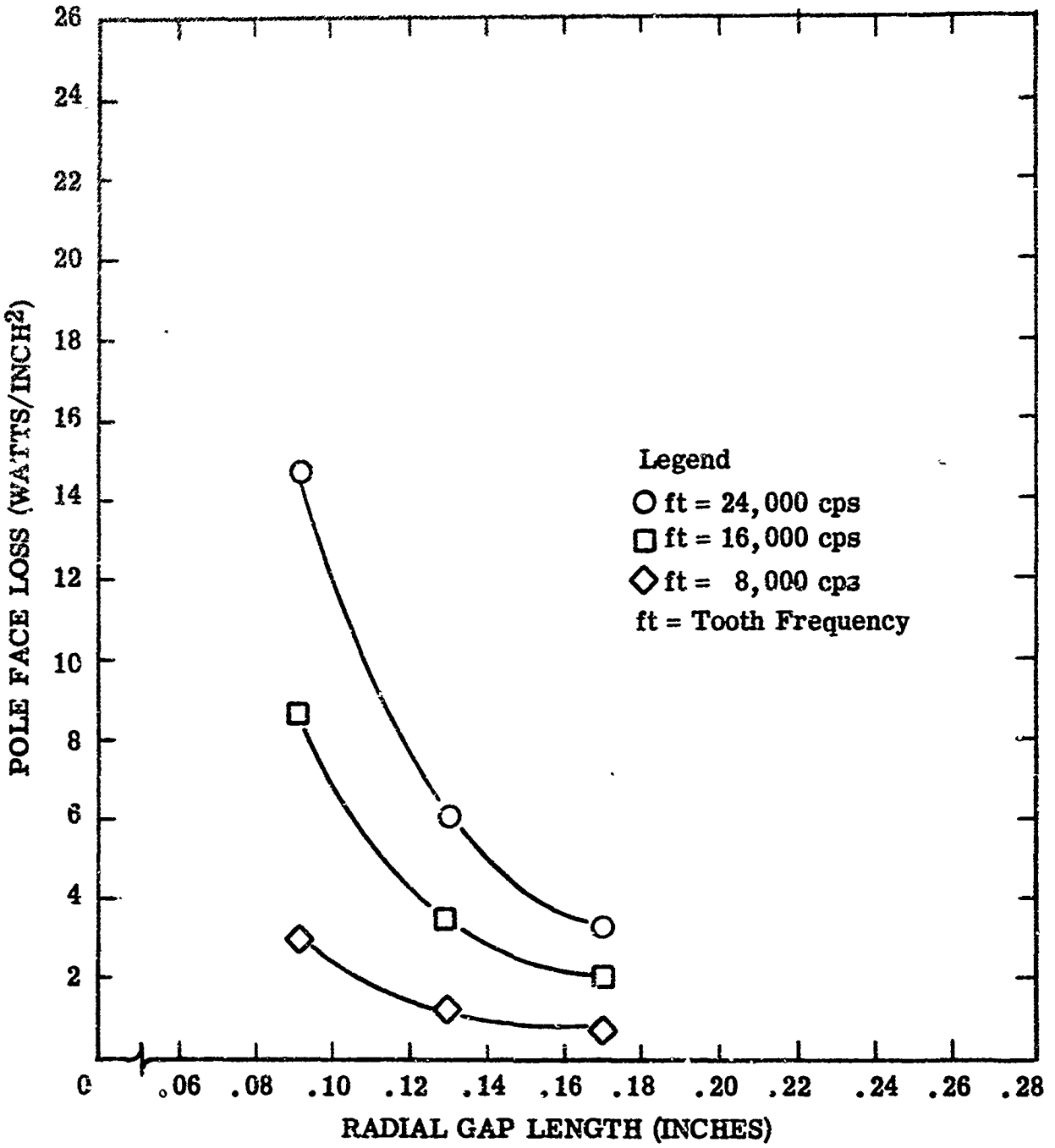

Figure 17. Pole Face Loss Versus Radial Gap for a Pole Face Flux Density of 56.5 Kilolines per Square Inch

where P = pole face loss and E = electrical loss for a large air gap. For an air gap of approximately 0.1 inch the value of E/P was about two. Therefore, the error associated with the pole face losses represented by the three points in Figure 18 could have been ± 25 percent. The final experimental points shown in Figure 18 are probably more accurate since conformity of the experimental values was obtained by plotting various dependent quantities against the independent variables of the experiment. In general, this allowed values for the dependent variable to be obtained from curves which represented the locus of the experimental values and eliminated part of the error caused by measurement accuracy. Unfortunately, the accuracy of the windage torque data could not be improved since windage torque measurements could only be obtained before and after the test fixture was magnetized for a particular calibration. These readings varied by ± one percent. When the combined torque values were taken from curves without the normal variation of points, the accuracy of the combined torque data was improved from ± one percent to ± 0.2 percent. Therefore, the error associated with the electrical loss was reduced from ± five percent to ± 2.6 percent for cases with a windage loss less than or equal to 200 percent of the electrical loss. The error associated with the pole face loss was therefore reduced from ± 25 percent to ± 13 percent for cases with a small air gap. Nevertheless, the possibility of a larger error exists for the point given for 48,000 cps in Figure 18 since the loss curve had to be extrapolated from 24,000 to 48,000 cps using three data points which may be in error by 13 percent. Extrapolations on a logarithmic plot were made using the three data points given in Figure 18 with ± 13 percent variation of the values. A straight line extension through the maximum point at 24,000 cps and the minimum point at 8,000 cps and vice versa resulted in a variation of 32 percent at 48,000 cps. It is logical to assume that this variation represents the possible error for the extrapolated value at 48,000 cps. The extrapolation gives a pole face loss of 31.7 ± 10.1 watts per square inch for a pole face temperature of 75°F. A temperature calculation performed for the experimental generator with an average coolant temperature of 600°F gave a pole face temperature of about 980°F. The loss decreases with increasing temperature due to a change in the resistivity of the pole face material. A correction for a change in resistance as outlined in Section V gives 23.0 ± 7.4 watts per square inch for the pole face loss at 980°F. The pole face area for the experimental generator is 77.5 square inches and when multiplied by the above loss density results in a total loss of 1783 ± 590 watts. This is the loss component induced in the rotor pole faces by the flux "bundling" effect of the armature teeth.

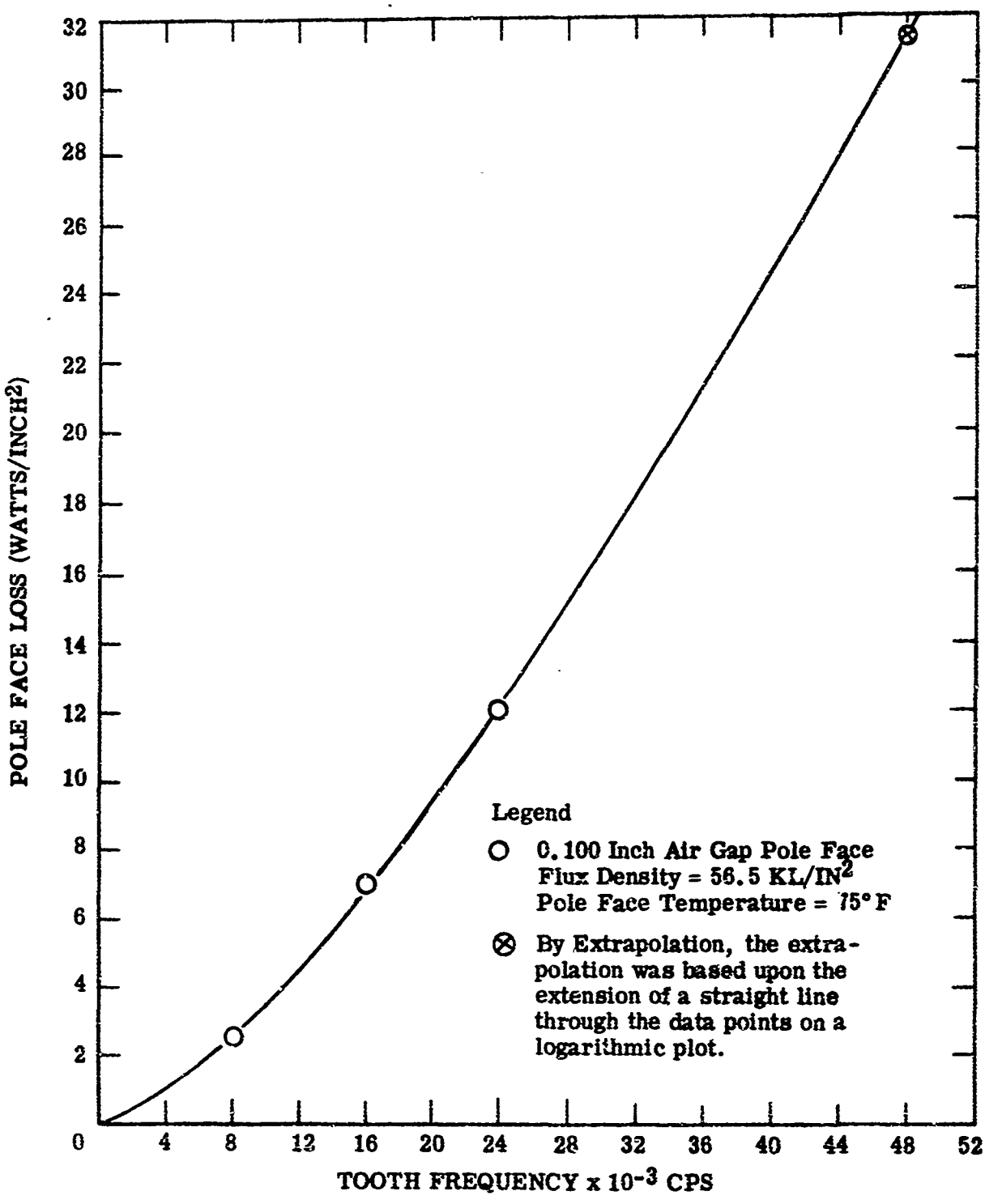

Figure 18. Pole Face Loss Versus Tooth Ripple Frequency for Radial Gap of 0.100 Inch and a Pole Face Flux Density of 56.5 Kilolines per Square Inch

SECTION IV

THEORETICAL TREATMENT OF POLE FACE LOSSES

A. Eddy-Current Loss

In practice the characteristic dimensions of the slots as shown by Figure 19a are small when compared with the dimensions of the rotor. Therefore, a mathematical treatment of the problem shall be made using rectangular coordinates as illustrated in Figure 19b.

The field equations can be used to analytically describe the flux, current, and the eddy-current loss in the pole material. Maxwell's equation from Faraday's law gives:

$$\nabla \times E = -\frac{\partial B}{\partial t}$$

and the differential form of Maxwell's equation derived from Ampere's law is:

$$\nabla \times H = 4\pi \left(J + \frac{\partial D}{\partial t}\right)$$

Maxwell's magnetic field equation as derived from Gauss's law gives the differential or point relation:

$$\nabla \cdot B = 0$$

Thus far, we have stated three of Maxwell's four equations which apply at a point in a time-changing field. The fourth is Maxwell's electric field equation as derived from Gauss's law:

$$\nabla \cdot D = \text{Charge density}$$

Since we are concerned with the eddy-current loss in a conducting medium we shall assume that the medium is free of charge and has zero dielectric constant. Thus, the displacement current:

$$J \text{ disp.} = \frac{dD}{dt} = \varepsilon \frac{dE}{dt} = 0$$

With this assumption the field equations in electromagnetic units are:

$$-\frac{\partial B}{\partial t} = \nabla \times E \qquad (1)$$

$$4\pi J = \nabla \times H \qquad (2)$$

$$\nabla \cdot B = 0 \qquad (3)$$

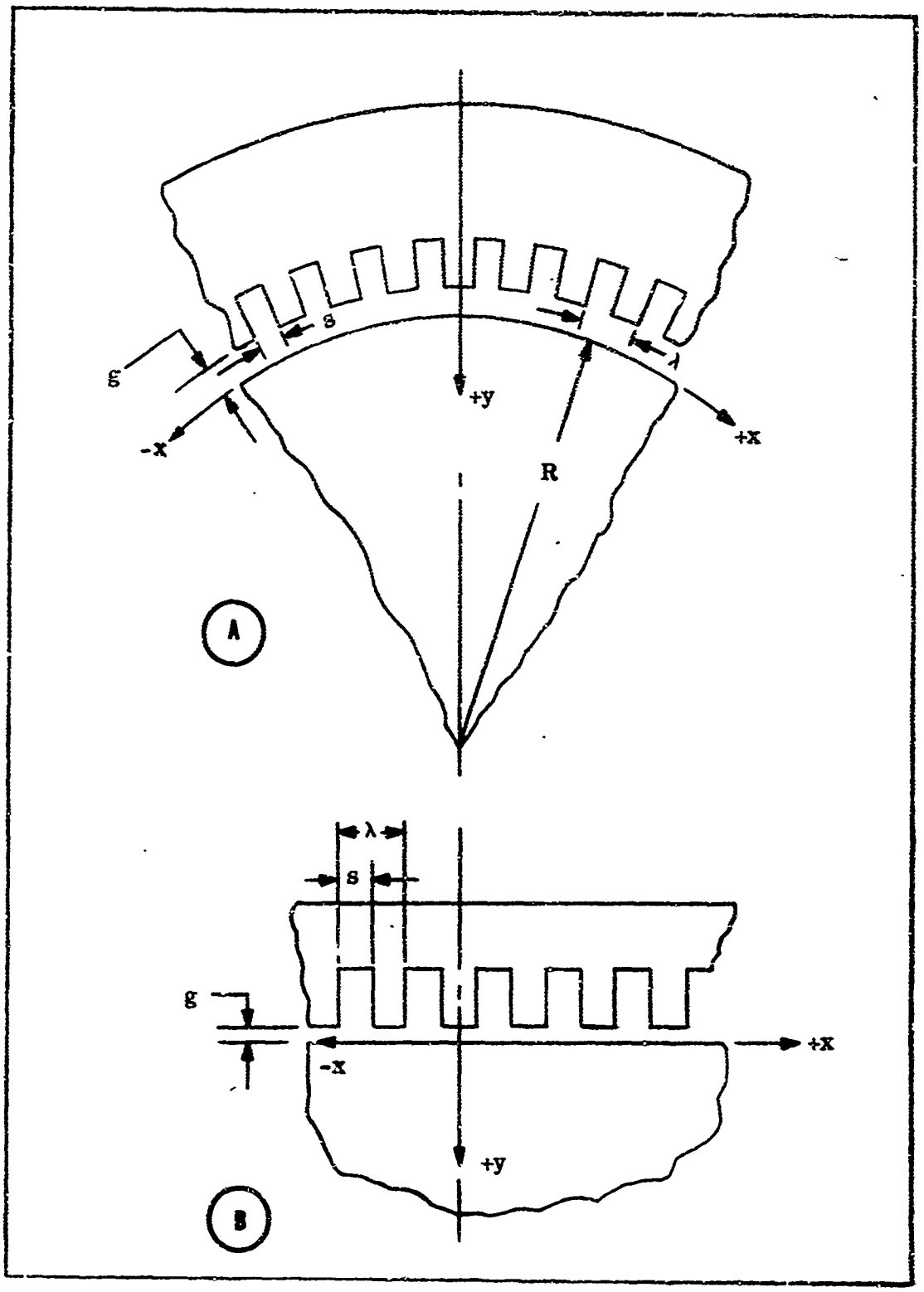

Figure 19. Mathematical Model of Rotor and Armature

Along with Maxwell's equations certain other fundamental relations are required to establish the eddy-current at a point within the system. They are:

$$\rho' J = E \tag{4}$$

$$B = \mu H \tag{5}$$

$$\nabla \cdot J = 0 \tag{6}$$

With these relations, we can write Maxwell's curl equations in terms of B and J. Thus,

$$-\frac{1}{\rho'}\frac{B}{\partial t} = \nabla X J \tag{7}$$

$$4\pi\mu J = \nabla X B \tag{8}$$

Therefore:

$$-\frac{4\pi\mu}{\rho'}\frac{\partial B}{\partial t} = \nabla X \nabla X B$$

$$= \nabla \cdot (\nabla \cdot B) - \nabla^2 B$$

Equation (3) shows that $\nabla \cdot B = 0$; thus,

$$\nabla^2 B = \frac{4\pi\mu}{\rho'}\frac{\partial B}{\partial t} \tag{9}$$

Writing Equation (9) in terms of the three rectangular components of B gives:

$$i\nabla^2 B_x + j\nabla^2 B_y + k\nabla^2 B_z = \frac{4\pi\mu}{\rho'}\left(i\frac{\partial B_x}{\partial t} + j\frac{\partial B_y}{\partial t} + k\frac{\partial B_z}{\partial t}\right) \tag{10}$$

Equation (10) is the vector sum of these scalar equations. Hence,

$$\frac{\partial^2 B_x}{\partial x^2} + \frac{\partial^2 B_x}{\partial y^2} + \frac{\partial^2 B_x}{\partial z^2} = \frac{4\pi\mu}{\rho'}\frac{\partial B_x}{\partial t} \tag{11}$$

$$\frac{\partial^2 B_y}{\partial x^2} + \frac{\partial^2 B_y}{\partial y^2} + \frac{\partial^2 B_y}{\partial z^2} = \frac{4\pi\mu}{\rho'}\frac{\partial B_y}{\partial t} \tag{12}$$

$$\frac{\partial^2 B_z}{\partial x^2} + \frac{\partial^2 B_z}{\partial y^2} + \frac{\partial^2 B_z}{\partial z^2} = \frac{4\pi\mu}{\rho'}\frac{\partial B_z}{\partial t} \tag{13}$$

A set of scalar equations for J can also be developed by differentiation of Equation (8) with respect to time. Which gives:

$$4\pi\mu\frac{\partial J}{\partial t} = \nabla x \frac{\partial B}{\partial t} \tag{14}$$

and combining Equation (7) with (14) gives:

$$-\frac{4\pi\mu}{\rho'}\frac{\partial J}{\partial t} = \nabla x \nabla x J$$

$$= \nabla \cdot (\nabla \cdot J) - \nabla^2 J$$

Equation (6) shows that $\nabla \cdot J = 0$. Therefore

$$\nabla^2 J = \frac{4\pi\mu}{\rho'} \frac{\partial J}{\partial t} \tag{15}$$

writing Equation (15) in terms of the three rectangular components of J gives an equation which is the vector sum of three scalar equations. Hence,

$$\frac{\partial^2 J_x}{\partial x^2} + \frac{\partial^2 J_x}{\partial y^2} + \frac{\partial^2 J_x}{\partial z^2} = \frac{4\pi\mu}{\rho'} \frac{\partial J_x}{\partial t} \tag{16}$$

$$\frac{\partial^2 J_y}{\partial x^2} + \frac{\partial^2 J_y}{\partial y^2} + \frac{\partial^2 J_y}{\partial z^2} = \frac{4\pi\mu}{\rho'} \frac{\partial J_y}{\partial t} \tag{17}$$

$$\frac{\partial^2 J_z}{\partial x^2} + \frac{\partial^2 J_z}{\partial y^2} + \frac{\partial^2 J_z}{\partial z^2} = \frac{4\pi\mu}{\rho'} \frac{\partial J_z}{\partial t} \tag{18}$$

a set of scalar equations can be developed from Maxwell's first curl equation which gives a relationship between the rectangular components of B and J. Since,

$$\nabla XE = \nabla x\rho' J = -\frac{\partial B}{\partial t} \tag{19}$$

we can express J and B in terms of the rectangular components to give:

$$-\frac{1}{\rho'} \frac{\partial}{\partial t} (iB_x + jB_y + kB_z) = i\left(\frac{\partial J_z}{\partial y} - \frac{\partial J_y}{\partial z}\right) + j\left(\frac{\partial J_x}{\partial z} - \frac{\partial J_z}{\partial x}\right) + k\left(\frac{\partial J_y}{\partial x} - \frac{\partial J_x}{\partial y}\right) \tag{20}$$

Equation (20) is the vector sum of three scalar equations. Hence,

$$-\frac{1}{\rho'} \frac{\partial B_x}{\partial t} = \frac{\partial J_z}{\partial y} - \frac{\partial J_y}{\partial z} \tag{21}$$

$$-\frac{1}{\rho'} \frac{\partial B_y}{\partial t} = \frac{\partial J_x}{\partial z} - \frac{\partial J_z}{\partial x} \tag{22}$$

$$-\frac{1}{\rho'} \frac{\partial B_z}{\partial t} = \frac{\partial J_y}{\partial x} - \frac{\partial J_x}{\partial y} \tag{23}$$

In addition we have from Equation (6)

$$\nabla \cdot J = 0 = \frac{\partial J_x}{\partial x} + \frac{\partial J_y}{\partial y} + \frac{\partial J_z}{\partial z} \tag{24}$$

Equations (11) through (13) are differential equations for B in terms of the independent variables (x, y, z, and t) of the system. A solution for the distribution of current density must start with a solution of equations (11) through (13) since we can define the boundary values for the flux. Once we have developed the flux distribution, we can then develop

the current distribution by using equations (16) through (18) and equations (21) through (24).

The solution for the rectangular components of B shall be based upon the following specific assumptions:

(1) The flux does not vary in the z direction and $B_z = 0$ or

$$B_z = \frac{\partial^2 B_x}{\partial z^2} = \frac{\partial^2 B_y}{\partial z^2} = \frac{\partial B_x}{\partial z} = \frac{\partial B_y}{\partial z} = 0$$

(2) $B_y = B_x = 0$ at $y = \infty$

(3) $B_y = \sum_{m=1}^{\infty} B_{ym} \operatorname{Cos} 2\pi m \left(ft \pm \frac{X}{\lambda}\right)$ at $y = 0$

With these assumptions Equations (11) through (13) become

$$\frac{\partial^2 B_x}{\partial x^2} + \frac{\partial^2 B_x}{\partial y^2} = \frac{4\pi\mu}{\rho'} \frac{\partial B_x}{\partial t} \qquad (25)$$

$$\frac{\partial^2 B_x}{\partial x^2} + \frac{\partial^2 B_y}{\partial y^2} = \frac{4\pi\mu}{\rho'} \frac{\partial B_y}{\partial t} \qquad (26)$$

Since we have established the boundary conditions for the B_y component we shall find a solution of equation (25) by the method of separation of variables.

We shall assume a solution of the form

$$B_y = X \cdot Y \cdot T$$

where $X = B_y(x)$ = a function of x only

$Y = B_y(y)$ = a function of y only

$T = B_y(t)$ = a function of t only

From Equation (25) we obtain

$$\frac{X''}{X} + \frac{Y''}{Y} - \frac{4\pi\mu T'}{\rho' T} \equiv 0$$

Now this condition requires that the functions $\frac{X''}{X}, \frac{Y''}{Y}$, and $\frac{T'}{T}$ must have a constant value since their sum must always be the same value. Therefore we shall let

$$\frac{X''}{X} = -a_1^2, \quad \frac{Y''}{Y} = a_2, \quad \frac{T'}{T} = a_3 \qquad (27), (28), (29)$$

and

$$-a_1^2 + a_2 - \frac{4\pi\mu}{\rho'} a_3 \equiv 0$$

Equations (27), (28), and (29) are ordinary differential equations. In our case the constants, a_1, a_2, and a_3 must equal

$$\frac{X''}{X} \equiv -a_1^2 \equiv 4\pi^2 m^2/\lambda^2 \tag{30}$$

$$\frac{T'}{T} \equiv a_3 \equiv inm2\pi f \tag{31}$$

$$\frac{Y''}{Y} \equiv a_2 \equiv 4\pi^2 m^2/\lambda^2 + i8\pi^2 nm\mu f/\rho' \tag{32}$$

The solutions of these equations for the case where n = 1 are:

$$X = A_1 \exp(i2\pi mx/\lambda) + B_1 \exp(-i2\pi mx/\lambda)$$

$$Y = C_1 \exp(2\pi m\sqrt{\omega_1}\, y/\lambda) + D_1 \exp(-2\pi m\sqrt{\omega_1}\, y/\lambda)$$

$$T = E_1 \exp(im2\pi ft)$$

where

$$\omega_1 = \left(1 + \frac{i\mu 2f^2\lambda^2}{\rho' m}\right)$$

The solutions of Equations (27), (28), and (29) for the case where n = -1 are

$$X = A_{-1} \exp(i2\pi mx/\lambda) + B_{-1} \exp(-i2\pi mx/\lambda)$$

$$Y = C_{-1} \exp(2\pi m\sqrt{\omega_{-1}}\, y/\lambda) + D_{-1} \exp(-2\pi m\sqrt{\omega_{-1}}\, y/\lambda)$$

$$T = E_{-1} \exp(-i2\pi mft)$$

where

$$\omega_{-1} = 1 - i\mu 2f\lambda^2/\rho' = \text{conjugate of } \omega_1 = \bar{\omega}_1$$

For the case where n = 1, we have

$$B'_{ym} = [A_1 \exp(i2\pi mx/\lambda) + B_1 \exp(-i2\pi mx/\lambda)]\ [C_1 \exp(2\pi m\sqrt{\omega_1}\, y/\lambda) + D_1 \exp(-2\pi m\sqrt{\omega_1}\, y/\lambda)]\ E_1 \exp(im2\pi ft) \tag{33}$$

and for the case where n = -1, we have

$$B'_{ym} = [A_{-1} \exp(i2\pi mx/\lambda) + B_{-1} \exp(-i2\pi mx/\lambda)]\ [C_{-1} \exp(2\pi m\sqrt{\bar{\omega}_1}\, y/\lambda) + D_{-1} \exp(-2\pi m\sqrt{\bar{\omega}}\, y/\lambda)]\ E_{-1} \exp(-im2\pi ft) \tag{34}$$

We must now examine the complex form of $\sqrt{\omega_1}$ and $\sqrt{\bar{\omega}_1}$, In order for $B_{ym} \to 0$ when $y \to \infty$, it is necessary that

$$\exp(\pm\sqrt{\omega_1}y) = \exp[(-U_m \pm iV_m)y] \quad \text{and} \quad \exp(\pm\sqrt{\bar{\omega}_1}y) = \exp[(-U_m \pm iV_m)y]$$

This can be accomplished by selection of the proper root of $\sqrt{\omega_1}$ and $\sqrt{\bar{\omega}_1}$. If we illustrate ω_1 and ω_1 and their roots in the complex plane, we have

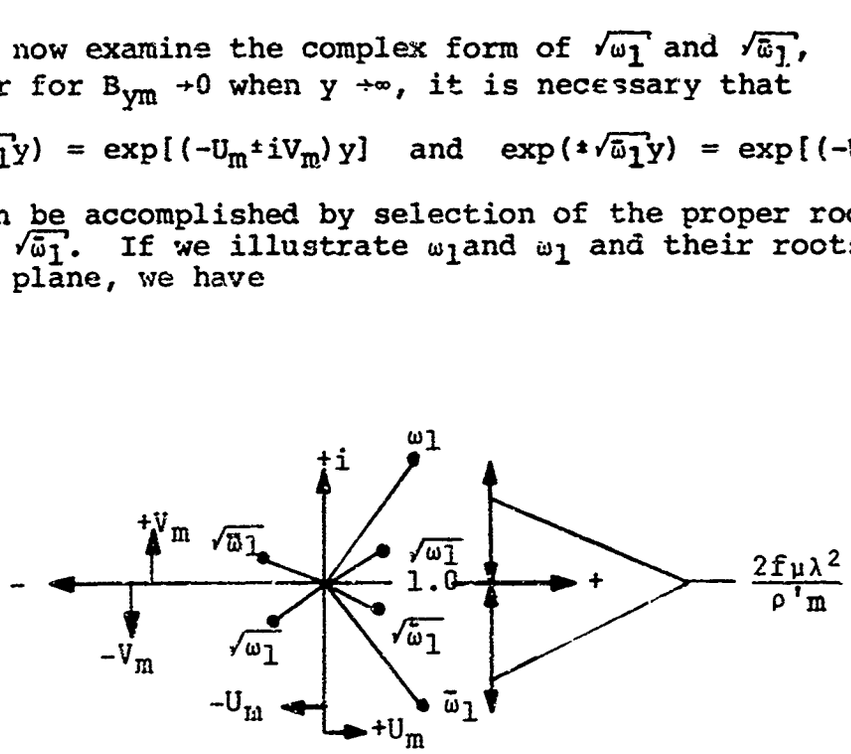

and the roots of $\sqrt{\omega_1} = U_m + iV_m$ and $-U_m - iV_m$
while the roots of $\sqrt{\bar{\omega}_1} = U_m - iV_m$ and $-U_m + iV_m$
This means that equations (33) and (34) become

$$B'_{ym} = E_1[A_1\exp(i2\pi mx/\lambda) + B_1\exp(-i2\pi mx/\lambda)]\exp[(2\pi m/\lambda)(-U_m y - iV_m y + if\lambda t)] \quad (35)$$

$$B'_{ym} = E_{-1}[A_{-1}\exp(i2\pi mx/\lambda) + B_{-1}\exp(-i2\pi mx/\lambda)]\exp[2\pi m/\lambda)(-U_m y + iV_m y - if\lambda t)] \quad (36)$$

We can now combine the particular solutions given by equations (35) and (36) by letting

$B_1 = A_{-1} = 0$
$A_1 = B_{-1} = 1$
$E_1 = E_{-1} = B_{ym}$

Adding the equations together gives:

$$B'_{ym} = B_{ym}\exp(-2\pi m U_m y/\lambda)\{\exp[(im2\pi)(ft + x/\lambda - V_m y/\lambda)] + \exp[(-im2\pi)(ft + x/\lambda - V_m y/\lambda)]\}$$

or

$$B'_{ym} = B_{ym}\exp(-2\pi m U_m y/\lambda)\cos(m2\pi/\lambda)(f\lambda t+x-V_m y) \qquad (37)$$

Before going any further, we must express U_m and V_m in terms of μ, λ, f, ρ' and m. Since U_m and V_m are the real and imaginary parts of $\sqrt{\omega_1}$, it is necessary to find the square root of this complex term.

$$\sqrt{\omega_1} = \left(1+\frac{i\mu 2f\lambda^2}{\rho' m}\right)^{1/2}$$

$$= \sqrt{R}\{\cos(\beta/2+\pi k)+i\sin(\beta/2+\pi k)\}$$

$$k = 0 \text{ and } 1$$

Since we previously examined all the roots of $\sqrt{\omega_1}$ and $\sqrt{\bar{\omega}_1}$, we only need to evaluate this case for k = 0 to determine U_m and V_m.

Thus,

$$\sqrt{\omega_1} = \sqrt{R}\{\cos\beta/2+i\sin\beta/2\}$$

where

$$\beta = \tan^{-1}\frac{2f\mu\lambda^2}{\rho' m}$$

$$\sqrt{R} = \left(1+\frac{4f^2\mu^2\lambda^4}{\rho'^2 m^2}\right)^{1/4}$$

Since

$$\cos\beta/2 = \sqrt{1/2(1+\cos\beta)}$$

and

$$\sin\beta/2 = \sqrt{1/2(1-\cos\beta)}$$

The equation for $\sqrt{\omega_1}$ can be written as

$$\sqrt{\omega_1} = \left(1+\frac{4f^2\mu^2\lambda^4}{\rho'^2 m}\right)^{1/4} \frac{1}{\sqrt{2}}\{\sqrt{1+\cos\beta} + i\sqrt{1-\cos\beta}\}$$

It can be noted from the illustration on page 35 that

$$\cos\beta = \left(1+\frac{4f^2\mu^2\lambda^4}{\rho'^2 m^2}\right)^{-1/2}$$

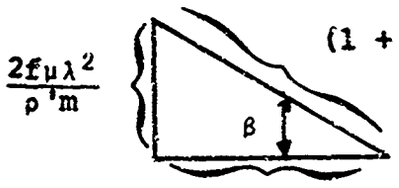

Thus,

$$\sqrt{\omega_1} = \sqrt{\frac{1}{2}} \left\{ \left[\left(1+\frac{4f^2\mu^2\lambda^4}{\rho'^2 m^2} \right)^{1/2} + 1 \right]^{1/2} + i \left[\left(1+\frac{4f^2\mu^2\lambda^4}{\rho'^2 m^2} \right)^{1/2} - 1 \right]^{1/2} \right\}$$

and

$$U_m = \sqrt{\frac{1}{2}} \left\{ \left(1+\frac{4f^2\mu^2\lambda^4}{\rho'^2 m^2} \right)^{1/2} + 1 \right\}^{1/2} \tag{38}$$

$$V_m = \sqrt{\frac{1}{2}} \left\{ \left(1+\frac{4f^2\mu^2\lambda^4}{\rho'^2 m^2} \right)^{1/2} - 1 \right\}^{1/2} \tag{39}$$

We can now form a series of solutions which will satisfy the boundary condition at $y = 0$ and $y = \infty$. By letting

$$B_y = \sum_{m=1,\ 2,\ 3}^{\infty} B'_{ym}$$

we have the solution for the B_y component of the flux density in the pole or

$$B_y = \sum_{m=1,\ 2,\ 3} B_{ym} \exp(-2\pi m U_m y/\lambda) \cos(m2\pi/\lambda)(f\lambda t + x - V_m y) \tag{40}$$

In this case, the values of V_m and U_m are given by Equation (38) and (39) and B_{ym} equals the coefficients for the cosine terms in a series which give the "Y" component of flux density at $y = 0$. We can also form a series of solutions for the B_x component of flux density since

$$\nabla \cdot B = 0 = \frac{\partial B_x}{\partial x} + \frac{\partial B_y}{\partial y}$$

we have

$$\frac{\partial B_x}{\partial x} = -\frac{\partial B_y}{\partial y} = \sum_{m=1,2,3} B_{ym} \exp\frac{2\pi m}{\lambda} \exp(-2\pi m U_m y/\lambda)\left[U_m \cos\frac{2\pi m}{\lambda}(f\lambda t + x - V_m y) - V_m \sin\frac{2\pi m}{\lambda}(f\lambda t + x - V_m y)\right]$$

and integrating this equation with respect to "x" gives:

$$B_x = \sum_{m=1,2,3} B_{ym} \exp(-2\pi m U_m y/\lambda)\left[U_m \operatorname{Sin}\frac{m2\pi}{\lambda}(f\lambda t + x - V_m y) + V_m \operatorname{Cos}\frac{m2\pi}{\lambda}(f\lambda t + x - V_m y)\right] + f_1(y,t) \qquad (41)$$

The question, "Are their functions such as $f_1(y, t)$ which are a part of the complete solution for the B_x component of the flux density?", can not be answered since we have no boundary values for this part of the problem. In general, the solution given by Equation (41) for $f_1(y, t) = 0$ apparently satisfies the only know boundary conditions for this problem which are:

(1) $B_x = 0$, $y \to \infty$

(2) B_x = periodic function of time

(3) $\nabla \cdot B = 0$

(4) $\frac{\partial^2 B_x}{\partial x^2} + \frac{\partial^2 B_x}{\partial y^2} = \frac{4\pi\mu}{\rho'}\frac{\partial B_x}{\partial t}$

In addition, we can perform two integrations which shows that the flux entering the pole surface is conserved. The flux, ϕ_y, entering the surface when ft = any integer is

$$\phi_y = \int_{\lambda}^{\lambda+1/4\lambda} B_y\Big|_{y=0} dx \qquad \text{or} \qquad \phi_y = \int_{\lambda}^{\lambda+1/4\lambda} B_{ym} \operatorname{Cos}\frac{m2\pi x}{\lambda} dx = \frac{\lambda B_{ym}}{2\pi m}$$

This flux must equal B_x when $B_y = 0$ or

$$\phi_x = \int_0^{\infty} B_x\Big|_{B_y = 0} dy = \int_0 B_{ym} \exp(-2\pi m U_m y/\lambda) dy = \frac{\lambda B_{ym}}{2\pi m}$$

The lines of flux in the pole can be graphically illustrated for the simple case when m = 1. To accomplish this task we must first form an equation for the slope of a flux line.

Since,

$$\frac{dx}{dy} = \frac{B_x}{B_y}$$
$$= \frac{U_1 \text{ Sin } \theta + U_1 \text{ Cos } \theta}{\text{Cos } \theta} = U_1 \tan \theta + V_1$$

where

$$\theta = \frac{2\pi}{\lambda} (f\lambda t + x - V_1 y) = f(x,y,t)$$

and since

$$d\theta = \frac{\partial f}{\partial x} dx + \frac{\partial f}{\partial y} dy + \frac{\partial f}{\partial t} dT$$

we will let ft = any integer and dT = 0. Then

$$\frac{dx}{dy} = \frac{\frac{d\theta}{dy} - \frac{\partial f}{\partial y}}{\frac{df}{dx}} = \frac{\frac{d\theta}{dy} + \frac{2\pi}{\lambda} V_1}{\frac{2\pi}{\lambda}} = U_1 \tan \theta + V_1$$

Thus

$$\frac{d\theta}{dy} = \frac{2\pi}{\lambda} U_1 \tan \theta$$

and after integrating

$$\frac{2\pi}{\lambda} U_1 \, y = \ln \left| \text{Sin } \theta \right| + \text{constant}$$

Since we can let $\theta_0 = \theta$ at the point where y = 0, the equation for y as a function of θ becomes

$$\frac{2\pi U_1}{\lambda} y = \ln \left| \frac{\text{Sin } \theta}{\text{Sin } \theta_0} \right|$$

The lines of flux for a typical simple case are illustrated in Figure 20. The only parameter which one needs to define to

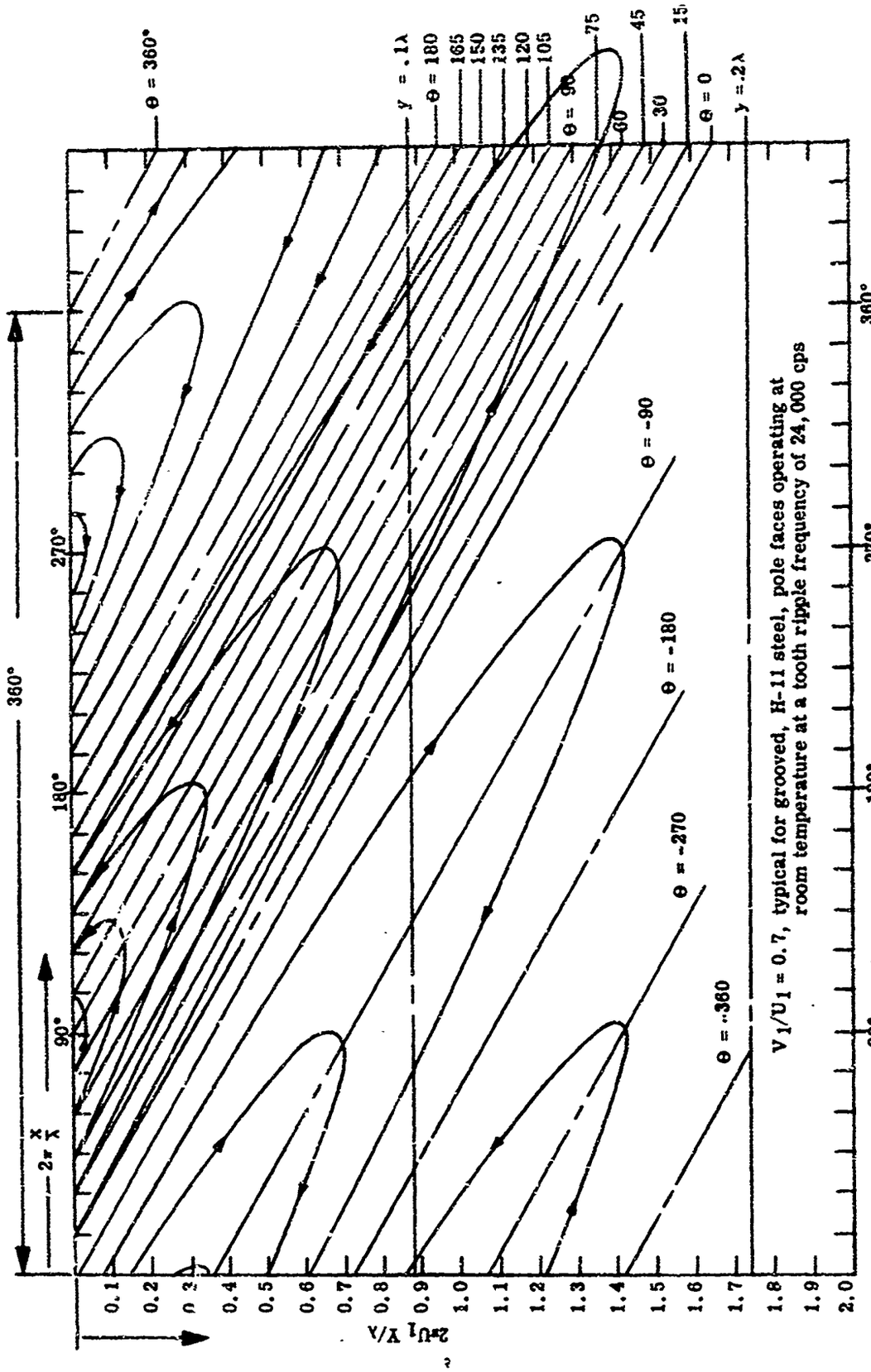

Figure 20. Flux Lines in Pole Face

make a plot line the one shown in Figure 20 is the ratio of V_1/U_1 since

$$\theta = \frac{2\pi x}{\lambda} - \left(\frac{2\pi U_1 y}{\lambda}\right)\left(\frac{V_1}{U_1}\right)$$

We have now defined the rectangular components of "B" in terms of the independent variables of the system. The next task is to define the eddy-current which is produced by the flux. Our solution for the current density shall be based upon the following considerations:

(1) Since we have assumed a uniform flux in the "z" direction which does not vary with time, we shall also assume $J_x = J_y = 0$. Thus, Equations (16) and (17) are of no importance and Equation (18) becomes:

$$\frac{\partial^2 J_z}{\partial x} + \frac{\partial^2 J_z}{\partial y^2} = \frac{4\pi\mu}{\rho'}\frac{\partial J_z}{\partial t}$$

and Equations (21), (22), and (23) reduce to

$$-\frac{1}{\rho'}\frac{\partial B_x}{\partial t} = \frac{\partial J_z}{\partial y}$$

$$\frac{1}{\rho'}\frac{\partial B_y}{\partial t} = \frac{\partial J_z}{\partial x}$$

(2) Since B_x (x, y, t) and B_y (x, y, t) have been defined and since J_z must satisfy the same partial differential equation as B_y and B_x, we can obtain J_z from the equations listed above. However, this work can be avoided by using Equation (8). For this case we have

$$4\pi\mu J_z = \frac{\partial B_y}{\partial x} - \frac{\partial B_x}{\partial y} \qquad (42)$$

The solution for J_z is obtained by forming the right-hand side of Equation (42)

$$4\pi\mu J_z = \sum_{m=1,2,3} \left[(U_m^2 - V_m^2 - 1)\frac{2\pi m}{\lambda}\operatorname{Sin}\frac{2\pi m}{\lambda}(f\lambda t + x - V_m y) \pm 4\,U_m V_m \frac{\pi m}{\lambda}\operatorname{Cos}\frac{2\pi m}{\lambda}(f\lambda t + X - V_m y)\right]\exp(-2\pi m U_m y/\lambda)$$

Since $U_m^2 - V_m^2 - 1 = 0$ and $U_m V_m = \frac{f\mu\lambda^2}{\rho' m}$, this equation reduces to

$$J_z = \frac{f\lambda}{\rho'} \sum_{m=1,2,3} B_{ym} \exp(-2\pi m U_m y/\lambda) \cos\frac{2\pi m}{\lambda}(f\lambda t + X - V_m y) \tag{43}$$

$$J_z = \frac{f\lambda}{\rho'} B_y \tag{44}$$

The eddy-current loss per unit of pole-face is

$$P = \frac{1}{\lambda} \int_0^{\infty} \int_d^{d+\lambda} \rho' J_z^2 dx dy \tag{45}$$

We shall evaluate this integral for the case when ft = any integer. Equation (43) becomes

$$J_z = \sum_{m=1,2,3} B_{ym} \frac{\lambda f}{\rho'} \exp(-2\pi m U_m y/\lambda) \cos\frac{m2\pi x}{\lambda} \cos\frac{2\pi m}{\lambda} V_m y +$$

$$\sum_{m=1,2,3} B_{ym} \frac{\lambda f}{\rho'} \exp(-2\pi m U_m y/\lambda) \sin\frac{m2\pi x}{\lambda} \sin\frac{2\pi m}{\lambda} V_m y$$

If we form the product of $\rho' J_z^2$, the terms in the series would be as follows:

$$B_{my} B_{ny} \frac{\lambda^2 f^2}{\rho'} \exp[-(mU_m + nU_n) 2\pi y/\lambda] \cos\frac{2\pi n V_n y}{\lambda} \cos\frac{2\pi m V_m y}{\lambda} \cos\frac{2\pi n x}{\lambda} \cos\frac{2\pi m x}{\lambda} +$$

$$B_{my} B_{ny} \frac{\lambda^2 f^2}{\rho'} \exp[-(mU_m + nU_n) 2\pi y/\lambda] \sin\frac{2\pi n V_n y}{\lambda} \sin\frac{2\pi m V_m y}{\lambda} \sin\frac{2\pi n x}{\lambda} \sin\frac{2\pi m x}{\lambda} +$$

$$2B_{my} B_{ny} \frac{\lambda^2 f^2}{\rho'} \exp[-(mU_m + nU_n) 2\pi y/\lambda] \cos\frac{2\pi n V_n y}{\lambda} \sin\frac{2\pi m V_m y}{\lambda} \cos\frac{2\pi n x}{\lambda} \sin\frac{2\pi m x}{\lambda}$$

where

$n = 1$ and $m = 1, 2, 3 \text{---} k$
$n = 2$ and $m = 1, 2, 3 \text{---} k$
$n = 3$ and $m = 1, 2, 3 \text{---} k$
$n = k$ and $m = 1, 2, 3 \text{---} k$

We need the following definite integrals to evaluate the integral in Equation (45).

$$\int_d^{d+\lambda} \text{Cos } m \frac{2\pi x}{\lambda} \text{ Cos } n \frac{2\pi x}{\lambda} \, dx = \begin{cases} 0 & \text{when } m \neq n \\ \frac{1}{2} & \text{when } m = n \end{cases}$$

$$\int_d^{d+\lambda} \text{Sin } m \frac{2\pi x}{\lambda} \text{ Sin } n \frac{2\pi x}{\lambda} \, dx = \begin{cases} 0 & \text{when } m \neq n \\ \frac{1}{2} & \text{when } m = n \end{cases}$$

$$\int_d^{d+\lambda} \text{Cos } n \frac{2\pi x}{\lambda} \text{ Sin } m \frac{2\pi x}{\lambda} \, dx = 0$$

With these definite integrals, all integrals with $\sin m \frac{2\pi x}{\lambda} \cos n \frac{2\pi x}{\lambda}$ vanish and all integrals for the cases when m is not equal to n vanish. Hence, integration with respect to "x" gives:

$$P = \frac{\lambda^2 f^2}{2\rho'} \int_0^{\infty} \sum_{m=1,2,3} B_{ym}^2 \exp(-4\pi U_m m y/\lambda) dy$$

$$= \frac{\lambda^3 f^2}{8\pi\rho'} \sum_{m=1,2,3} \frac{B_{ym}^2}{mU_m} \qquad (46)$$

The tasks that remain are (1) to determine the distribution of flux and the amplitude of flux oscillation on the surface of the pole, (2) to determine the effective resistivity of the material when the pole face has been grooved, (3) compare the experimental results with results obtained from theoretical

considerations, and (4) to determine the effective permeability of the material.

B. Amplitude of Flux Oscillation on the Surface of the Poles

A solution for the flux distribution on the surface of the pole requires a solution of the Laplacian differential equation

$$\frac{\partial^2 F}{\partial x^2} + \frac{\partial^2 F}{\partial y^2} = 0$$

An analytic solution of this equation can be obtained by conformal mapping the geometry of the slots and the opposing rotor in the x-y-plane onto a complex plane. One then constructs a complex potential solution in order to determine the value of field vectors in the complex field. Field vectors are then expressed in terms of the dimensions of the x-y-plane. In general, this approach is limited to idealized configurations and can not be used when the slots are closed partially. A numerical or graphical solution of the Laplacian differential equation is required when the configuration of the slots is complex.

Since the magnetostatic field is analogue of a stationary temperature field, one can use numerical methods developed for heat transfer problems to determine the flux distribution on the surface of the pole. In this case the correspondence of quantities in the fields are:

Quantity	Magnetostatic Field	Stationary Temp. Field
Potential Function	F_1 magnetostatic potential	T, temperature
Basic differential equation of the potential function	$\Delta^2 F = 0$	$\Delta^2 T = 0$
Characteristic constant of medium	μ, absolute permeability	k, thermal conductivity
Potential gradient	$H = -\Delta F$, magnetizing force	$U = -\Delta T$, temperature gradient
Associated field vector	$B = \mu H$, Magnetic flux density	$Q/A = kU$, heat power flow density
Flux of the associated vector	$\phi = \int B_n ds$, magnetic flux	$Q = \int Q/A \, dA$, heat power flow

The problem which must be solved is to determine the magnetic flux density distribution on the surface of the pole as shown below.

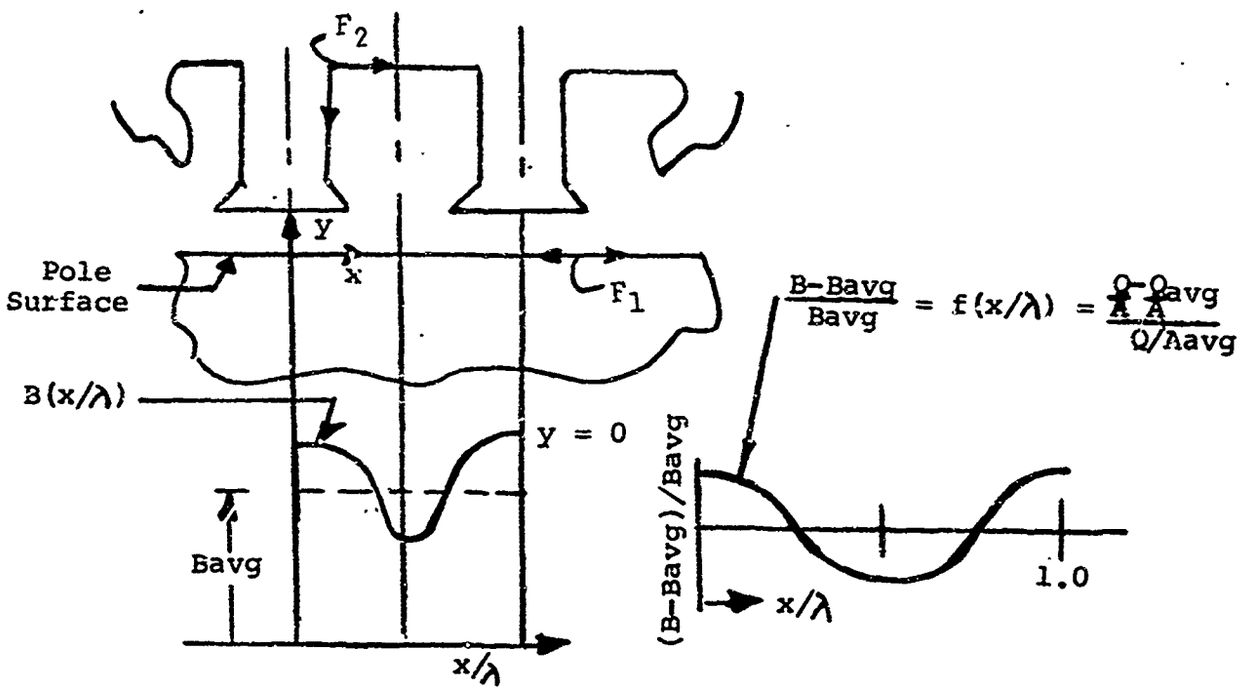

The equivalent heat transfer problem is to determine the heat power flow density into the surface of pole with the surface of teeth at a temperature of T_1 and with the surface of the pole at a temperature of T_2. The average heat power flow density on the surface of the pole would be subtracted from the value obtained at each point. This difference would then be divided by the average heat power flow density to give:

$$\frac{Q/A - Q/Aavg}{Q/Aavg} = \frac{B-Bavg}{Bavg} = f(x/\lambda)$$

A computer program is available to IBM 7090 users through the Share Library which will solve this problem by a numerical

approach. The program is called TOSS and was written by David Bagwell, Union Carbide Nuclear Company, Oak Ridge Gaseous Diffusion Plant, Oak Ridge, Tennessee (AEC R & D Report No. K-1494). TOSS is a proven digital computer program for finding the transient and/or steady-state temperature distributions of a three-dimensional irregular body. To solve the problem the body is divided into a number of cells. Each cell is associated with an interior node. Surfaces of cells which lie on the boundary of the body are associated with a surface node. Conditions external to the system which affect the temperatures of the system are associated with boundary nodes. With this nodal description of a system, a set of finite difference equations is used to solve heat transfer problems that are restrained by

$$k\left(\frac{\partial^2 T}{\partial x^2} + \frac{\partial^2 T}{\partial y^2} + \frac{\partial^2 T}{\partial z^2}\right) + \dot{q} = \delta C \frac{\partial T}{\partial t}$$

Internal heat generation may be a function of space and time and boundary temperature may be a function of time.

A nodal network which described the space between the rotor teeth and the opposing pole face in test fixture was defined for an air gap of 0.100 inches. The network consisted of 302 interior nodes, 50 surface nodes, and 2 boundary nodes. The first boundary node represented the surface temperature of the rotor teeth and the second boundary node represented the surface temperature of the pole. A steady-state solution of the problem was obtained which gave the heat power flow density at 18 points along one-half of the tooth pitch. Figure 21 gives the magnetic flux density distribution on the pole surface that was obtained with TOSS.

In general, the magnetic flux density distribution on the pole surface is a periodic function of (x/λ) which possesses certain symmetric properties since

$$f(-x/\lambda) = f(x/\lambda)$$

and

$$\int_0^1 \frac{B-Bavg}{Bavg}\, d(x/\lambda) = 0$$

A series expansion of (Bavg-B)/Bavg is simple since it is an even function of (x/λ) and contains no sine terms. The coefficient for the cosine terms can be obtained by making an harmonic analysis of the periodic function.

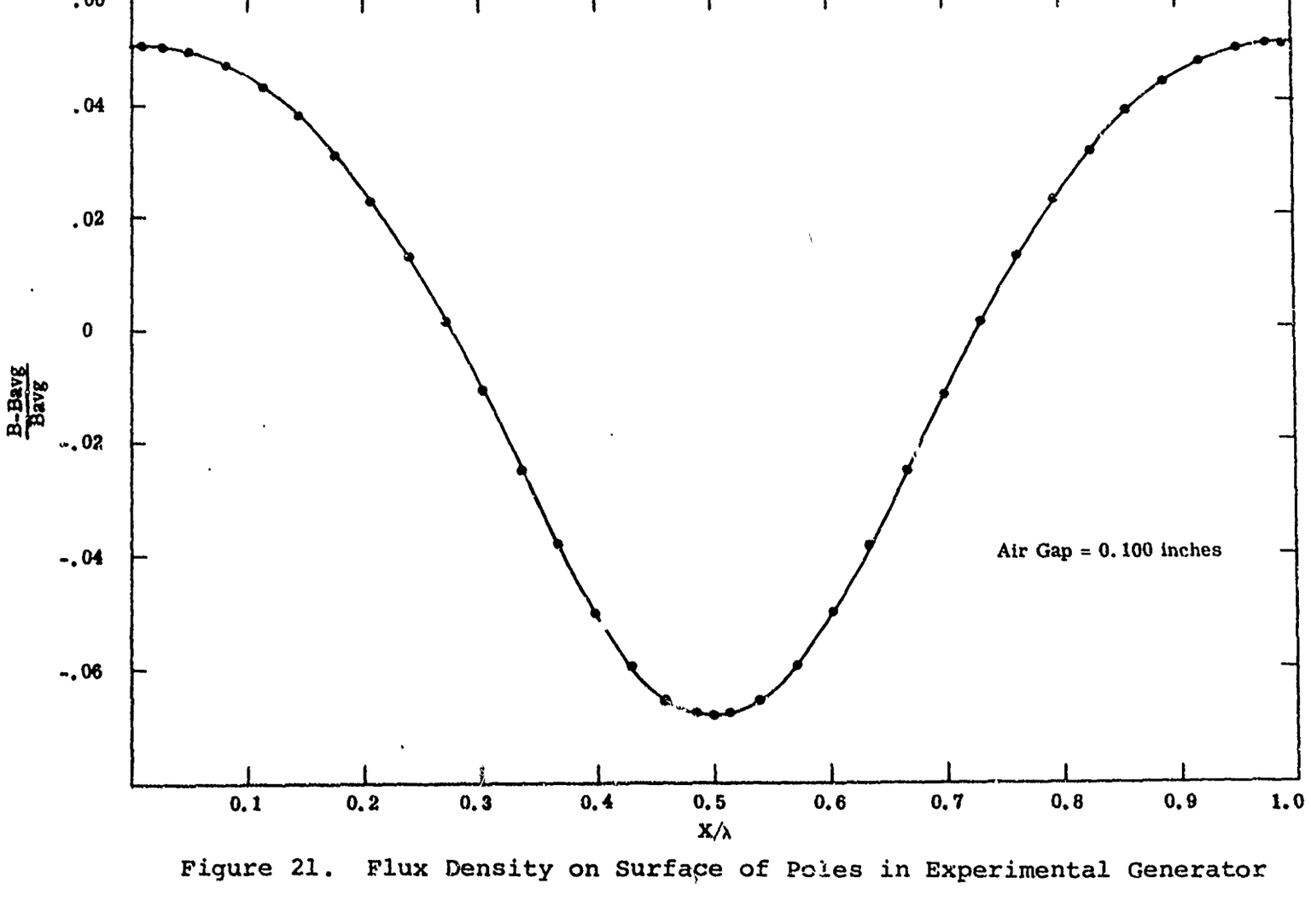

Figure 21. Flux Density on Surface of Poles in Experimental Generator

A series expansion for the alternating flux density becomes

$$B_y = Bavg \sum_{m=1,2,3} A_m \cos m \frac{2\pi}{\lambda} x$$

where A_m equals the coefficients obtained from the harmonic analysis. Letting Bavg A_m = Bym, this equation becomes

$$B_y = \sum_{m=1,2,3} Bym \cos m \frac{2\pi}{\lambda} x$$

Up to this point we have considered "By" on the surface of the pole to be only a function of "x". Since "By" varies with time at any point on the surface of the pole, we must describe the entire function in order to establish the boundary values for the problem.

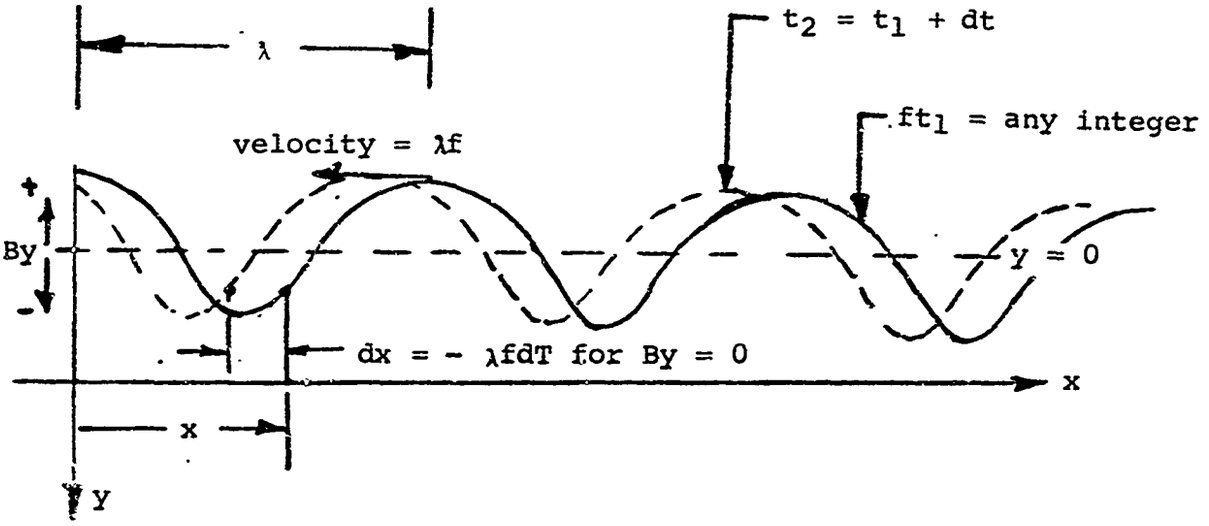

To do this we shall consider the wave shown in the illustration above to be traveling to the left at a velocity equal to λf. We shall also let "x" = 0 at a point on the surface of the pole where "By" has its maximum value and the product of frequency and time is equal to any integer. Since By = f (x, t), we can write

$$dB_y = \frac{\partial f}{\partial x} dx + \frac{\partial f}{\partial t} dT$$

and since $dB_y = 0$ when $-dx = \lambda f dT$ we can write

$$\lambda f \frac{\partial f}{\partial x} = \frac{\partial f}{\partial t}$$

If we let $f(x,t) = X \cdot T$

then

$$f\lambda\frac{X'}{X} \equiv \frac{T'}{T} \equiv \pm\, im2\pi\lambda f$$

and the solution becomes

$$B_y = \sum_{m=1,2,3} B_{ym} \cos\frac{m2\pi}{\lambda}(f\lambda t+x) \qquad (47)$$

Equation (47) gives the boundary values which were used to obtain By (x, y, t) as described in Section IV-A.

The coefficients for the cosine terms in an expansion of the flux distribution shown in Figure 21 are

m	A_m (coefficient)	Cosine Term
1	0.0588	$\cos 2\pi x/\lambda$
2	-0.0087	$\cos 4\pi x/\lambda$
3	0.0008	$\cos 6\pi x/\lambda$
4	0.0004	$\cos 8\pi x/\lambda$
5	0.0001	$\cos 10\pi x/\lambda$

The coefficients given in this table are for an air gap of 0.100 inches or for the air gap that has been specified for the experimental generator. It is interesting to note that for this particular case, over 98% of the pole face loss in the generator will be associated with the fundamental frequency of the periodic function. The loss for each harmonic frequency is proportional to

$$\frac{A_m^2}{mU_m} = \frac{A_m^2\sqrt{2}}{m\left[\left[1 + \frac{4f^2\mu^2\lambda^4}{\rho'^2 m}\right]^{1/2} + 1.0\right]^{1/2}}$$

For values of $\frac{4f^2\mu^2\lambda^4}{\rho'^2 m} >> 1$, the loss is proportional to $A_m^2/\sqrt{m}$. For the experimental generator and for a 0.100 inch air gap in the test fixture, the breakdown of eddy-current loss is

m	$A_m^2/\sqrt{m}$	Proportion of Total Loss
1	34.55×10^{-4}	98.5%
2	53.5×10^{-6}	1.5%
3	37.0×10^{-8}	0

C. Effective Resistivity of a Grooved Pole Face

It is possible to reduce the eddy-current loss by grooving the pole face (reference 4). The grooves must be placed along the face of the pole in a direction parallel to the motion of the rotor so they cross the path of the eddy-currents. This increases the length and thus the resistance of the eddy-current path. The emf from end to end of the pole face is unaffected by the groove.

The resistance of the path under the grooves is directly proportional to the depth of the grooves which suggests that the deeper the grooves the greater will be the reduction in loss. However, the eddy-currents can take an alternate path and use the radial face of each groove to form a closed loop. The depth of the groove does not affect the resistance of the path which is parallel to the grooves.

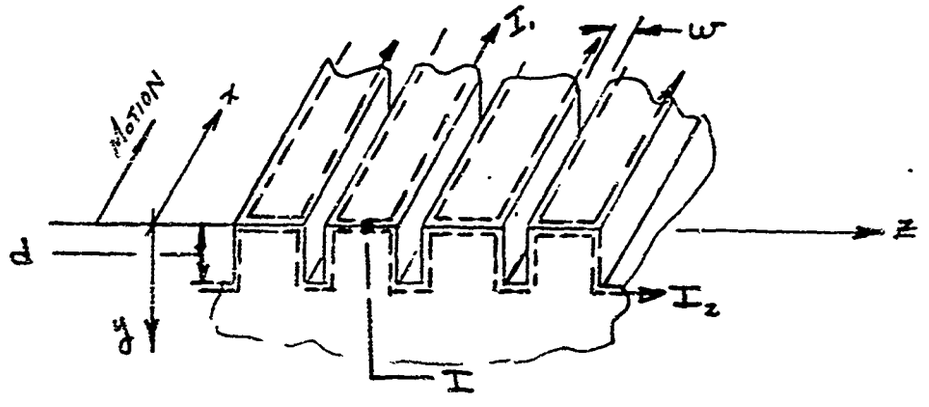

Since $I = I_1 + I_2$

where I_2 = current flowing under the grooves

I_1 = current flowing parallel to grooves

The total resistance offered by a groove is

$$R_g = \frac{R_1 R_2}{R_1 + R_2}$$

The specific resistance of the path under the groove

$$R_2 = \{2d + w\}\rho$$

In previous work it has been shown that the resistance of the path parallel to the grooves is

$$R_1 = 0.263 \frac{\lambda}{} \rho$$

Thus

$$Rg + \frac{(2d + w)\cdot 263\lambda\rho}{2d + w + .263\lambda}$$

The resistance R_g is in series with the natural resistance of the pole face material. Therefore,

$$\frac{\rho eff}{\rho} = 1 + \frac{(2d + w)\cdot 263\lambda b}{l\,(2d + w + .263\lambda)} = 1 + \frac{(2d + w).263\lambda}{\lambda_g(2d + w + .263\lambda)} \qquad (48)$$

where

d = depth of groove
w = width of groove
b = number of grooves
l = length of pole face
λ = tooth pitch
λ_g = groove pitch
ρ_{eff} = effective resistivity of pole face material
ρ = natural resistivity of material

For the pole face loss test fixture,

d = 0.070 inches,
w = 0.007 inches,
g = 0.0325 inches,
λ = 0.314 inches, and
$\frac{\rho_{eff}}{\rho}$ = 2.63

SECTION V

COMPARISON OF EXPERIMENTAL RESULTS WITH RESULTS OBTAINED FROM THEORETICAL CONSIDERATIONS

The eddy-current loss per unit area of the pole surface (watts per cm^2) versus the permeability of the material is given in Figure 22. These eddy-current losses were calculated using Equations (38) and (46) from Section IV-B for conditions which correspond to a radial air gap of 0.100 inches and average flux density in the air gap of 56.5 kilolines per square inch (8750 gauss). Equation (48) was used to calculate the effective resistivity of the material in the grooved pole faces. The eddy-current losses given by Figure 22 are those losses associated with the fundamental frequency of the periodic flux variation since it has been demonstrated in Section IV-B that the losses associated with the harmonic frequencies are not significant for this particular case.

Figure 22 also shows the pole face losses that were derived from the experimental data obtained in the pole face loss test fixture. A comparison of losses derived from the experimental data and the losses based upon theoretical consideration indicates that the effective permeability of the material is extremely low. In fact, the experimental loss at 8000 cps is greater than the losses calculated for a material which has a permeability of one. Since the effective permeability appears to be low, we must determine the maximum induction in the pole to determine if the material is saturated. The maximum flux density occurs on the surface of the pole or when y = 0. Therefore,

$$B_{max} = [(B_{avg} + B_y)^2 + B_x^2]^{.5}$$

$$= B_{avg} \left[1 + A_1^2 U_1^2 + 2A_1 (\cos\theta + .5A_1U_1V_1\sin 2\theta)\right]^{.5}$$

where

$$\theta = \frac{2\pi}{\lambda} (f\lambda t + x)$$

Figure 23 give B_{max} as a function of θ for a fundamental frequency of 24,000 cps and for a value of U_1, V_1 and A_1 which corresponds with the loss observed in the test fixture. The maximum flux density for this case was only 6.2% greater than the average flux density in the air gap. Figure 24 shows the maximum and minumum flux density at the surface for μ (effective) = 10.5 on a normal magnetization curve for the H-11 material.

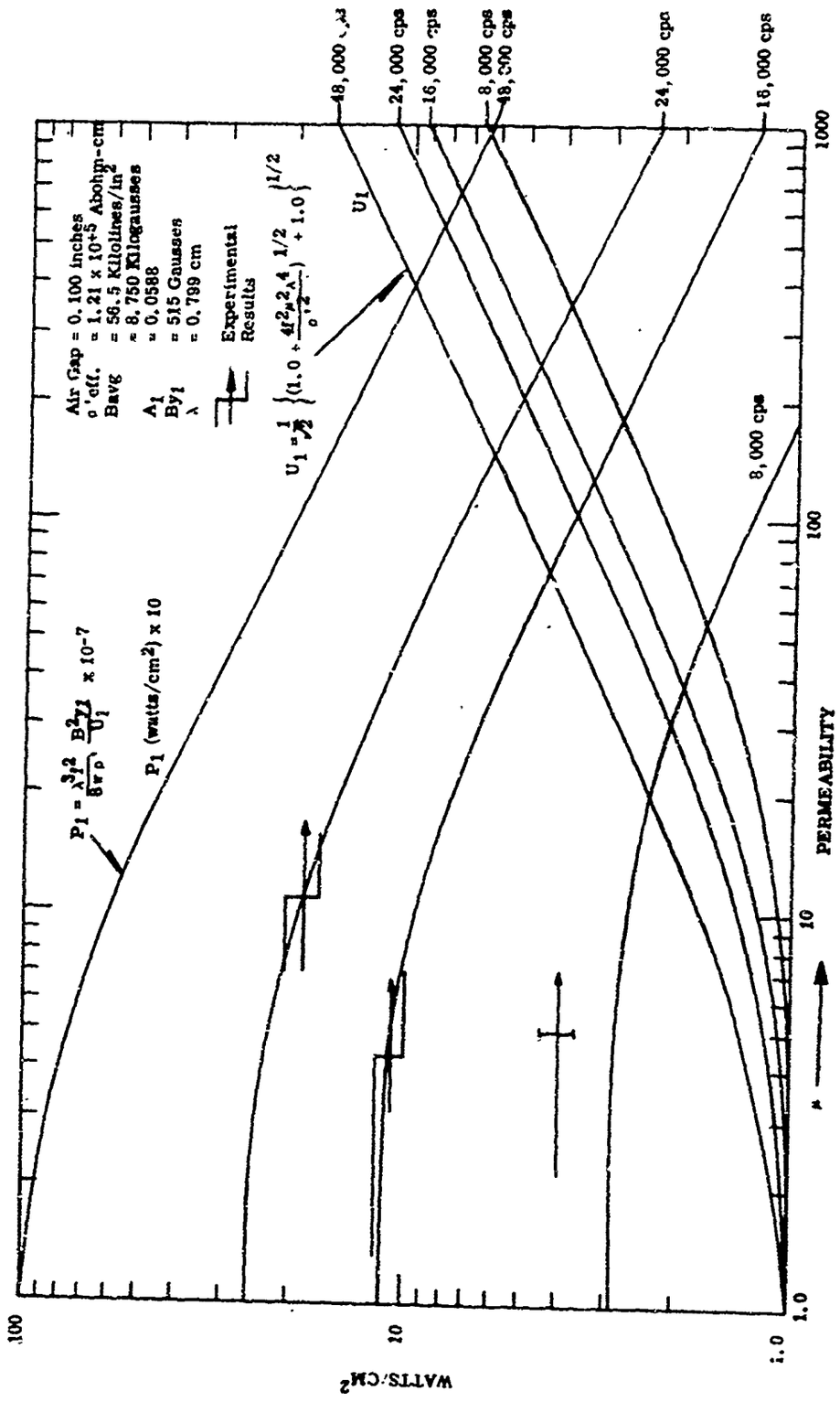

Figure 22. Eddy-Current Loss Versus Permeability of Material

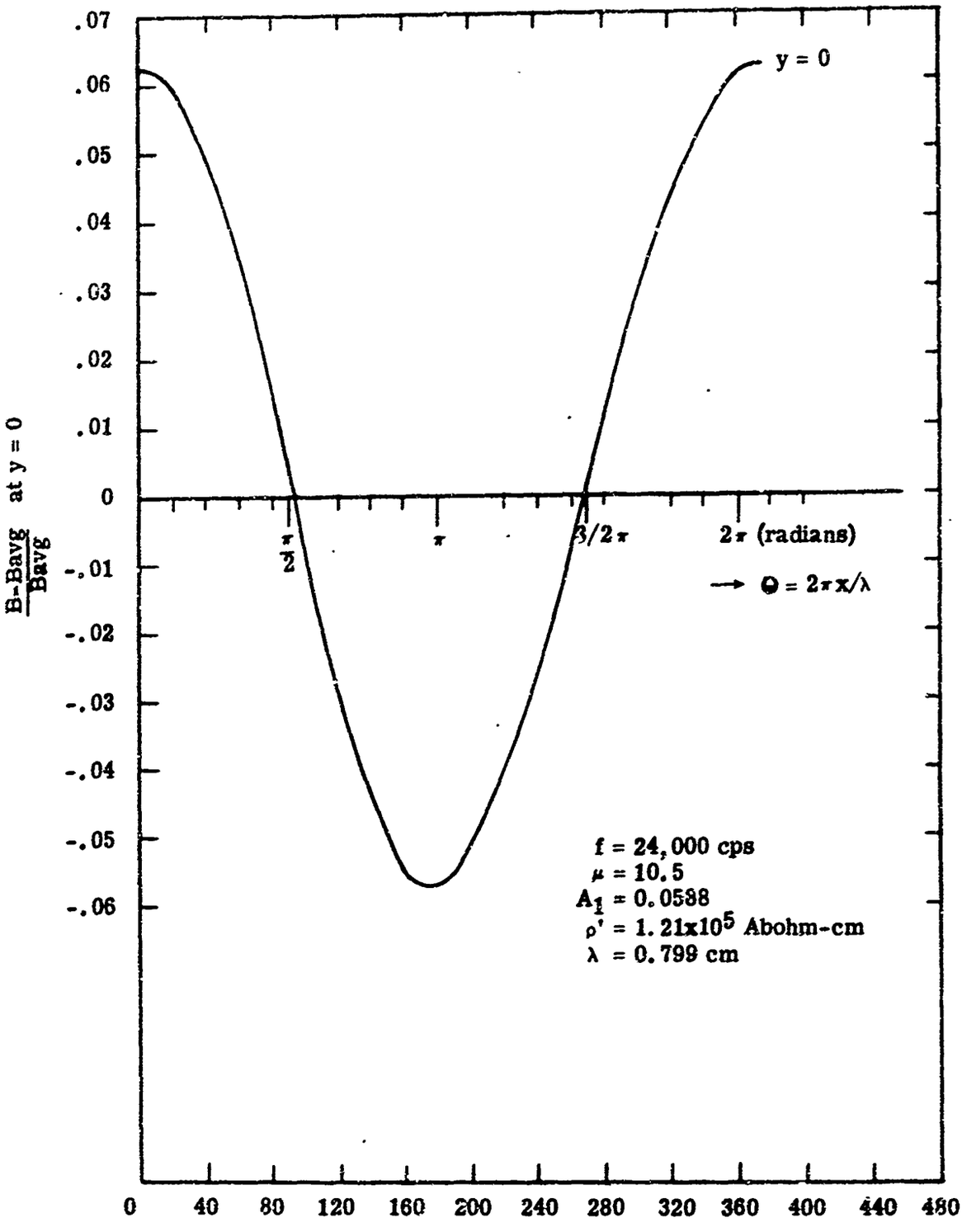

Figure 23. Maximum Flux Density in Pole Faces at 24,000 cps

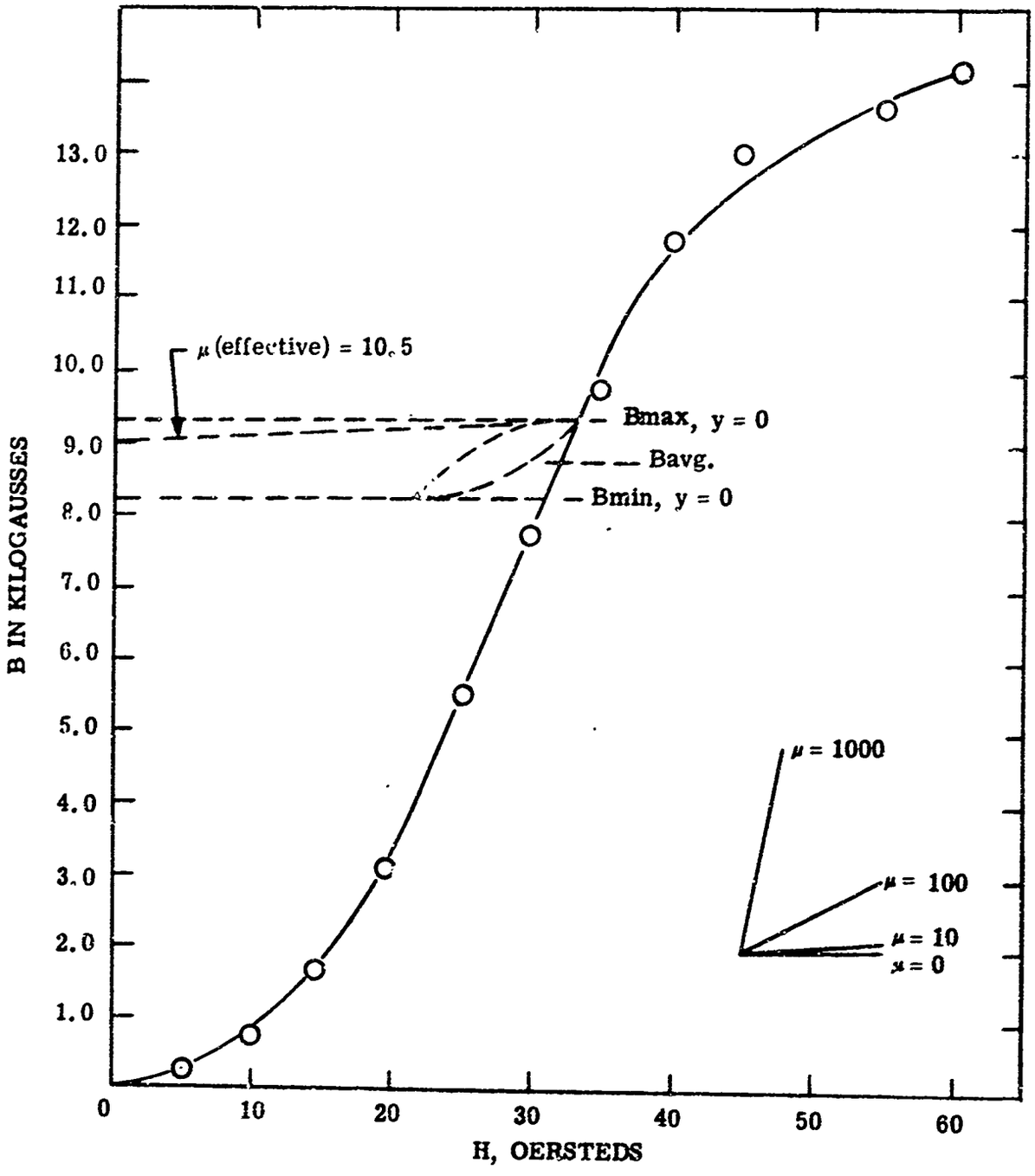

Figure 24. Maximum and Minimum Flux Density in Pole Face at 24,000 cps Graphically Illustrated on a Normal Magnetization Curve for H-11 Steel

It can be noted that the maximum induction is well below the point of saturation. Thus, the low value of μ (effective) can not be associated with points of saturation within the pole face. The low value of μ (effective) may also be due to the fact that a significant portion of the tooth ripple loss is produced by hysteresis loss. Minor hysteresis loops are produced by the varying field which are superposed upon the normal magnetization curve as shown in Figure 24. A different loop would exist for each point in the pole. The loop would represent the variation of B and H with time for a constant value of X and y. The hysteresis loss in watts per cubic cm at a point is

$$P\Big|_{\substack{x=c_1\\y=c_2}} = \frac{f \times 10^{-7}}{8\pi} \int_c B(t)\Big|_{\substack{x=c_1\\y=c_2}} d[H(t)]$$

and the total hysteresis loss per unit of surface area would be

$$P\Big|_{x=c_1} = \frac{fx10^{-7}}{8\pi} \int_0^{\infty} \left[\int_c B(t)\Big|_{\substack{x=c_1\\y=c}} d[H(t)] \right]_{\substack{x=c\\y=0 \text{ to } \infty}} dy$$

In general, the area within a hysteresis loop can only be evaluated experimentally. However, some conclusions can be obtained if one assumes the following:

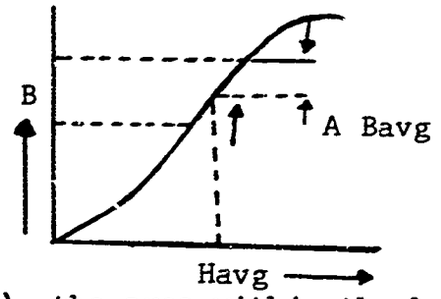

(a) the area within the hysteresis loop at y = 0 and X = 0 shall be assumed to be equal to

$$\int_c Bdh = 2A_1 \text{ Bavg Havg}$$

which is probably several times greater than the actual case.

(b) the area within the hysteresis loops at X = 0 shall be assumed to decrease with y in accordance with the relation

$$\text{Area} = (\text{Area})_{y=0} \exp(-2\pi U_1 y/\lambda)$$

This relationship is based upon the assumption that the area within a hysteresis loop is proportional to the amplitude of cyclically changing flux density. In the actual case the area would also be proportional to the amplitude of the cyclically changing field-strength. Thus,

$$\text{Area} = (\text{Area})_{y=0} \exp(-4\pi U_1 y/\lambda)$$

is probably more correct than the relationship assumed for the calculation presented in this report.

With these assumptions hysteresis loss per unit of surface area becomes

$$P_H = \frac{A_1 B_{avg}\, H_{avg}\, \lambda\, f \times 10^{-7}}{8\pi^2 U_1} \qquad (\text{watt/cm}^2) \qquad (49)$$

Equation (49) gives an extravagant value for the hysteresis loss. Thus, if the value of hysteresis loss obtained from this equation is small compared with the calculated eddy-current loss, the inclusion of hysteresis loss would not be essential. Figure 25 gives pole face losses with and without the inclusion of hysteresis loss. In general, this comparison shows that hysteresis loss probably is not a significant part of the total tooth ripple loss for these operating conditions. The inclusion of hysteresis loss means that the effective permeability for eddy-current calculations would have to be increased slightly to provide for a small decrease of eddy-current loss that is required for the same combined losses. Figure 25 shows the eddy-current loss is predominant over hysteresis loss at high tooth ripple frequencies. Therefore, the inclusion of hysteresis loss is not essential for the operating conditions which establish the maximum heat load for the rotor cooling system.

The only reasonable explanations for the low values of effective permeability that were derived from the experimental data are: (1) that H-11 steel had a low reversible permeability, and (2) that the incremental permeabilities associated with the minor hysteresis loops were also low. Figure 26 illustrates how minor hysteresis loops under various conditions in iron appear on a normal magnetization curve. The reversible permeability, μ_r, for value of H_b and B_b lying on a normal magnetization curve can be determined by two ways (reference 5). The first procedure is illustrated on Figure 26b. In this case the biasing field strength is held constant and the incremental permeability, $\mu_\Delta = \Delta B/\Delta H$, is determined for an increasing ΔH. The reversible is then obtained by extrapolating μ_Δ to $\Delta H = 0$. The second procedure is illustrated on Figure 26c. For this case, a steady field is applied in one direction, and the

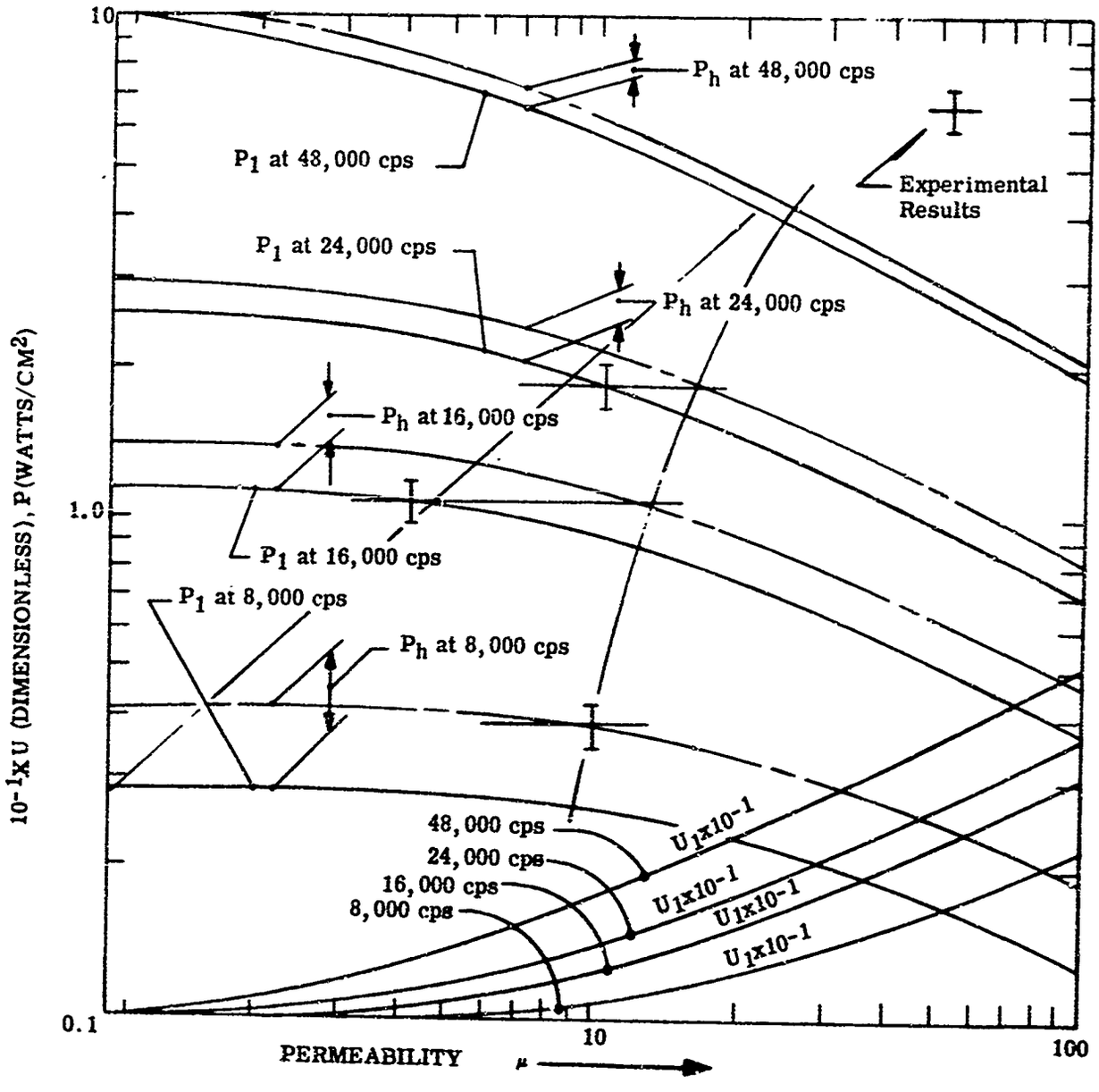

Figure 25. Pole Face Losses with the Inclusion of Hysteresis Loss

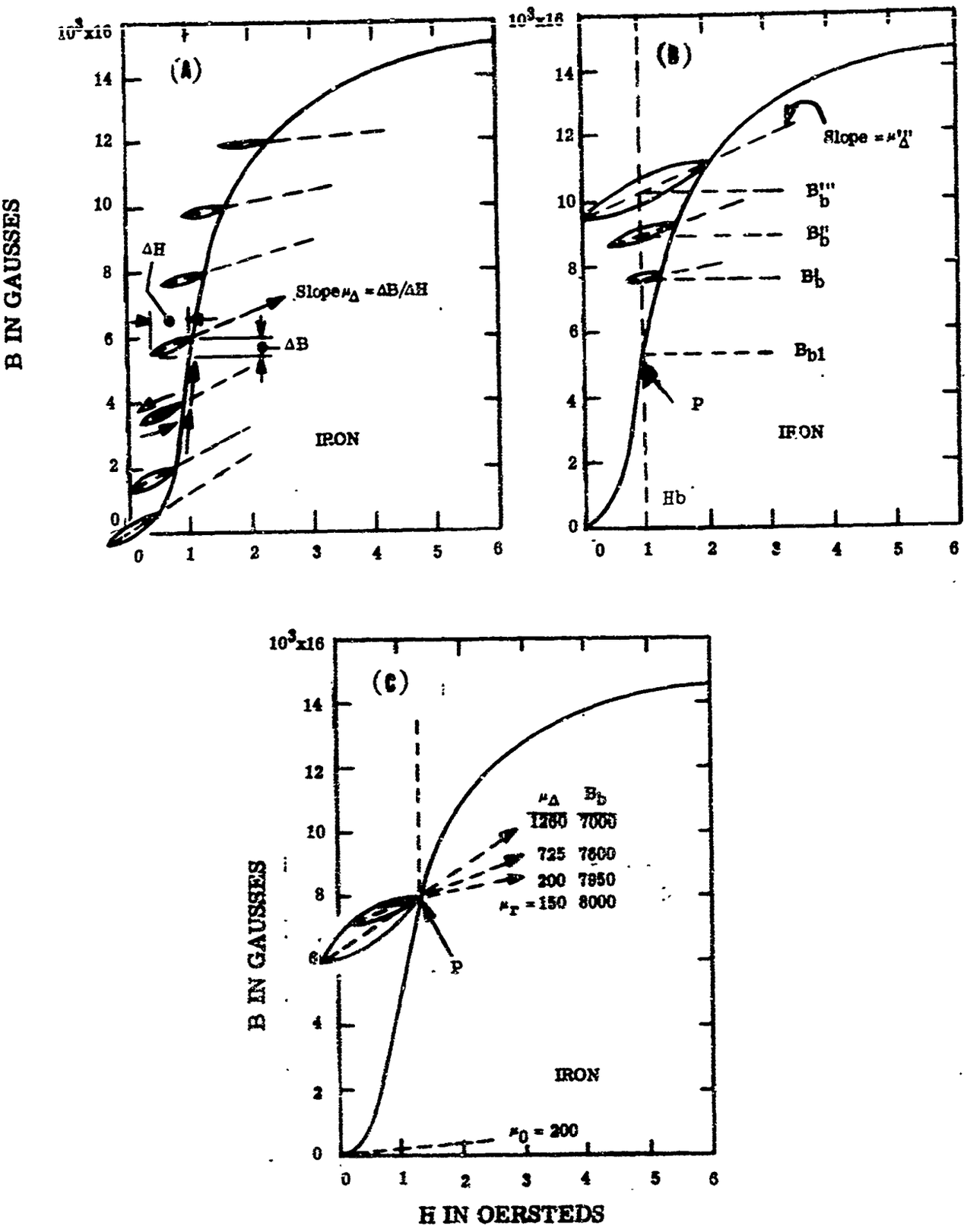

Figure 26. Minor Hysteresis Loops Taken Under Various Conditions in Iron, Taken From Reference 5

alternating field is applied first in the opposite direction. The incremental permeability, $\mu_\Delta = \Delta B/\Delta H$, is determined for an increasing ΔH and the reversible permeability is determined by extrapolating to $\Delta H = 0$.

The reversible permeability of the pole face material is an important parameter since it is the applicable value of permeavility to be used in the pole face loss equations when the value of ΔH or ΔB approach zero. In the actual case ΔH and ΔB approach zero at points under the surface. Therefore, the reversible permeability would be the exact value of permeability to be used for eddy-current losses at these points. At a point in the pole where ΔB has a finite value, the permeability approaches the incremental permeability of the minor hysteresis loop which is produced at this point. The incremental permeability represents the average change of B with respect to changes of H along the hysteresis loop.

The applicable value for the permeability for calculating pole face losses can be determined by a numerical integration. Equation 46 gives the pole face loss as

$$P = (\lambda^2 f^2/2\rho') \int_0^\infty \sum_{m=1,2,3} B^2_{ym} \exp(-4\pi U_m m y/\lambda)\, dy$$

The integrands of this equation are equal to the square of the y component of flux density for each harmonic frequency along a path where $(ft + x/\lambda - V_m y/\lambda)$ equals any integer. If we consider each harmonic frequency separately, the loss for each frequency becomes

$$P_m = (\lambda^2 f^2/2\rho') \int_0^\infty B_y^2\, dy$$

Since

$$B_y = B_{ym} \exp(-2\pi m U_m y/\lambda)$$

$$dy = (\lambda/2\pi U_m m B_y)\, d\, By$$

we can express the loss for each frequency as

$$P_m = (\lambda^3 f^3/8\pi m\rho') \int_0^{B_{ym}} \frac{d(B^2 y)}{U_m}$$

In order to simplify the numerical integration of this equation, we shall assume that $4f^2\mu^2\lambda^4/\rho'^2 m^2 >> 1$ and it can be noted from Equation 38 that U_m becomes equal to $\lambda\sqrt{f\mu/\rho' m}$. Thus,

$$P_m = (\lambda^2 f^{3/2}/8\pi\sqrt{\rho^{-1}m}) \int_0^{B_{ym}} \frac{d(B^2 y)}{\sqrt{\mu}} \qquad (50)$$

The integrand, $1/\sqrt{\mu}$, in the equation shall be considered to be a variable quantity and equal to $C_H/\sqrt{\mu_\Delta}$. By is equal to the amplitude of the y component of the flux density for a constant value of "y". If we consider a constant value of "y", the flux density has a sinusoidal variation with "x" or time which produces minor hysteresis loops as illustrated by Figure 26C. The ΔB associated with each loop is equal to $2B_y$. The biasing induction, B_b, will be constant and equal to the average flux density in the pole. A different loop exists for each value of "y". Since μ_Δ varies with the amplitude of the loop, a numerical integration of Equation (50) is required as illustrated in Figure 27. The parameter "C_H" is a correction for the fact that the slope at a point on a minor hysteresis loop is not equal to μ_Δ. The previous derivations were based upon the assumption that $\mu = \mu_\Delta$ and that the loss per unit volume was proportional to $B_y\sqrt{\mu_\Delta}$. A large portion of a minor hysteresis loop has a slope which is less than μ_Δ at points where By^2 is large. Therefore, a significant error was introduced when $(\Delta B/2)^2(1/\sqrt{\mu_\Delta})\cos^2 2\pi x/\lambda$ was integrated with respect to "x". The factor required to correct this error is

$$C_H = \frac{B_\Delta^2 \int_0^{2\pi} (1/\sqrt{\mu}) \cos^2(2\pi x/\lambda) d(2\pi x/\lambda)}{\frac{B_\Delta^2}{\sqrt{\mu_\Delta}} \int_0^{2\pi} \cos^2(2\pi x/\lambda) d(2\pi x/\lambda)}$$

where μ = the actual slope at a point on the hysteresis loop and $B_\Delta = \Delta B/2$. The evaluation of the integral requires a standardization of the hysteresis loops. The specific assumptions made regarding the shape of the loop as shown on page 64 are:

(1) the slope of the hysteresis loop is a linear function of the field strength
(2) the slope of the hysteresis loop for decreasing induction at $B_y/B_\Delta = 1$ is equal to the reversible permeability
(3) the slope of the hysteresis loop for increasing induction at $B_y/B_\Delta = -1$ is equal to the reversible permeability
(4) $\text{Cos}^{-1}(B_y/B_\Delta) = 2\pi x/\lambda$
(5) for $B_y/B_\Delta = 1$ $H/H_\Delta = 1$ and for $B_y/B_\Delta = -1$ $H/H_\Delta = -1$

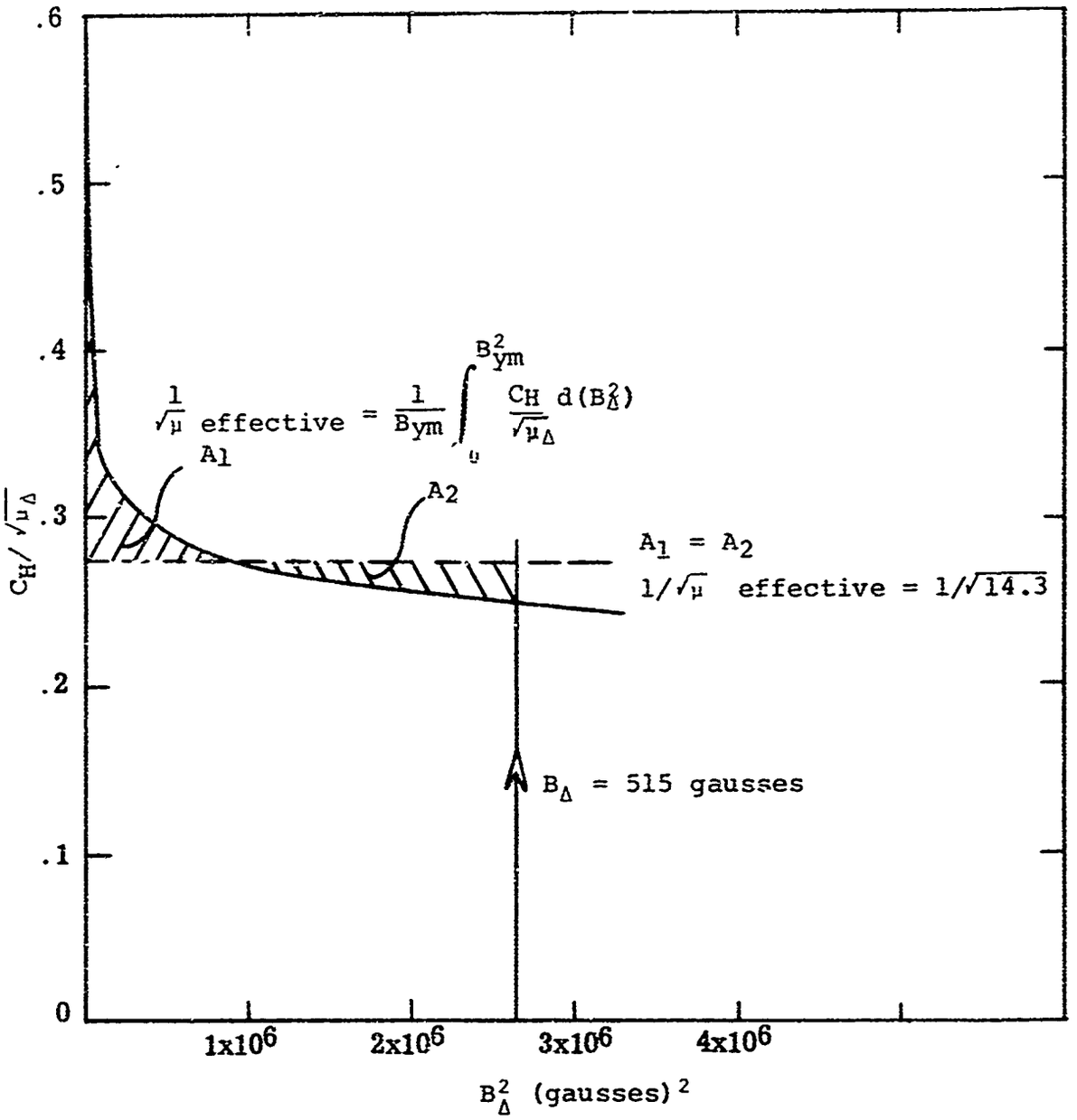

Figure 27. Effective Permeability of H-11 Steel Based Upon Theoretical Considerations

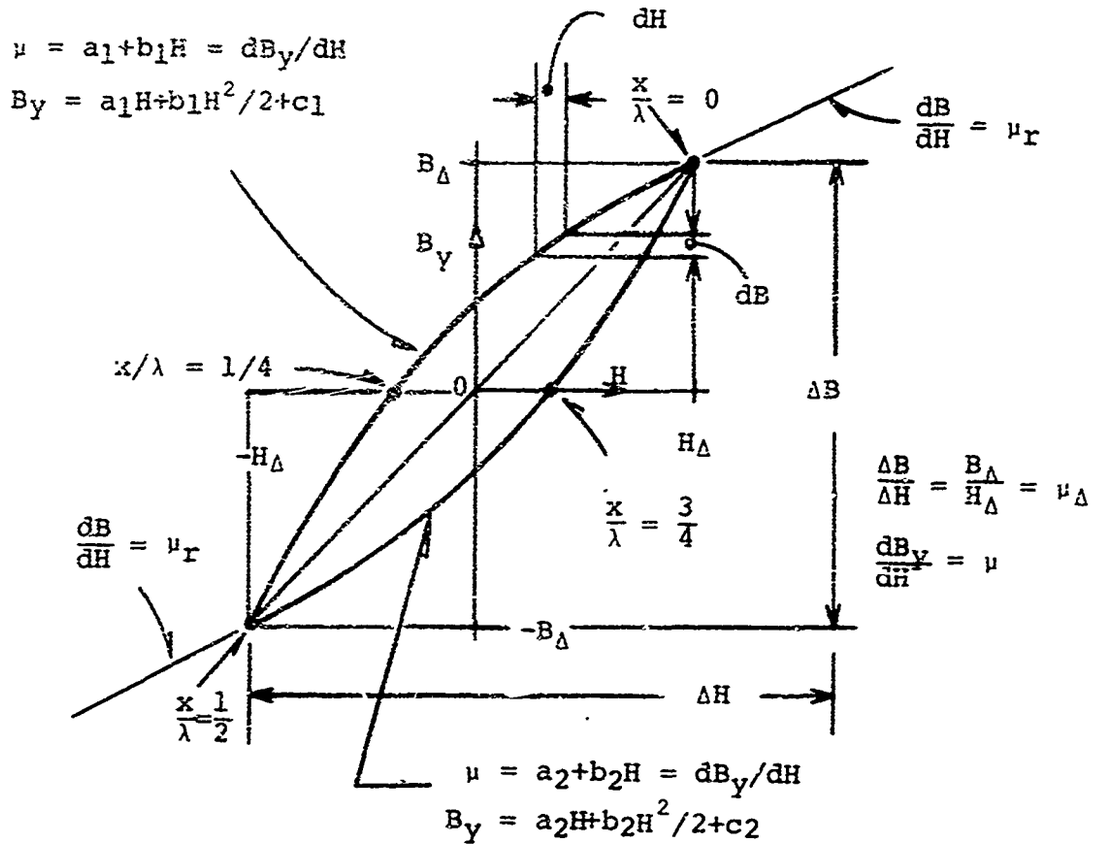

with these assumptions

$$a_1 = a_2 = \mu_\Delta$$
$$c_1 = c_2 = -(\mu_r-\mu_\Delta)H_\Delta/2$$
$$b_1 = -b_2 = (\mu_r-\mu_\Delta)/H_\Delta$$

and for the upper portion of the loop,

$$0 \leq x/\lambda \leq 1/2 \quad \begin{cases} \mu/\mu_\Delta = 1 + (\mu_r-\mu_\Delta)H/\mu_\Delta H_\Delta & (51) \\ B_y/B_\Delta = ((\mu_r-\mu_\Delta)/2\mu_\Delta)(H/H_\Delta)^2 + H/H_\Delta-(\mu_r-\mu_\Delta)/2\mu_\Delta & (52) \end{cases}$$

For the bottom portion of the loop the equations become

$$1/2 \leq x/\lambda \leq 1 \quad \begin{cases} \mu/\mu_\Delta = 1 - (\mu_r-\mu_\Delta)H/\mu_\Delta H_\Delta & (53) \\ B_y/B_\Delta = -((\mu_r-\mu_\Delta)/2\mu_\Delta)(H/H_\Delta)^2 + H/H_\Delta + (\mu_r-\mu_\Delta)/2\mu_\Delta & (54) \end{cases}$$

Since the correction factor for the upper portion of the loop will be equal to the correction factor for the lower portion, we only need to determine the factor for one-half of the loop. The task that remains is to form the integrals required to evaluate the correction factor. The correction factor can be expressed as

$$C_H = \frac{2}{\pi} \int_0^{\pi} \sqrt{\mu_\Delta/\mu}\,(B_y/B_\Delta)^2 d(2\pi x/\lambda)$$

Since B_Δ and μ_Δ are not a function of "x" and

$$B_y/B_\Delta = \cos 2\pi x/\lambda$$

By letting

$$C_H = 2/\pi \int_1^{-1} f(B_y/B_\Delta)\,d(B_y/B_\Delta) = 2/\pi \int_0^{\pi} \sqrt{\mu_\Delta/\mu}\,(B_y/B_\Delta)^2 d(2\pi x/\lambda)$$

we can form the integral on the left. because

$$\cos^{-1}(B_y/B_\Delta) = 2\pi\, x/\lambda$$

$$\frac{-d(B_y/B_\Delta)}{\sqrt{1-(B_y/B\Delta)^2}} = d(2\pi x/\lambda)$$

and from equations 51 and 52 it can be shown that

$$\sqrt{\mu_\Delta/\mu} = \left\{ 1 + \left(\frac{\mu_r-\mu_\Delta}{\mu_\Delta}\right)^2 + 2\left(\frac{\mu_r-\mu_\Delta}{\mu_\Delta}\right)\frac{B_y}{B_\Delta} \right\}^{1/4}$$

Therefore, the integral for the correction becomes

$$C_H = 2/\pi \int_{-1}^{1} \frac{-(B_y/B_\Delta)^2 d(B_y/B_\Delta)}{\sqrt{1-(B_y/B_\Delta)^2}\left\{1 + \left(\frac{\mu_r-\mu_\Delta}{\mu_\Delta}\right)^2 + 2\left(\frac{\mu_r-\mu_\Delta}{\mu_\Delta}\right)\frac{B_y}{B_\Delta}\right\}^{1/4}}$$

if we let $B_y/B_\Delta = \cos\theta$ and $(\mu_\Delta-\mu_r)/\mu_\Delta = \varepsilon$,

$$C_H = 2/\pi \int_0^{\pi} \frac{\cos^2\theta d\theta}{\{1+\varepsilon^2-2\varepsilon\cos\theta\}^{1/4}} \qquad (55)$$

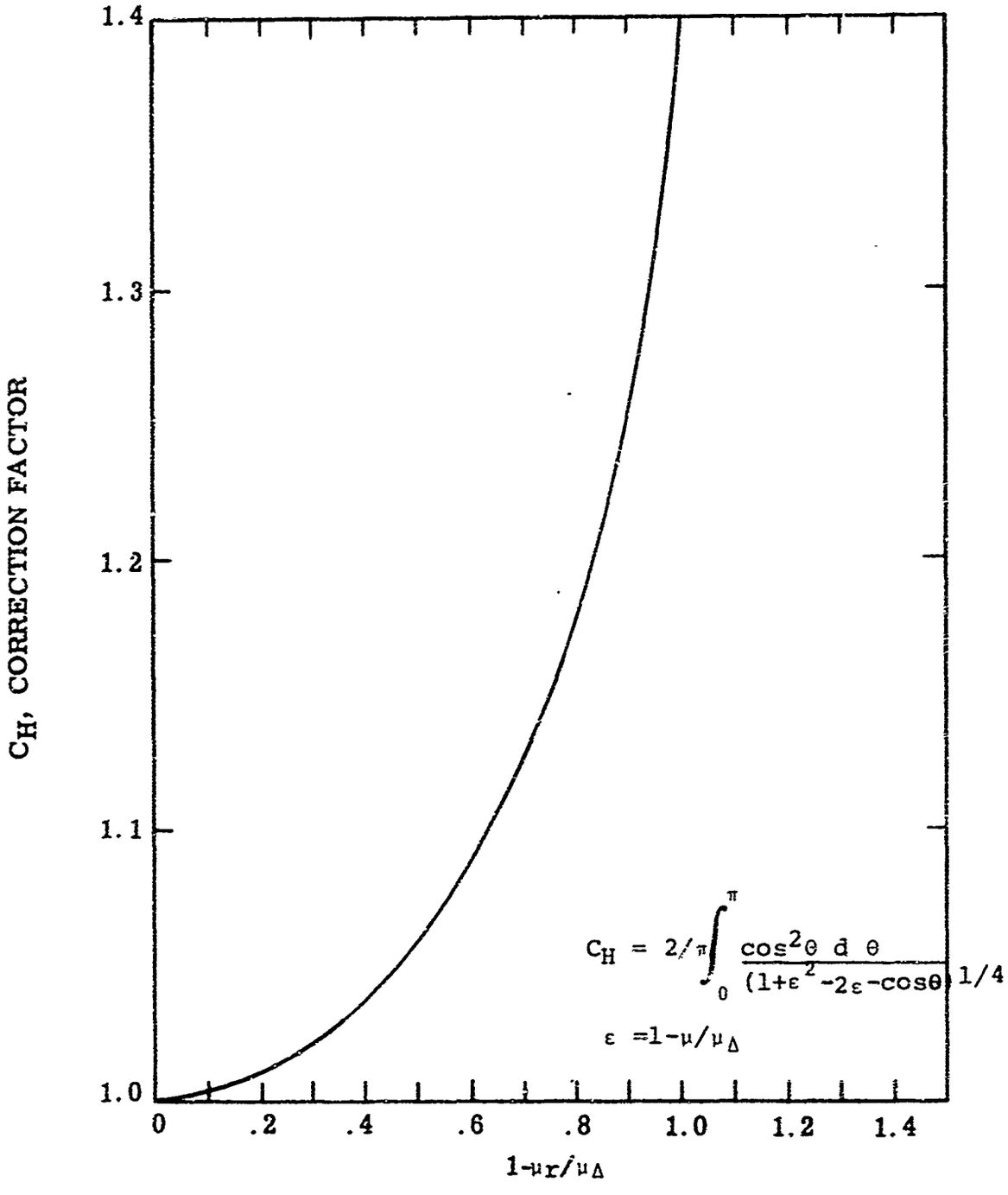

Figure 28. Correction Factor Versus $1-\mu_r/\mu_\Delta$

The correction factor for various values of ε was determined by Gaussian quadrature integration of Equation (55) as shown by Figure 28. The applicable value of permeability for pole face loss calculations can now be determined with the corrections given by Figure 28 and with the numerical integration shown on Figure 27. The material properties required for this integration are:

(1) the reversible permeability of the material at a steady induction equal to the average flux density in the poles and,

(2) the incremental permeabilities of the minor hysteresis loops which occur in the poles.

Since these quantities are intrinsic and measurable properties of the material the effective permeability is a predictable quantity once the flux distribution on the surface of the pole is known. Unfortunately, the reversible and incremental permeabilities of H-11 steel have not been measured and it is therefore necessary to derive a value for the effective permeability of H-11 steel from theoretical considerations. When the amplitude of the alternating field, H_Δ, is increased the incremental permeability is also generally increased. For small amplitudes this increase is linear and by analogy with Rayleigh's law, we can assume that

$$\mu_\Delta = \mu_r + V_\Delta H_\Delta$$

and

$$B_\Delta = \mu_r H_\Delta + V_\Delta H_\Delta^2$$

When the magnetization is sufficiently low Rayleigh's law may be used for the initial portion of the normal magnetization curve or

$$\mu = \mu_0 + VH$$

and

$$B = \mu_0 H + VH^2$$

For H-11 steel the initial portion of the normal magnetization curve gives

$$\mu_0 = 20$$
$$V = 6$$

Ebinger, reference 5, has measured V_Δ for a variety of materials and plotted V_Δ/V vs. $(B-H)/B_S$. He found that the points lie reasonably close to a single curve. For a biasing induction of 8.75 kilogausses on H-11 steel the ratio of V_Δ/V from Ebinger's curve is approximately 0.175 which means that value of V_Δ for H-11 steel at this induction is approximately one. Brown, reference 5, has shown for material with no direction of easy magnetization and with anisotropic domains that the ratio of μ_r/μ_0 equals approximately 0.15 for a proportionate induction, $(B-H)/B_S$, of 42% which means that μ_r for H-11 steel at an induction of 8.75 kilogausses would be approximately equal to three.

Thus, the equation for the incremental permeability becomes

$$\mu_\Delta = 3 + 1.05\ H_\Delta$$

and

$$B_\Delta = 3H_\Delta + 1.05H_\Delta^2$$

We can now express μ_Δ, μ_r/μ_Δ, B_Δ, and other parameters of interest in terms of H_Δ as shown below.

H	μ_Δ	B_Δ	μ_r/μ_Δ	C_H	$C_H/\sqrt{\mu_\Delta}$	B_Δ^2
oersteds		gausses				$(\text{gausses})^2$
0	3.0	0	1.0	1.0	0.577	0
2	5.1	10.2	0.588	1.038	0.460	0.000104×10^6
4	7.2	28.8	0.416	1.081	0.402	0.000830×10^6
6	9.3	55.8	0.322	1.115	0.368	0.00311×10^6
8	11.4	91.2	0.263	1.140	0.331	0.00781×10^6
10	13.5	135.0	0.222	1.160	0.316	0.0182×10^6
12	15.6	187.0	0.1922	1.180	0.299	0.035×10^6
14	17.7	248.0	0.1694	1.195	0.283	0.0615×10^6
16	19.8	317.0	0.1513	1.206	0.271	0.1003×10^6
18	21.9	394.0	0.137	1.216	0.260	0.1552×10^6
20	24.0	480.0	0.125	1.226	0.250	0.230×10^6
22	26.1	574.0	0.115	1.234	0.242	0.329×10^6

Since

$$\frac{1}{\sqrt{\mu}}\ \text{effective} = 1/B_{ym}^2 \int_0^{B_{ym}^2} \frac{C_H}{\sqrt{\mu_\Delta}}\, d(B_\Delta^2)$$

the applicable value of permeability can be determined by numerical integration of the integral as shown in Figure 27. This integration gives

$$1/\sqrt{\mu} \text{ effective} = 0.274$$

for B_{ym} = 515 gausses. Thus,

$$\mu \text{ effective} = 14.3$$

Although the above analysis may not be strictly accurate from a numerical standpoint due to the admission of approximations, it shows that the effective permeability of H-11 steel is low.

It also shows that the low permeability value required to obtain agreement between experimental and analytical results is reasonable.

The eddy-current losses given by Figures 22 and 25 are based upon conditions pertinent to the experimental generator except for resistivity of the material. The losses given by Figures 22 and 25 were calculated using resistivity which corresponds to room temperature conditions. Figure 29 gives the eddy-current loss with a correction for a change in resistivity based upon the estimated operating temperature of the pole face in the generator.

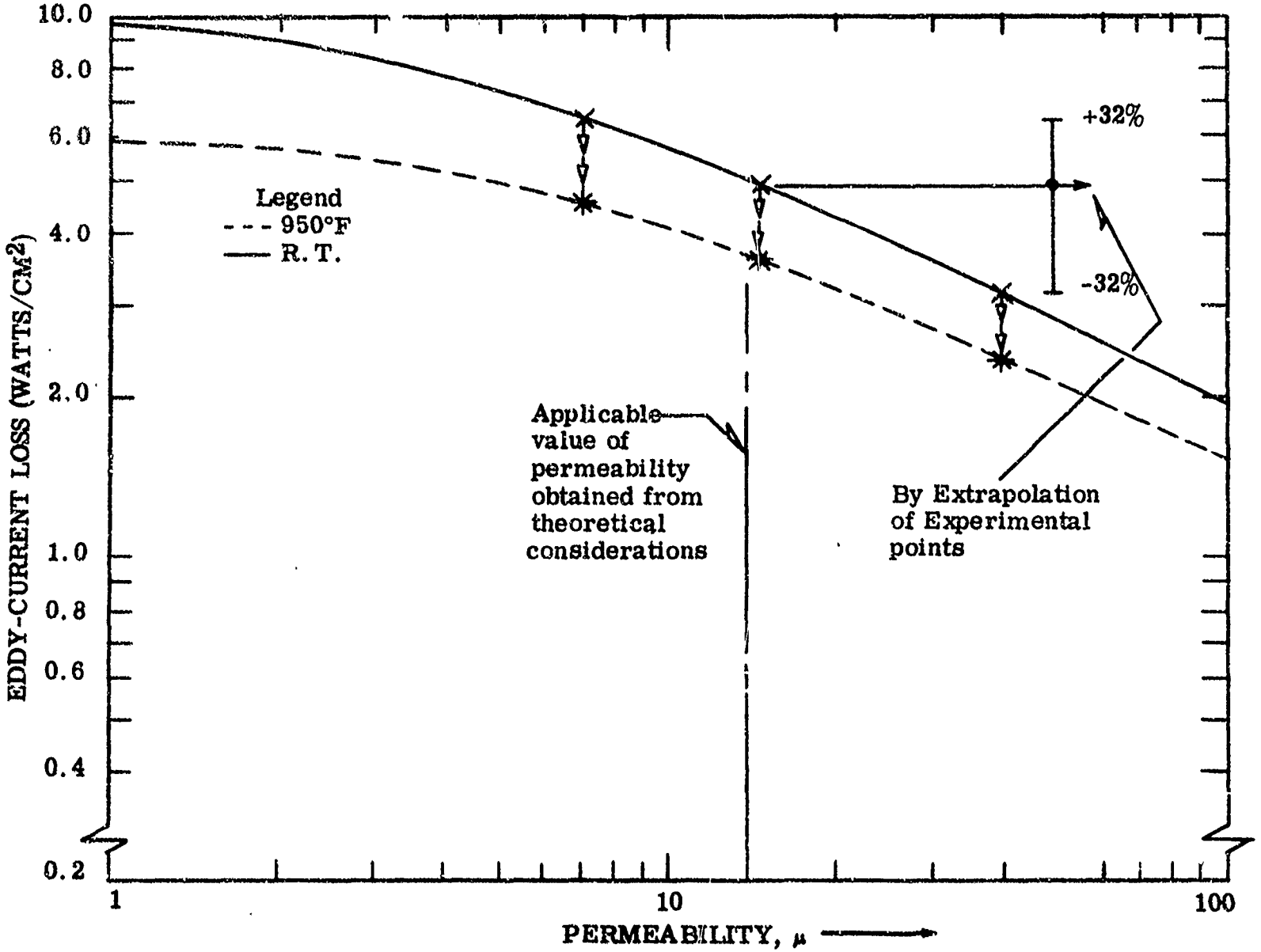

Figure 29. Eddy-Current Loss in Experimental Generator at Room Temperature and 950°F

SECTION VI

POLE FACE LOSSES CAUSED BY ARMATURE REACTION

The eddy-currents produced by the stray rotating fields of the armature reaction were calculated by using the equations from Reference 2. These equations were published in 1955 by G. Barello and his derivations shall be taken for granted. His results give:

$$W = \sum \frac{5.65 \left[\frac{N}{100}\right]^2 \left[\frac{I}{100}\right]^2 \left[\frac{fen}{n}\right]^2 (n \pm 1)^{3/2} f_1^{3/2}}{\sqrt{\mu_r \rho}\left(\left[\sinh\frac{\pi n \delta}{T_1} + \frac{T_1 m}{\mu_r \pi n}\cosh\frac{\pi n \delta}{T_1}\right]^2 + \left[\frac{T_1 m}{\mu_r \pi n}\cosh\frac{\pi n \delta}{T_1}\right]^2\right)}$$

where:

W = Loss in watts per square meter of pole surface

N = Number of conductors in series per pole per phase

I = Current per phase in amperes

f_1 = Nominal frequency of currents in windings, the base frequency of the machine in cps

n = The order of the harmonic being considered

$fen = K_\rho K_d$ for the nth harmonic being considered

μ_r = The relative permeability of the rotor material

ρ = Resistivity in ohm-meters

T_1 = Pole pitch of the machine in meters

δ = Air gap in meters

$m = \sqrt{\pi \mu (n \pm 1) f_1 / \rho}$ in meters

$\mu = \mu_0 \mu_r$

$\mu_0 = 1.256 \times 10^{-6}$

Barello found that a value of $\mu_r = 2000$ was a suitable value for the relative permeability of the rotor material. In general, this value gave good agreement between calculated losses and the losses measured on tests with similar machines.

The calculated eddy-current losses produced by the stray rotating fields of the armature reaction for the experimental generator are presented in Table I. For this case the losses are 20.9 kilowatt per square meter. Since the total area of the pole faces in the generator is 0.050 square meters, the losses due to the stray rotating field of the armature reaction will be 1050 watts.

Unfortunately, the original calculated value for the losses due to armature reaction was 210 watts and the rotor cooling system was designed for a combined value of pole face losses equal to approximately 2000 wats. Thus, with 1050 watts of loss due to armature reaction and 1793 watts loss due to tuffs of flux from the stator teeth, over-heating of the rotor will occur if the generator is operated at design conditions. This conclusion is supported by the fact that the calculated loss due to armature reaction was based upon a relative permeability, μ_r, of 2000 for the rotor material. This value had an empirical derivation based upon test data from average machines and it is reasonable to assume the applicable value was influenced by the actual permeability of the rotor material. Since the material in the rotor of the experimental generator has an unusually low permeability, it is problematical that the losses due to armature reaction will even be higher than the calculated value of 1050 watts based upon Barello's equation. In any case, the loss due to armature reaction constitute a large portion of the total estimated pole face losses.

TABLE I. Pole Face Losses Caused by Stray Rotating Fields of Armature Reaction Losses by Barello Method

n	n±1	$(n\pm1)^{3/2}$	n^2	$\frac{n\pm1}{n}$	b	α	sinh α	cosh α
2	3	5.2	4	0.866	0.0297	0.282	0.284	1.04
4	3	5.2	16	0.433	0.0148	0.564	0.59	1.16
5	6	14.7	25	0.49	0.0168	0.705	0.76	1.26
7	6	14.7	49	0.35	0.0120	0.988	1.16	1.26
8	9	27.1	64	0.375	0.0129	1.13	1.39	1.53
10	9	27.1	100	0.300	0.0103	1.41	1.93	2.17
11	12	41.6	121	0.315	0.0108	1.55	2.25	2.46
13	12	41.6	169	0.266	0.0091	1.83	3.04	3.20
14	15	58.0	196	0.276	0.0094	1.97	3.52	3.66
16	15	58.0	256	0.242	0.0083	2.26	4.74	4.84
17	18	96.4	289	0.249	0.0085	2.40	5.69	5.78
19	18	76.4	361	0.224	0.0077	2.68	7.26	7.33

n	Y	X	X^2	Y^2	X^2+Y^2	C	$(fen)^2$	$\frac{\text{Watts}}{\text{Meter}^2}$
2	0.0309	0.315	0.0991	0.00096	0.1001	8.170	0.00784	11,660
4	0.0172	0.607	0.368	0.00029	0.3683	0.555	0.00885	892
5	0.0212	0.781	0.611	0.0045	0.6114	0.602	0.0300	3,280
7	0.0184	1.178	1.39		1.39	0.136	0.0167	419
8	0.0220	1.408	1.98		1.98	0.134	0.0167	401
10	0.0223	1.948	3.8		3.80	0.045	0.0300	226
11	0.0266	2.277	5.19		5.19	0.042	0.0088	73
13	0.0291	3.066	9.4		9.4	0.016	0.0078	236
14	0.0344	3.55	12.6		12.6	0.015	0.829	2,240
16	0.0402	4.779	14.3		14.3	0.010	0.829	1,510
17	0.0492	5.742	33.0		33.0		0.0885	-------
19	0.0563	7.314	53.6		53.6		0.0946	-------
							TOTAL	20,900

$b = \frac{T_1 m}{\mu_r \pi n} = 0.0343 \frac{\sqrt{n\pm1}}{n}$

$\alpha = \frac{\pi n \delta}{T_1} = .141n$

$C = \frac{5.65(NI)^2(n\pm1)^{3/2}10^{-8}}{\sqrt{\rho \mu_r (x^2+4^2)n^2}}$

$Y = b \cosh \alpha$

$X = \sinh \alpha + Y$

$N = 0.625$

$I = 1298$ Amperes

$f_1 = 3200$ cps

$T_1 = 0.0565$ meters

$\delta = 0.00254$ meters

$\mu_r = 2000.$

$\rho = 67 \times 10^{-4}$ ohm-meters

SECTION VII

SUMMARY AND CONCLUSIONS

The pole face losses caused by the alternating flux density that is produced by the slots and teeth of the armature for the 467 kva experimental generator were experimentally evaluated by using an eddy-current dyanamometer. Design factors which influence pole face losses in the generator were duplicated in the test fixture as close as possible. Centrifugal stress limited the rotor speed in the test fixture to one-half the speed of the generator. It was, therefore, necessary to extrapolate the data from a tooth ripple frequency of 24,000 cps to 48,000 cps to determine the face losses in the generator. No attempt was made to control the temperature of the pole faces. Thus, the test results had to be corrected for a change of resistivity since the pole faces will operate at a much higher temperature in the generator. The pole face losses due to tooth flux ripple for the generator as derived from the experimental data are 1783 $\pm$ 590 watts for pole face temperature of 950°F.

An analysis of the losses associated with tooth flux ripple based upon theoretical considerations was made. A procedure for dealing quantitatively with the magnetic flux density distribution at the surface of the pole face was outlined. A knowledge of the distribution of flux density on the surface is essential, because it is the non-uniformity of this flux which causes all tooth-ripple losses. Harmonic frequencies and losses due to each harmonic frequency were considered. This analysis showed that 98.5% of the tooth-ripple losses in the experimental generator are associated with the fundamental frequency of the cyclically changing induction in the pole faces. The amplitude of the cyclically changing flux density for the fundamental frequency was found to be 5.88% of the average flux density in the radial gap. Solid and grooved pole faces were considered in the analysis. The losses in grooved pole faces were calculated by using an effective resistivity for the pole face material which was based upon the increase in the resistance of the eddy-current path caused by the grooves. The resistivity of the pole face material was effectively increased by 2.63-folds. Thus, grooving the pole faces reduced the pole face losses by approximately 38.5%. Hysteresis losses in the pole faces could not be separated from the other losses since no theoretical relationship exists between the amplitude of flux density oscillation and the area within a hysteresis loop. In order to determine if hysteresis losses were of importance a relationship between the area of a hysterssis loop and the amplitude of flux density oscillation was

assumed which would give an extravagant value for the hysteresis loss. Even for these conditions it was found that hysteresis loss was of minor importance and that eddy-current loss was predominant over hysteresis loss.

The theoretical equations for the calculations of the eddy-current losses contain a parameter which is equal to the permeability of the pole face material. The derivations of these equations were based upon the assumption that the permeability of the material is a constant. In the actual case the permeability of the material is a variable and an applicable value of this parameter must be used to obtain a reasonable estimation of the eddy-current losses from theoretical consideration. The experimental results present in this report demonstrate that the applicable value of permeability is associated with the incremental permeability of the minor hysteresis loops that are produced in the pole face material. In general, the incremental permeability of a minor hysteresis loop in a particular material can vary widely since the slope of a loop usually increases when the amplitude of the oscillating induction increases. A procedure for dealing with a varying incremental permeability was outlined. The applicable value can be obtained by a numerical integration which also considers the varying permeability around each minor hysteresis loop.

The eddy-current loss produced by the stray rotating fields of the armature reaction were calculated using Barello's equations. It was concluded from these calculations that the rotating fields of armature reaction will produce a loss of 1050 watts. Unfortunately, the rotor cooling system was designed for only 210 watts of loss due to armature reaction. This dilemma results from inadvertant error in the original calculations. It is therefore generally concluded that overheating of rotor would occur if the generator was operated at full load with a 575°F coolant inlet temperature. This particular dilemma was not resolved by redesigning the cooling system since the redirected test plans for the generator allows a low temperature coolant to be used. Nevertheless, it is a logical conclusion that the eddy-current loss produced by the rotating fields of the armature reaction will constitute a large portion of the rotor face losses in this type of generator.

The design of an electromagnetic generator with a high-speed, high-temperature solid rotor must cope with the problem of reducing the pole face losses if temperature is to be attained which do not impose serious design limitations upon rotor materials. There are certain parameters which can be varied to reduce the rotor pole face losses. Some of the parameters which have a significant influence upon the pole face losses are the radial gap, the ratio of the width of the slot opening

and tooth pitch, tooth pitch, pole pitch, and the direct axis synchronous reactance of the machine. In general, these parameters can be varied to reduce the amplitude of flux density variations on the surface of the pole faces. However, serious performance and weight penalties can be incurred in the overall design when these parameters are optimized only from the standpoint to pole face losses. The designer is therefore obliged to look for other methods for reducing pole face losses. The most promising solutions of the dilemma would be to combine a material which offers excellent properties for the reduction of eddy-current losses in the pole faces with a material that offers excellent creep strength and d-c magnetic properties for a solid rotor. Pole face losses are reduced by selection of a material for the pole tips which has a high resistivity and a high reversible permeability. Unfortunately, materials which have the best combination of d-c magnetic and strength properties for a high speed and high temperature rotor have inferior properties from the standpoint of pole face losses. For example, the pole face losses in Westinghouse NIVCO alloys will be approximately 2 to 3-folds greater than the pole face losses in H-11 steel. The losses in H-11 steel are approximately 4-folds greater than the losses in soft iron. The increase in heating in the pole faces may more than offset the advantage offered by the additional high-temperature creep strength of a particular material.

Generally a material which has a high normal permeability at a particular value of induction also has high incremental and reversible permeabilities at this level of induction. The normal permeability of the cobalt-iron alloys at inductions up to 10 kilogausses are relatively high. Thus, these materials and probably others are candidates for pole face materials. It should be noted that a material of much lower creep strength can be used on the pole tips since the stress is much lower on the outer radius of the rotor than at the root of the pole bodies or in the rotor core. In addition the creep strain may be allowed to approach 1 to 1-1/2% since the length of this material will be small. A creep strain over 1/2% for other parts of the rotor may be considered excessive since this amount of strain would cause a large change of the radial gap in the generator.

A large increase in resistance to the flow of eddy-current can be obtained with laminated pole tips. Consequently, arrangement for attaching the pole tips should permit a laminated construction to be used. Eddy-current losses can be decreased by approximately 2-folds by using laminations in place of grooved pole faces.

The overall decrease of eddy-current losses with a laminated material which has been chosen for its high a-c magnetic permeability can approach 16-folds when compared with the losses associated with H-11 steel or other materials that have been selected for their creep strength or other criteria except their a-c magnetic permeability. The reduction of pole face losses which is offered by a material which has been selected for its high magnetic permeability may eliminate a critical need for a high temperature material and the need for special and complicated cooling passages in the rotor.

RECOMMENDATIONS

1. The only ways by which tooth ripple losses can be reduced with the present design concepts are by (a) increasing the radial gap, (b) minimizing the amplitude of the flux density variation on the surface of the pole face by maintaining the optimum ratio of slot width and slot pitch, and (c) increasing the length or the effective resistance of the eddy-current path by incorporating grooves in pole faces in a direction parallel to the motion of the rotor. The main disadvantages incurred by using these methods for reducing the pole face losses are (a) additional excitation is required, (b) leakage reactance in the armature is increased, and (c) slotting the pole faces is a very expensive operation and only increases the effective resistance of the material by a factor of approximately 2.6. It is therefore recommended that other techniques for the reduction of pole face losses be investigated. The most promising solution of the dilemma would be to combine a material which offers excellent magnetic properties for the reduction of eddy-current losses with a material that offers excellent creep strength and d-c magnetic properties for a solid rotor. In this case the pole tips would be made of a laminated material of excellent a-c magnetic properties and attached to the pole bodies. The use of a material that is selected for its high a-c magnetic permeability about the operating flux density can reduce pole face eddy-current losses by as much as 7-fold. This method also permits a laminated construction with interlaminar insulation which provides a large increase in the effective electrical resistance to eddy-currents. It is estimated that the laminated construction can cause a 5 to 6-fold increase of the resistance when compared with the resistance of grooved pole faces. Thus, the eddy-current losses can be decreased by approximately 2-folds by using a laminated construction in place of grooved pole faces. The overall decrease of eddy-current losses with a laminated material which has been chosen for its high a-c magnetic permeability can

approach 16-folds when compared with losses associated with material that has been selected for its creep strength or other criteria except its a-c magnetic permeability. The greatly decreased eddy-current losses will permit much cooler operation of the rotor which will enhance the strength of the rotor. The reduction in heating may also allow the rotor coolant temperature to be increased and even eliminate the need for special and complicated cooling passages in the rotor.

2. An estimate of the eddy-current losses in pole faces from theoretical considerations requires a knowledge of the incremental and reversible permeabilities of the material in the pole. Therefore, experiments should be performed to determine these properties for the materials which are candidates for a solid rotor and for pole tips. Since H-11 steel will be used in the experimental, 467 kva generator, it is relatively important that the incremental permeabilities of this material be evaluated so that a comparison of theoretical data and experimental data can be made. This comparison can be used to confirm the general validity of the theoretical equations.

The incremental permeabilities of materials would be evaluated by applying a steady induction on a specimen and by applying an alternating induction first in the opposite direction. The incremental permeability would be determined from the minor hysteresis loops produced by the alternating induction. The alternating induction would be varied from zero to 15% of the steady induction. The reversible permeability would be determined by extrapolating $\Delta B = 0$. The permeabilities would be evaluated along the normal magnetization curve and with descending and ascending value of the steady induction.

Generally a material which has a high normal permeability at a particular value of induction also has high incremental permeabilities at this level of induction. The normal permeability of the cobalt-iron alloys at inductions up to 10 kilogausses are relatively high. Thus, these materials are potentially useful for the reduction of pole face losses since their incremental permeabilities are most likely high. It is recommended that incremental permeabilities of these materials be evaluated to determine their capabilities as materials for the reduction of pole face losses.

The material which offers the best combination of a-c magnetic and strength properties for use as pole tips should then be tested in the experimental generator for comparison with a material that has been selected for the best combination of creep strength and d-c magnetic properties for the highly stressed main rotor body.

Unclassified

Security Classification

DOCUMENT CONTROL DATA - R&D

(Security classification of title, body of abstract and indexing annotation must be entered when the overall report is classified)

1 ORIGINATING ACTIVITY (Corporate author) Westinghouse Electrical Corporation Aerospace Electrical Division Lima, Ohio	2a REPORT SECURITY CLASSIFICATION Unclassified 2b GROUP

3 REPORT TITLE

EVALUATION OF POLE FACE LOSSES FOR THE 467 KVA EXPERIMENTAL GENERATOR

4 DESCRIPTIVE NOTES (Type of report and inclusive dates)

Final January 1965 - July 1966

5 AUTHOR(S) (Last name, first name, initial)

McCabria, Jack L.
Kouba, Carroll C.

6 REPORT DATE	7a TOTAL NO. OF PAGES	7b NO. OF REFS
February, 1967	79	5

8a CONTRACT OR GRANT NO. AF33(615)2326 b. PROJECT NO. c. d.	9a ORIGINATOR'S REPORT NUMBER(S) WAED 66.55E 9b OTHER REPORT NO(S) (Any other numbers that may be assigned this report) AFAPL-TR-66-143

10 AVAILABILITY/LIMITATION NOTICES

11 SUPPLEMENTARY NOTES	12 SPONSORING MILITARY ACTIVITY

13 ABSTRACT

The pole face losses associated with the alternating flux density that is produced by the slot and teeth in the armature for the 467 kva experimental generator were experimentally evaluated by using an eddy-current dynamometer. The design factors which influence pole face losses in the generator were duplicated in the test fixture as close as possible. Centrifugal stress in the rotor limited the tooth ripple frequency to one-half the tooth ripple frequency of the generator and it was necessary to extrapolate the data from 24,000 cps to 48,000 cps to determine the pole face losses at these conditions. No attempt was made to control the temperature of the pole faces. Therefore, the test results had to be corrected for a change of resistivity since the pole faces will operate at a much higher temperature in the generator.

A complete analysis of the pole face loss problem based upon theoretical considerations is presented in the report. The problem of dealing quantitatively with the magnetic flux density distribution at the surface of the poles is treated analytically. Harmonic frequencies and the losses due to each harmonic frequency were considered. The effect of grooves in the pole faces were also considered in the theoretical analysis. The theoretical equations show that the eddy-current losses are a function of permeability of the pole face material. In the actual problem this quantity is a variable and a method for

DD FORM 1 JAN 64 1473

Unclassified

Security Classification

Unclassified

Security Classification

14. KEY WORDS	LINK A		LINK B		LINK C	
	ROLE	WT	ROLE	WT	ROLE	WT
Eddy-current loss in rotor Tooth ripple loss in rotor Analytical treatment of flux distribution on rotor surface. Reduction of pole face losses						

INSTRUCTIONS

1. ORIGINATING ACTIVITY: Enter the name and address of the contractor, subcontractor, grantee, Department of Defense activity or other organization *(corporate author)* issuing the report.

2a. REPORT SECURITY CLASSIFICATION: Enter the overall security classification of the report. Indicate whether "Restricted Data" is included. Marking is to be in accordance with appropriate security regulations.

2b. GROUP: Automatic downgrading is specified in DoD Directive 5200.10 and Armed Forces Industrial Manual. Enter the group number. Also, when applicable, show that optional markings have been used for Group 3 and Group 4 as authorized.

3. REPORT TITLE: Enter the complete report title in all capital letters. Titles in all cases should be unclassified. If a meaningful title cannot be selected without classification, show title classification in all capitals in parenthesis immediately following the title.

4. DESCRIPTIVE NOTES: If appropriate, enter the type of report, e.g., interim, progress, summary, annual, or final. Give the inclusive dates when a specific reporting period is covered.

5. AUTHOR(S): Enter the name(s) of author(s) as shown on or in the report. Enter last name, first name, middle initial. If military, show rank and branch of service. The name of the principal author is an absolute minimum requirement.

6. REPORT DATE: Enter the date of the report as day, month, year; or month, year. If more than one date appears on the report, use date of publication.

7a. TOTAL NUMBER OF PAGES: The total page count should follow normal pagination procedures, i.e., enter the number of pages containing information.

7b. NUMBER OF REFERENCES: Enter the total number of references cited in the report.

8a. CONTRACT OR GRANT NUMBER: If appropriate, enter the applicable number of the contract or grant under which the report was written.

8b, 8c, & 8d. PROJECT NUMBER: Enter the appropriate military department identification, such as project number, subproject number, system numbers, task number, etc.

9a. ORIGINATOR'S REPORT NUMBER(S): Enter the official report number by which the document will be identified and controlled by the originating activity. This number must be unique to this report.

9b. OTHER REPORT NUMBER(S): If the report has been assigned any other report numbers *(either by the originator or by the sponsor)*, also enter this number(s).

10. AVAILABILITY/LIMITATION NOTICES: Enter any limitations on further dissemination of the report, other than those imposed by security classification, using standard statements such as:

(1) "Qualified requesters may obtain copies of this report from DDC."

(2) "Foreign announcement and dissemination of this report by DDC is not authorized."

(3) "U. S. Government agencies may obtain copies of this report directly from DDC. Other qualified DDC users shall request through _____."

(4) "U. S. military agencies may obtain copies of this report directly from DDC. Other qualified users shall request through _____."

(5) "All distribution of this report is controlled. Qualified DDC users shall request through _____."

If the report has been furnished to the Office of Technical Services, Department of Commerce, for sale to the public, indicate this fact and enter the price, if known.

11. SUPPLEMENTARY NOTES: Use for additional explanatory notes.

12. SPONSORING MILITARY ACTIVITY: Enter the name of the departmental project office or laboratory sponsoring *(paying for)* the research and development. Include address.

13. ABSTRACT: Enter an abstract giving a brief and factual summary of the document indicative of the report, even though it may also appear elsewhere in the body of the technical report. If additional space is required, a continuation sheet shall be attached.

It is highly desirable that the abstract of classified reports be unclassified. Each paragraph of the abstract shall end with an indication of the military security classification of the information in the paragraph, represented as *(TS), (S), (C), or (U)*.

There is no limitation on the length of the abstract. However, the suggested length is from 150 to 225 words.

14. KEY WORDS: Key words are technically meaningful terms or short phrases that characterize a report and may be used as index entries for cataloging the report. Key words must be selected so that no security classification is required. Identifiers, such as equipment model designation, trade name, military project code name, geographic location, may be used as key words but will be followed by an indication of technical context. The assignment of links, rules, and weights is optional.

Unclassified

Security Classification

13. Abstract - Concluded

determining the applicable value of this variable is presented.

The general conclusions derived from this work are: (1) materials which offer the best combination of d-c magnetic and strength properties for a high speed, high temperature, solid rotor have inferior properties from the standpoint of pole face losses and (2) a 16-fold decrease of eddy-current losses can be obtained by using a laminated material for the pole tips which has been chosen for its high a-c magnetic permeability when compared with the losses associated with material that has been selected for its creep strength or other criteria except its a-c magnetic permeability.

(This abstract is subject to special export controls and each transmittal to foreign governments or foreign nationals may be made only with prior approval of the Air Force Aero Propulsion Laboratory, APIP-1.)